THE UNIVERSITY OF CHICAGO

EXACTLY SOLVABLE MODELS: QUANTUM CRITICALITY, DYNAMICS, AND
TOPOLOGY

A DISSERTATION SUBMITTED TO
THE FACULTY OF THE DIVISION OF THE THE PHYSICAL SCIENCES
IN CANDIDACY FOR THE DEGREE OF
DOCTOR OF PHILOSOPHY

DEPARTMENT OF PHYSICS

BY
CAROLYN CHUCHU ZHANG

CHICAGO, ILLINOIS
JUNE 2023

To my parents, who have climbed both literal and figurative mountains for me.

TABLE OF CONTENTS

LIST OF FIGURES

ACKNOWLEDGMENTS

This PhD journey was made not only possible, but also truly enjoyable, by the amazing people who accompanied me along the way.

Michael has been one of the best parts of graduate school. Recently, after meeting with him to discuss some ideas, I couldn't help say, "I love talking physics with Michael so much!" Michael's patience with me helped me feel less afraid of asking questions and making mistakes. He always took my questions and ideas seriously, and explained things at a level I could understand. He was also generous with his time – there were so many instances where I knocked on his door and said, "Can I ask a quick question?" only to proceed to take up his entire afternoon.

Michael taught me to sit patiently with problems I care about, and to value the physical intuition behind mathematical statements. He also taught me that it takes time and deliberation to write a good paper or prepare a clear talk. I thank him for his thoughtful and thorough feedback on my talks and papers, even those on which he was not a coauthor. Working with Michael made doing physics a joy, and I view him as a role model for the kind of advisor I want to be in the future.

I've had the great fortune of working with two other excellent advisors earlier on in my PhD. Dave's enthusiasm and encouragement re-inspired me during a period of burn-out, and the community of Schusterlab felt like family during my first year in grad school. I thank Erez for helping me persevere through my first theory project in grad school, and for hosting me at Weizmann while folks in Chicago suffered through the polar vortex of winter 2019.

I'm also especially thankful for Clay, for the practical and moral support he gave me during my postdoc applications. He became not just a coauthor, but also a mentor. He contributed greatly to the collaborative culture at the Kadanoff center, and instigated many fun conversations at lunch, at the coffee machine, and in the hallways.

I'm grateful for my committee members, which include Son and Cheng in addition to

also thankful for my UQM community: Sal, Arkya, Marvin, Ethan, Patrick, Arpit, Hart, Brenden, Senthil, Ashvin, Xie, and John M, among others. I always look forward to the UQM meetings, especially the late night hotel lobby conversations. I'm thankful for other folks in physics that I've come to know over the years, including Tyler, Ho Tat, Sergio, Danny, Naren, Ruihua, Roman, Liujun, Zhuxi, Bowen, Wilbur, Ryan, Ruben, Abi, Ryohei, Rahul, Saran, Juven, Arthur, Dan B, Dan M, Henry, Zongping, Shuoguang, Zhiqiang, Nandu, Jukka, Max, Tarun, Peter, Leon, and Cameron. Thankfully, I get to meet them all somewhat regularly at conferences!

Outside of physics, I enjoyed living with Caroline and then with Janeen. I couldn't have asked for a better quarantine/ vacation/ triathlon/ prayer/ climbing/ gardening buddy than Caroline (and sometimes Ethan), and I'm thankful for Janeen's thoughtful listening, enthusiasm, and encouragement. I also thank the Vue53 doorman Ray, who brightens every morning. I thank my Avatar quarantine bubble Jair, Allen, and Jarret for bringing joy in a difficult time. I'm grateful to also have old friends Claudia, Lucy, Natalie, Barbara, and Julia, some of which also ended up in Chicago. I'm especially thankful for baby Grace; she has brought more joy to my life than she knows.

I thank my climbing coach Luca and fellow pupils Bruno and Davi, and other climbing partners James, John M, Sakina, Mac, Justin, and Jason for keeping me in climbing shape. I'm grateful for Adam, Brian, Trevor, John M, and Linnea for getting me out the door for morning runs even in the winter. I also thank my Mon night plank call crew, which includes some of the above together with Jair and Winnie.

I've been blessed by my graduate Christian fellowship community (shoutout to Brian, Ahn, Jair, Jenn, Kaleb, Joe, Lyndon, Adam, Susan, Caitlin, John H, Andrew W, Phillip, Irene, Jeremiah, Venezah, Hannah, Thao, Trevor, Chunny, Xiaoyang, Michaela, Andrew X, Ellen, Jun Yi, Olivia, and Clara); I've learned and grown so much through our conversations. I'm grateful for An, who began as my mentee, but become a close confidante and mountain

ABSTRACT

We present a collection of three short stories on the applications of simple toy models in different topics in condensed matter theory. These stories describe examples of new toy models and methods for solving them exactly, as well as limitations of certain kinds of toy models. The models we construct provide to a refined understanding of complex physical phenomena, by distilling the phenomena down to their minimal ingredients.

The first story describes an exactly solvable model for an unusual kind of phase transition called a deconfined quantum critical point (DQCP). While these kinds of quantum critical points have been hypothesized and intensely studied from field theory and numerical perspectives, their exact nature is still disputed. Our model provides the first example of a DQCP that can be solved exactly on the lattice, and gives a clear picture of the physical mechanism behind the transition. The second story presents a simple, exactly solvable model for a transition in the entanglement dynamics of a quantum system. Like DQCPs, entanglement transitions have been explored mainly through numerical work and field theory approximations, with very limited exact results. We present both the model and a novel means of solving it – by a mapping to Möbius transformations. The third story is about limitations of exactly solvable models. We show that, although these models can be constructed for broad classes of topological phases of matter, they cannot be constructed for certain phases – namely those with a nonzero Hall conductance.

CHAPTER 1

INTRODUCTION

1.1 Toy models in physics

Much of our understanding of condensed matter physics has come from simple toy models. Some examples of these models are:

- The Ising model[2, 3]

- The Haldane model[4], the Kitaev wire[5], and other free fermion models[6]

- The Haldane chain[7] and the AKLT model[8]

- The SYK model[9, 10]

- The toric code[11]

- The Kitaev honeycomb model[12]

- String-net models[13, 14] and generalizations[15, 16]

- Fracton stabilizer models, such as the Chamon model[17], the Haah models[18], the X-cube model[19], and others[20]

Simple toy models are powerful tools for demystifying complex theories and giving physical intuition for abstract mathematical concepts. They are particularly useful in the field of topological phases of matter, which connects deep mathematical results in topology and category theory to the physical world. This PhD thesis reviews some ways in which my collaborators and I used simple toy models to better understand aspects of three very different topics in condensed matter theory: quantum criticality, quantum dynamics, and topological phases. The toy models we study are so simple that they can be solved exactly, and capture the minimal ingredients for various interesting physical phenomena.

In the following, we will briefly discuss the three topics in condensed matter theory listed above, introducing along the way our new results. We will explore thse topics much more in depth in the following chapters.

1.2   Symmetries of phases of matter and how to break them

In the 1930s and 1940s, Lev Landau developed a paradigm for understanding phases of matter and transitions between them[21]. Within the Landau paradigm, phases are classified by their symmetries, and systems undergo "spontaneous symmetry breaking" phase transitions when their symmetry group is reduced to a subgroup. An example of such a transition is the liquid to solid transition. In this example, the liquid has a continuous translation symmetry because its particle density is uniform in space. On the other hand, a solid has a discrete translation symmetry due to its crystal lattice structure. The symmetry of the latter is a subgroup of the former, and the transition between these two phases is described by spontaneous symmetry breaking.

Transitions between different phases are particularly interesting when they are *continuous*[22]. In a continuous phase transition, the correlation length diverges, so microscopic details of the system are washed away. As a result, two entirely different systems can demonstrate precisely the same properties at criticality, a phenomenon known as universality. For example, the uni-axial magnet at its paramagnetic to ferromagnet transition and water at its critical point, where the difference between liquid and gas disappears, actually have identical critical properties.

Within the spontaneous symmetry breaking picture, it would seem unlikely to have a continuous transition between phases that have different symmetries. Specifically, this is the case where the symmetry group of one phase is not a subgroup of the symmetry group of the other. A priori, there is no reason for there to be a direct transition; such a transition may secretly be two spontaneous symmetry breaking transitions finely tuned to occur at the

same point. When the transition is indeed continuous and not finely tuned, the transition is known as a *deconfined quantum critical point*. Ch. 2 presents the first exactly solvable model for this kind of unusual quantum critical point.

1.3   Entanglement transitions: competition between scrambling and measurement

Sec. 1.2 discussed phases of stationary, time-independent systems. There are also interesting phases of dynamical systems, where the interactions between particles change in time and we also allow for observers to probe the quantum system via measurement[23, 24, 25, 26]. The dynamical phases we will focus on are distinguished by the entanglement of the steady state. Here, we will give some physical intuition for the result we will present from an information-theoretic perspective.

Suppose that we have a 1D chain of qubits and initialize the system in a quantum state. This quantum state encodes a message. For example, in a particularly simple kind of state known as a product state on a chain of N qubits, the state can be labeled by a binary string of length N such as $(0, 0, 1, 0, \ldots, 1)$ where each entry indicates the state of a qubit. If we now add interactions to the qubits, then the state will change over time, and the message of the initial state becomes "scrambled," or encrypted. If we also perform measurements on the system, we can extract information about the system, thereby removing information that was originally stored by the initial state. However, if there is sufficient scrambling, then the message gets encrypted well enough that small amounts of measurement do not destroy the message – the message can still be at least partially recovered.

The competition between scrambling and measurement leads to *measurement-induced phase transitions*, which are phase transitions in dynamical systems related to properties of the long-time steady-state, i.e. if that steady-state can still carries information about the initial message. Ch. 3 presents a simple model of such a phase transition, where we can

3

compute universal properties of the critical point exactly.

1.4   Topological phases and commuting projector Hamiltonians

Many phases are classified by their symmetries. However, more recently, it has been shown that phases with the same symmetries can still be distinct[1]. Such phases are known as *topological phases*[27, 6].

The integer quantum Hall effect is the prototypical example of a topological phase of matter in two dimensions[28]. In fact the experimental discovery of the quantum Hall phase marked the beginning of the study of topological phases of matter[29]. In a 2D slab, the bulk is a boring insulator, but the boundary can host dissipationless current. This dissipationless current is proportional to the Hall conductance, which is the topological invariant labeling the phase of matter.

There is a recipe for constructing exactly solvable models, called *commuting projector Hamiltonians*, for broad classes of topological phases[1, 14, 15, 16]. However, it was recently shown using abstract and highly nontrivial results in algebraic geometry that the integer quantum Hall phase, and in fact any topological phase with a nonzero Hall conductance, cannot be realized by a commuting projector Hamiltonian[30]. In Sec. 4, we prove this no-go theorem on exactly solvable models in a completely different, and more physically intuitive way.

---

1. To be clear, by symmetry in this context we mean refer to 0-form symmetries

CHAPTER 2

STORY 1: INTERTWINED SYMMETRIES AND UNUSUAL PHASE TRANSITIONS

2.1 Introduction: Deconfined quantum criticality

The notion of deconfined quantum criticality was introduced in Refs. [31, 32]. The paradigm of such a critical point, as explained in those original papers, describes the transition between a valence-bond solid (VBS) phase and a Néel antiferromagnet on a square lattice. The system has both an $SO(3)$ internal rotation symmetry and a C_4 lattice rotation symmetry due to the square lattice. In the VBS phase, neighboring spins pair into singlets, so the $SO(3)$ symmetry is respected but the C_4 lattice rotation symmetry is spontaneously broken. This results in four degenerate ground states. In the Néel phase, the C_4 rotation symmetry is respected but the $SO(3)$ symmetry is spontaneously broken. Therefore, a direct transition between the two phases would be a transition between phases that have different symmetries: C_4 is not a subgroup of $SO(3)$ and $SO(3)$ is not a subgroup of C_4.

One physical indication for a direct transition is in the structure of the C_4 vortices. If we start in the VBS phase, then we restore the C_4 symmetry by proliferating domain walls of the symmetry. The structure of the vortices, where four domain walls meet, show that the symmetries are intertwined: the vortices carry spin$-1/2$'s, i.e. spinons. Therefore, proliferating vortices also proliferates spinons, so restoring the C_4 symmetry results in spontaneously breaking the $SO(3)$ symmetry[1].

Initial numerical work agreed with the hypothesis of a direct, continuous phase transition[33, 34]. However, later work in numerics and conformal bootstrap led to growing evidence against a continuous phase transition[35, 36, 37, 38]. It is now believed that this transition is actually weakly first order rather than continuous.

Inspired by the picture of vortices of one symmetry carrying fractional charge of the other
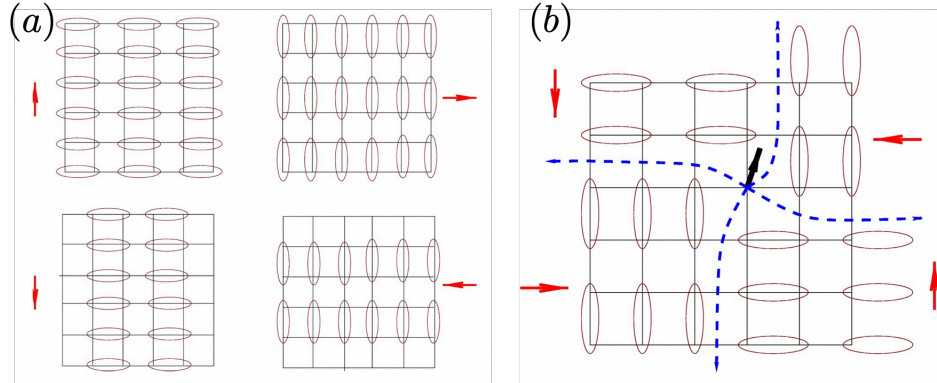
Figure 2.1: (a) The four degenerate ground states resulting from spontaneously breaking the C_4 rotation symmetry in the VBS phase. (b) Four C_4 domain walls form a vortex, which charries an uncompensated spin$-1/2$ moment. These figures are obtained from Ref. [1].

symmetry, we construct a model that implements a similar physical picture in a simpler setting. We obtain a model in 1D where the domain walls of one symmetry carry fractional charge of another symmetry. Using an exact mapping to a well-known spontaneous symmetry breaking transition, we show that indeed the DQCP in this case exists, and is exactly solvable on the lattice.

2.2 Exactly solvable model for a deconfined quantum critical point in 1D

This chapter is reprinted with permission from:

Carolyn Zhang and Michael Levin. Exactly solvable model for a deconfined quantum critical point in 1D. Phys. Rev. Lett. 130,026801, Jan 2023.

© 2020 American Physical Society

Abstract

We construct an exactly solvable lattice model for a deconfined quantum critical point (DQCP) in (1+1) dimensions. This DQCP occurs in an unusual setting, namely at the edge of a (2+1) dimensional bosonic symmetry protected topological phase (SPT) with $\mathbb{Z}_2 \times \mathbb{Z}_2$

symmetry. The DQCP describes a transition between two gapped edges that break different $\mathbb{Z}_2$ subgroups of the full $\mathbb{Z}_2 \times \mathbb{Z}_2$ symmetry. Our construction is based on an exact mapping between the SPT edge theory and a $\mathbb{Z}_4$ spin chain. This mapping reveals that DQCPs in this system are directly related to ordinary $\mathbb{Z}_4$ symmetry breaking critical points.

2.2.1   Introduction

Deconfined quantum critical points (DQCPs) describe unusual "Landau forbidden" phase transitions in which the unbroken symmetry group of one phase is not a subgroup of the unbroken symmetry group of the other phase[31, 32]. The paradigm of this kind of critical point is the hypothesized (2+1) dimensional DQCP between the valence bond solid (VBS) phase and the Néel phase on a square lattice. The VBS phase has internal $SO(3)$ rotation symmetry but spontaneously breaks C_4 lattice rotation symmetry, while the Néel phase has C_4 symmetry but breaks $SO(3)$ symmetry. Crucially, the two symmetries are intertwined: vortices of the C_4 symmetry carry uncompensated spin-1/2 moments[1]. As a result, disordering with respect to the C_4 symmetry can cause ordering under the $SO(3)$ symmetry, resulting in a hypothesized direct transition between the two phases.

Thus far, DQCPs have been studied primarily using field theory and numerical methods[33, 34]. One reason for this is the lack of analytically tractable lattice models for DQCPs. In this work, we take a step towards a more analytical microscopic approach, by constructing an *exactly solvable* lattice model for a (1+1) dimensional DQCP. The exact solvability of our model makes explicit the mechanism for the DQCP, which lies in the unusual structure of the domain walls. This DQCP has a similar field theory description to the (1+1) dimensional DQCP that was analyzed in Refs. [39, 40, 41] using bosonization (see also Ref. [42, 43]). However, our DQCP involves a different lattice realization with different (non-spatial) symmetries.

The key idea behind our solvable lattice model is to consider a DQCP in an unusual
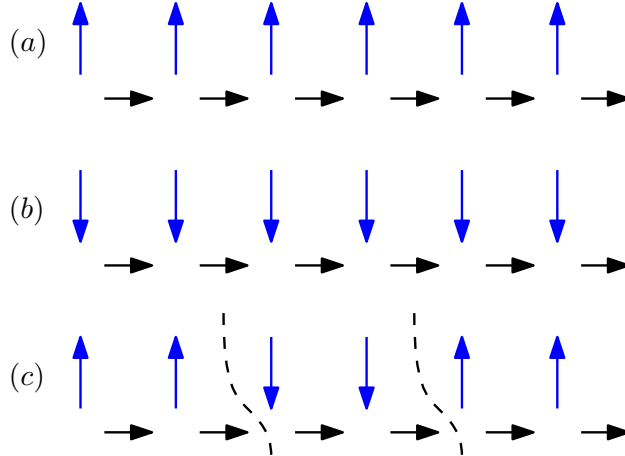
Figure 2.2: (a)-(b) The two degenerate ground states of the Hamiltonian (2.2) that spontaneously breaks $\mathbb{Z}_{2a}$. The blue arrows represent the σ_j spins and the black arrows represent the $\tau_{j+1/2}$ spins. Both states are eigenstates of U_b with eigenvalue $+1$. (c) Domain walls occur at the boundaries between these states. A state with two $\mathbb{Z}_{2a}$ domain walls (indicated by the dashed lines) has eigenvalue -1 under U_b, meaning two $\mathbb{Z}_{2a}$ domain walls fuse to a $\mathbb{Z}_{2b}$ charge.

setting – namely, at the *edge* of a (2+1) dimensional symmetry protected topological (SPT) phase. SPT edge theories provide a natural setting for DQCPs because they also have intertwined symmetries[44, 45]. In particular, an SPT with a "mixed anomaly" between two symmetries has an edge theory where domain walls of one symmetry carry fractional charge of the other symmetry[46, 47, 48]. Like in the VBS/Néel system, disordering with respect to one symmetry, by proliferating domain walls of that symmetry, may cause ordering with respect to the other symmetry, thereby realizing a DQCP.

We consider the simplest example of such an SPT edge theory: the edge theory of a 2D $\mathbb{Z}_2 \times \mathbb{Z}_2$ symmetric bosonic SPT with a mixed anomaly between the two $\mathbb{Z}_2$ symmetries. Using an exact mapping between the SPT edge theory and a $\mathbb{Z}_4$ spin chain, we rigorously establish the existence of a DQCP and derive the full critical theory.

2.2.2 $\mathbb{Z}_{2a} \times \mathbb{Z}_{2b}$ SPT edge theory

Our model for the SPT edge theory consists of a chain of spin-1/2's with two spins σ_j and $\tau_{j+1/2}$ in each unit cell, labeled by j. The two $\mathbb{Z}_2$ symmetries, denoted by $\mathbb{Z}_{2a}$ and $\mathbb{Z}_{2b}$, are generated by unitary operators U_a and U_b with

$$U_a = \prod_j \sigma_j^x \qquad U_b = \prod_j \tau_{j+1/2}^x i^{\frac{1-\sigma_j^z \sigma_{j+1}^z}{2}}. \tag{2.1}$$

Note that U_b does not act "on-site" in this representation: this is allowed since (2.1) describes the effective action of the symmetries on the *edge* degrees of freedom; in the original 2D spin system that describes the bulk SPT phase, both symmetries act onsite.

The above symmetry action (2.1) carries a mixed anomaly between the two symmetries. One manifestation of this mixed anomaly is that a pair of $\mathbb{Z}_{2a}$ domain walls is charged under $\mathbb{Z}_{2b}$. To see this, consider the Hamiltonian

$$H = -\sum_j \sigma_j^z \sigma_{j+1}^z - \sum_j \tau_{j+1/2}^x. \tag{2.2}$$

The two degenerate ground states of this Hamiltonian, which are illustrated in Fig. 3.1(a)-(b), spontaneously break $\mathbb{Z}_{2a}$. Now consider a state with two domain walls $|\psi_{2\mathrm{dw}}\rangle$, as shown in Fig. 3.1(c). From (2.1), we can see that such a state is actually charged under $\mathbb{Z}_{2b}$: $U_b|\psi_{2\mathrm{dw}}\rangle = -|\psi_{2\mathrm{dw}}\rangle$. Evidently, two $\mathbb{Z}_{2a}$ domain walls carry a $\mathbb{Z}_{2b}$ charge, so each domain wall can be associated with "half" a $\mathbb{Z}_{2b}$ charge.

Another way to think about this anomaly is in terms of the fusion rules for domain walls. There are actually four kinds of domain walls for this system if we distinguish between states that carry different quantum numbers under the unbroken $\mathbb{Z}_{2b}$ symmetry. These four kinds of domain walls are shown in Fig. 3.2: (1) a "no-domain wall" state; (2) a (bare) $\mathbb{Z}_{2a}$ domain wall; (3) a $\mathbb{Z}_{2b}$ charge; (4) a composite of a $\mathbb{Z}_{2a}$ domain wall and a $\mathbb{Z}_{2b}$ charge. The fact that

9
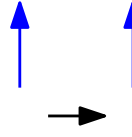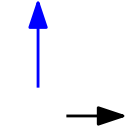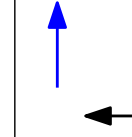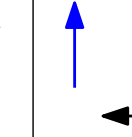
$C_j^\dagger C_{j+1}$	1	i	-1	$-i$
domain wall				

Figure 2.3: A mapping between the four kinds of domain walls in the SPT edge theory and the four kinds of domain walls in the $\mathbb{Z}_4$ spin chain, which are labeled by their eigenvalues $\{1, i, -1, -i\}$ under $C_j^\dagger C_{j+1}$. As discussed in the main text, two $\mathbb{Z}_{2a}$ domain walls (second configuration) fuse to a U_b charge, which is equivalent to a $\tau_{j+1/2}$ spin flip (third configuration).

two $\mathbb{Z}_{2a}$ domain walls fuse to a $\mathbb{Z}_{2b}$ charge means that the fusion rules for the domain walls have a $\mathbb{Z}_4$ group structure rather than the usual $\mathbb{Z}_2 \times \mathbb{Z}_2$ structure. This $\mathbb{Z}_4$ fusion structure points to a connection between our edge theory with an anomalous $\mathbb{Z}_{2a} \times \mathbb{Z}_{2b}$ symmetry given by (2.1) and an ordinary (non-anomalous) $\mathbb{Z}_4$ spin chain (this was also noted in Ref. [49]).

2.2.3 $\mathbb{Z}_4$ spin chain

The $\mathbb{Z}_4$ spin chain is a spin chain where each spin can be in four different states. The two basic operators acting on the jth spin are the "clock" operator C_j and the "shift" operator S_j. These operators take the following form (in the clock eigenstate basis):

$$C_j = \begin{pmatrix} 1 & 0 & 0 & 0 \\ 0 & i & 0 & 0 \\ 0 & 0 & -1 & 0 \\ 0 & 0 & 0 & -i \end{pmatrix} \qquad S_j = \begin{pmatrix} 0 & 0 & 0 & 1 \\ 1 & 0 & 0 & 0 \\ 0 & 1 & 0 & 0 \\ 0 & 0 & 1 & 0 \end{pmatrix}. \tag{2.3}$$

Note that C_j and S_j satisfy the algebra

$$C_j^4 = S_j^4 = \mathbb{1} \qquad C_j S_j = i S_j C_j. \tag{2.4}$$

In this paper, we will be interested in $\mathbb{Z}_4$ spin chains with a global $\mathbb{Z}_4$ symmetry given by $U_{\mathbb{Z}_4} = \prod_j S_j$. Such spin chains are closely related to the $\mathbb{Z}_2 \times \mathbb{Z}_2$ SPT edge theory described above. To see the relation, consider a symmetry breaking Hamiltonian of the form $H = -\sum_j \frac{1}{2}(C_j^\dagger C_{j+1} + C_{j+1}^\dagger C_j)$. This system has four degenerate ground states, and likewise four different species of domain walls. The different types of domain walls can be conveniently labeled by fourth roots of unity, $\{1, i, -1, -i\}$; the label associated with each domain wall is given by $C_j^\dagger C_{j+1}$ (assuming the domain wall is located between spins at sites j and $j + 1$). The crucial point is that these domain walls obey $\mathbb{Z}_4$ fusion rules just like the domain walls for the $\mathbb{Z}_2 \times \mathbb{Z}_2$ SPT edge theory, suggesting that there may be a way to map one system onto the other.

2.2.4 Mapping between the models

We will now map the Hilbert space of the $\mathbb{Z}_2 \times \mathbb{Z}_2$ SPT edge theory onto the Hilbert space of the $\mathbb{Z}_4$ spin chain.

As we mentioned earlier, the basic idea is to map the four kinds of domain walls in the $\mathbb{Z}_4$ spin chain onto the four kinds of domain walls in the SPT edge theory. To do this, we need to map the spin chain operator $C_j^\dagger C_{j+1}$ (which measures $\mathbb{Z}_4$ domain walls) onto a corresponding domain wall operator in the SPT edge theory. The latter operator should have the four domain wall configurations in Fig. 3.2 as eigenstates, with eigenvalues $1, i, -1$, and $-i$. It should also be invariant under the $\mathbb{Z}_2 \times \mathbb{Z}_2$ symmetry, since we want our mapping to map $\mathbb{Z}_4$ symmetric operators in the spin chain (like $C_j^\dagger C_{j+1}$) onto $\mathbb{Z}_2 \times \mathbb{Z}_2$ symmetric operators in the SPT edge theory. These requirements are satisfied by the operator $\tau_{j+1/2}^x i^{(1-\sigma_j^z \sigma_{j+1}^z)/2}$, so we map

$$C_j^\dagger C_{j+1} \leftrightarrow \tau_{j+1/2}^x i^{(1-\sigma_j^z \sigma_{j+1}^z)/2}. \tag{2.5}$$

In addition to $C_j^\dagger C_{j+1}$, we also need to work out how our mapping acts on the shift

11
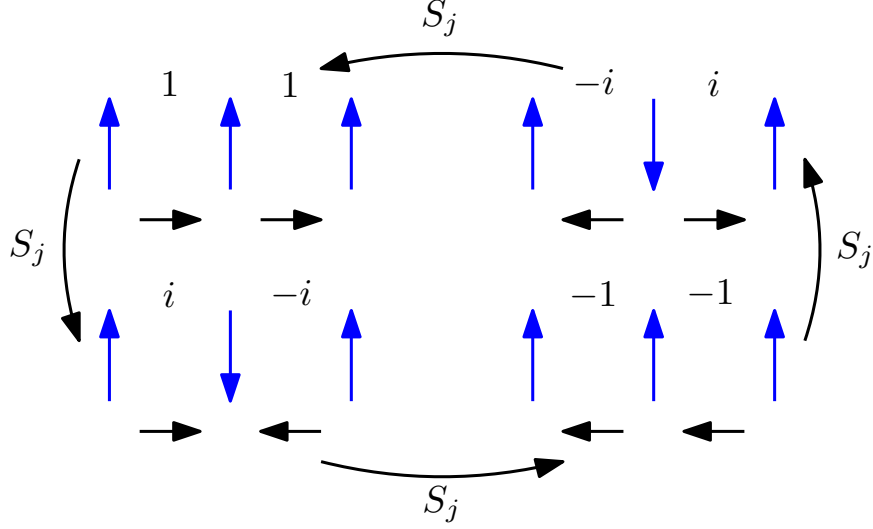
Figure 2.4: The action of S_j on domain wall states in the SPT edge theory: S_j shifts the domain wall measured by $C_{j-1}^\dagger C_j$ by i and the domain wall measured by $C_j^\dagger C_{j+1}$ by $-i$. Here, j labels the spin in the middle of each 5-spin configuration.

operator S_j. To do this, notice that S_j shifts the domain wall measured by $C_{j-1}^\dagger C_j$ by i and the domain wall measured by $C_j^\dagger C_{j+1}$ by $-i$. This means that S_j should map to an operator whose action on SPT domain wall states is of the form shown in Fig. 2.4. Another requirement is that S_j should map onto an operator that is invariant under the $\mathbb{Z}_2 \times \mathbb{Z}_2$ symmetry. These two requirements lead us to the mapping

$$
\begin{aligned}
S_j \leftrightarrow \sigma_j^x & \left[\left(\frac{1 + \sigma_{j-1}^z \sigma_j^z}{2} \right) + \left(\frac{1 - \sigma_{j-1}^z \sigma_j^z}{2} \right) \tau_{j-1/2}^z \right] \\
& \times \left[\left(\frac{1 + \sigma_j^z \sigma_{j+1}^z}{2} \right) \tau_{j+1/2}^z + \left(\frac{1 - \sigma_j^z \sigma_{j+1}^z}{2} \right) \right].
\end{aligned}
\tag{2.6}
$$

Eqs. (2.5-2.6) define a mapping between local $\mathbb{Z}_4$ symmetric operators in the spin chain and local $\mathbb{Z}_2 \times \mathbb{Z}_2$ symmetric operators in the SPT edge theory. To understand the *global* properties of this mapping, we note that straightforward algebra shows that

$$
\prod_j S_j \leftrightarrow U_a \qquad \prod_j C_j^\dagger C_{j+1} \leftrightarrow U_b.
\tag{2.7}
$$

12

These equations tell us how the various symmetry sectors map onto one another. In particular, we see that the two sectors of the SPT edge theory with $U_a = \pm 1$ and $U_b = 1$ map onto the two spin chain sectors with $\prod_j S_j = \pm 1$, and with *periodic* boundary conditions. On the other hand, the two SPT sectors with $U_a = \pm 1$ and $U_b = -1$ map onto spin chain sectors with $\prod_j S_j = \pm 1$ and *anti-periodic* boundary conditions. Here, the anti-periodic boundary condition can be implemented, on a closed loop of N sites, by using $C_{N+1} = -C_1$ instead of $C_{N+1} = C_1$ (which corresponds to the periodic case). Putting this all together, we see that the Hilbert space of the SPT edge theory maps onto the Hilbert space of the $\mathbb{Z}_4$ spin chain with a particular combination of sectors, namely the two symmetry sectors $\prod_j S_j = \pm 1$, with either periodic or anti-periodic boundary conditions.

Alternatively, one can think of this particular combination of sectors as describing a $\mathbb{Z}_4$ spin chain coupled to a $\mathbb{Z}_2$ gauge field $\{\nu_{j+1/2}\}$ with the gauge constraint $\nu^x_{j-1/2}\nu^x_{j+1/2} = S_j^2$. In the gauged spin chain, the two boundary conditions correspond to sectors with even and odd $\mathbb{Z}_2$ gauge flux, while the global constraint $\prod_j S_j = \pm 1$ is imposed by gauge invariance. In this paper, we will mostly work with the explicit sector description rather than the gauged spin chain language, but the latter is a completely equivalent way to think about our mapping.

2.2.5   Using the mapping

We will now use the mapping to understand the phases and phase transitions of the SPT edge theory. We start with the $\mathbb{Z}_4$ spin chain, which is expected to support three different gapped phases: an ordered phase where the $\mathbb{Z}_4$ symmetry is spontaneously broken, a disordered phase where the symmetry is unbroken, and a partially ordered phase where the $\mathbb{Z}_4$ symmetry is broken down to $\mathbb{Z}_2$[50]. We can diagnose each of these phases in terms of an order parameter

O, and a disorder parameter D defined as follows[1]:

$$O = \lim_{|i-j|\to\infty} \langle C_i^\dagger C_j \rangle \quad D = \lim_{|i-j|\to\infty} \left\langle \prod_{k=i}^{j} S_k \right\rangle.$$ (2.8)

Each phase has a different pattern of order and disorder parameters:

$$\text{Ordered phase}: \quad O \neq 0, \quad D = 0$$

$$\text{Disordered phase}: \quad O = 0, \quad D \neq 0$$

$$\text{Partially ordered phase}: \quad O = 0, \quad D = 0.$$ (2.9)

Now, according to (2.7), our mapping takes the order parameter O for the $\mathbb{Z}_4$ spin chain onto the symmetry transformation U_b restricted to an interval, which is, by definition, a disorder parameter for $\mathbb{Z}_{2b}$. Likewise, our mapping takes the $\mathbb{Z}_4$ disorder parameter D to a $\mathbb{Z}_{2a}$ disorder parameter. It follows that the ordered phase of the spin chain corresponds to a phase of the SPT edge theory with a vanishing $\mathbb{Z}_{2a}$ disorder parameter and a nonvanishing $\mathbb{Z}_{2b}$ disorder parameter – i.e. a phase with broken $\mathbb{Z}_{2a}$ symmetry and unbroken $\mathbb{Z}_{2b}$ symmetry. By the same reasoning, the disordered phase of the spin chain maps onto a phase with unbroken $\mathbb{Z}_{2a}$ symmetry and broken $\mathbb{Z}_{2b}$ symmetry. Finally, the partially ordered phase of the spin chain maps onto a phase where both $\mathbb{Z}_{2a}$ and $\mathbb{Z}_{2b}$ are broken.

The most important application of these results, for our purposes, involves phase *transitions*. In particular, consider a hypothetical critical point between the $\mathbb{Z}_{2a}$ broken ($\mathbb{Z}_{2b}$ unbroken) phase, and its partner, the $\mathbb{Z}_{2b}$ broken ($\mathbb{Z}_{2a}$ unbroken) phase. Applying our mapping, such critical points correspond to critical points between the ordered and disordered phase of the $\mathbb{Z}_4$ spin chain. This means that the problem of understanding DQCPs in the context of the SPT edge theory maps onto the problem of understanding ordinary symmetry

---

1. By some conventions, "order parameter" refers to the operator C_j. Here, we mean the two-point correlation function in (2.8), which is nonzero in the ordered phase and zero in the disordered phase.

breaking critical points for the $\mathbb{Z}_4$ spin chain. Since the latter critical points are known to exist and are well-understood, this proves the existence of DQCPs and also allows us deduce their structure.

2.2.6 Exactly solvable model

More concretely, we can use our mapping to construct an exactly solvable Hamiltonian that describes a continuous phase transition between the $\mathbb{Z}_{2a}$ broken ($\mathbb{Z}_{2b}$ unbroken) phase, and the $\mathbb{Z}_{2b}$ broken ($\mathbb{Z}_{2a}$ unbroken) phase of the SPT edge theory and therefore describes a DQCP. To build such a Hamiltonian, we start with an exactly solvable spin chain Hamiltonian that describes a $\mathbb{Z}_4$ symmetry breaking transition. In particular, we use the $\mathbb{Z}_4$ clock model:

$$H_{\text{clock}}(\alpha) = -(1-\alpha)\sum_j \frac{1}{2}\left(C_j^\dagger C_{j+1} + C_{j+1}^\dagger C_j\right) - \alpha\sum_j \frac{1}{2}\left(S_j + S_j^\dagger\right). \qquad (2.10)$$

Later, we will review how to solve H_{clock} exactly; for now, the only property we need is that H_{clock} belongs to the $\mathbb{Z}_4$ ordered phase for $\alpha < \frac{1}{2}$ and the disordered phase for $\alpha > \frac{1}{2}$, with a direct transition at $\alpha = \frac{1}{2}$.

To apply our mapping, we write

$$H_{\text{clock}}(\alpha) = (1-\alpha)H_{\text{a,clock}} + \alpha H_{\text{b,clock}}, \qquad (2.11)$$

where $H_{\text{a,clock}}$ and $H_{\text{b,clock}}$ describe the two sets of terms in (2.10). Notice that $H_{\text{a,clock}}$ and $H_{\text{b,clock}}$ are both sums of commuting terms. Furthermore, one can see that $H_{\text{a,clock}}$ and $H_{\text{b,clock}}$ belong to the ordered and disordered phases, respectively. Hence, applying our mapping to $H_{\text{a,clock}}$ gives a commuting Hamiltonian describing the $\mathbb{Z}_{2a}$ broken ($\mathbb{Z}_{2b}$

unbroken) phase of the SPT edge theory:[2]

$$H_a = -\sum_j \left(\frac{1 + \sigma_j^z \sigma_{j+1}^z}{2} \right) \tau_{j+1/2}^x. \tag{2.12}$$

Similarly, applying our mapping to $H_{b,\text{clock}}$, gives a commuting Hamiltonian for the $\mathbb{Z}_{2b}$ broken ($\mathbb{Z}_{2a}$ unbroken) phase:

$$H_b = -\sum_j \left[\sigma_j^x \left(\frac{1 + \sigma_{j-1}^z \sigma_{j+1}^z}{2} \right) \left(\frac{\tau_{j-1/2}^z + \tau_{j+1/2}^z}{2} \right) \right. \tag{2.13}$$
$$\left. + \sigma_j^x \left(\frac{1 - \sigma_{j-1}^z \sigma_{j+1}^z}{2} \right) \left(\frac{1 + \tau_{j-1/2}^z \tau_{j+1/2}^z}{2} \right) \right].$$

Our exactly solvable model that tunes between these two symmetry breaking phases is given by

$$H(\alpha) = (1 - \alpha) H_a + \alpha H_b. \tag{2.14}$$

Like H_{clock}, this Hamiltonian describes a direct transition between the two phases (and hence a DQCP) at $\alpha = \frac{1}{2}$.

2.2.7   Exactly solvable critical point

We now review how to solve the $\mathbb{Z}_4$ clock model $H_{\text{clock}}(\alpha)$ (2.10) and hence also $H(\alpha)$. The basic idea is to map H_{clock} onto two decoupled transverse field Ising models which undergo simultaneous symmetry breaking transitions. To do this, we map each four dimensional spin onto two spin-1/2 degrees of freedom, denoted by μ_j and ρ_j (note that μ_j and ρ_j should not be confused with σ_j and $\tau_{j+1/2}$). We then write

$$C_j = \frac{e^{-i\pi/4}}{\sqrt{2}} \left(\mu_j^z + i\rho_j^z \right) \tag{2.15}$$

---

2. Note that this Hamiltonian is not exactly the same as the Hamiltonian written under Eq. 2.1, whose ground states also spontaneously break U_a.

and

$$S_j = \mu_j^x \left(\frac{1 + \mu_j^z \rho_j^z}{2} \right) + \rho_j^x \left(\frac{1 - \mu_j^z \rho_j^z}{2} \right). \tag{2.16}$$

Using (2.15) and (2.16), we compute

$$C_j^\dagger C_{j+1} + C_{j+1}^\dagger C_j = \mu_j^z \mu_{j+1}^z + \rho_j^z \rho_{j+1}^z$$

$$S_j + S_j^\dagger = \mu_j^x + \rho_j^x. \tag{2.17}$$

Applying this map to the $\mathbb{Z}_4$ clock model in Eq. 2.10 gives

$$
\begin{aligned}
H_{\text{clock}} = -(1-\alpha) \sum_j \frac{1}{2} \left(\mu_j^z \mu_{j+1}^z + \rho_j^z \rho_{j+1}^z \right) \\
- \alpha \sum_j \frac{1}{2} \left(\mu_j^x + \rho_j^x \right),
\end{aligned}
\tag{2.18}
$$

which recovers the well-known fact that the $\mathbb{Z}_4$ clock model is unitarily equivalent to two decoupled transverse field Ising models.

This mapping implies that the DQCP that occurs at $\alpha = 1/2$ is equivalent to two copies of the critical Ising theory[51]. More precisely, the DQCP is equivalent to a particular combination of *sectors* of the Ising theory: translating the sectors $\prod_j S_j = \pm 1$ and $C_{N+1} = \pm C_1$ into the Ising language, we see that $H(\alpha)$ is described by the symmetry sector $\prod_j \mu_j^x \rho_j^x = 1$, with the same (periodic or anti-periodic) boundary conditions in both μ, ρ, i.e. $\mu_{N+1}^z = \pm \mu_1^z$ and $\rho_{N+1}^z = \pm \rho_1^z$.[3]

Using this mapping we can obtain all the critical exponents of the DQCP. For example, the correlation length ξ near the critical point diverges as $\xi \sim \frac{1}{|\alpha - \frac{1}{2}|^\nu}$ with $\nu = 1$. Also, the

---

3. To see that $\prod_j S_j = \pm 1$ translates to $\prod_j \mu_j^x \rho_j^x = 1$, notice that $S_j^2 = \mu_j^x \rho_j^x$ according to (2.16). Since $\prod_j S_j = \pm 1$, $\prod_j S_j^2 = \prod_j \mu_j^x \rho_j^x = 1$. The fact that the two Ising models must have the same boundary condition follows directly from $C_{N+1} = \pm C_1$, using the definition of C_j in (2.15).

two-point correlators for the $\mathbb{Z}_{2a}$ and $\mathbb{Z}_{2b}$ order parameters σ^z and τ^z are given by

$$\langle \sigma_i^z \sigma_j^z \rangle \sim \frac{1}{|i-j|^{1/2}} \qquad \langle \tau_{i+1/2}^z \tau_{j+1/2}^z \rangle \sim \frac{1}{|i-j|^{1/2}}. \tag{2.19}$$

Is the above DQCP stable to perturbations? The answer to this question depends on what additional symmetries we impose beyond $\mathbb{Z}_{2a} \times \mathbb{Z}_{2b}$. For example, suppose we impose both time reversal and parity symmetry. In this case, it is well known that the critical point of the $\mathbb{Z}_4$ clock model does not have any relevant symmetric operators beyond the tuning parameter α, but it does have a marginal operator corresponding to $\lambda \sum_j (C_j^2 C_{j+1}^2 + S_j^2)$. Adding this operator moves the system along a critical line[50, 52, 53]. Therefore the DQCP that we described above is actually part of deconfined quantum critical *line* with continuously varying exponents (see the Sec. 2.3 for more details). On the other hand, if we don't impose additional symmetries, then the critical point has other relevant symmetric operators that drive the system into a gapless phase, destroying the direct transition. These are known as "chiral perturbations," and are given by $\lambda_\varphi \sum_j \left(C_j^\dagger C_{j+1} e^{i\varphi} + h.c. \right)$ and $\lambda_\vartheta \sum_j \left(S_j e^{i\vartheta} + h.c. \right)$[54, 55, 56, 57]. More generally, if we consider the whole critical line, there is a region (i.e. a range of λ) where the chiral perturbations are irrelevant[52, 54, 55, 56] (see also Sec. 2.3). In this region, time reversal symmetry and parity symmetry are not required to stabilize the transition.

2.2.8   Self-duality at criticality

An interesting aspect of the above DQCP is that it is *self-dual*: there is a duality transformation that maps the critical point to itself and exchanges the $\mathbb{Z}_{2a}$ and $\mathbb{Z}_{2b}$ order parameters in (2.19). This self-duality is reminiscent of the self-duality that occurs in other DQCPs, such as in the XY antiferromagnet/VBS transition obtained from adding easy-plane spin anisotropy to the Néel/VBS theory[31, 32, 58].

The duality transformation – denoted by U_c – is easiest to understand in terms of the $\mathbb{Z}_4$ spin chain variables: in this description, U_c maps $C_j^\dagger C_{j+1}$ onto S_{j+1} and maps S_j onto $C_j^\dagger C_{j+1}$. This is similar to the Kramers-Wannier duality, but unlike standard Kramers-Wannier duality, U_c is both (1) unitary and (2) locality preserving, in the sense that it maps local operators to local operators. These properties are due to the unusual sector structure in our $\mathbb{Z}_4$ spin chain, or equivalently the fact that the $\mathbb{Z}_4$ spin chain is coupled to a $\mathbb{Z}_2$ gauge field (see the Sec. 2.3 for more details). One consequence of the unitarity and locality of U_c is that U_c can also be viewed as an ordinary symmetry, rather than a duality.

2.2.9 Discussion

As emphasized above, at the core of our construction is the mapping between the $\mathbb{Z}_2 \times \mathbb{Z}_2$ SPT edge theory and the $\mathbb{Z}_4$ spin chain (2.5-2.6). This mapping can be readily generalized to any $\mathbb{Z}_{N_1} \times \mathbb{Z}_{N_2}$ SPT edge theory with a primitive[4] mixed anomaly. Specifically, any edge theory of this kind can be mapped onto a $\mathbb{Z}_{N_1 N_2}$ spin chain in such a way that the Landau forbidden transition in the edge theory maps onto an ordinary symmetry breaking transition in the spin chain.

Moving forward, it would be interesting to find examples of these mappings for other kinds of anomalies, such as "type-III anomalies"[48, 47], or for non-Abelian symmetry groups. Examples of this kind could give solvable DQCPs with richer structure. It would also be interesting to generalize to higher dimensional systems, though this is not straightforward since our construction relies on charges and domain walls having the same dimensionality, as shown in Fig. 3.2.

Another interesting generalization is to add disorder to our model, by drawing the coefficients of the terms in $H_{a,\text{clock}}$ and $H_{b,\text{clock}}$ from random distributions. It was shown in Refs. [60, 61, 62] that strongly disordered $\mathbb{Z}_N$ clock models have continuous transitions with

---

4. By "primitive" we mean that the topological invariant $e^{i\Theta_{12}}$ defined in Ref. [59] is a primitive dth root of unity where $d = \gcd(N_1, N_2)$.

critical properties that can be obtained exactly using a renormalization group analysis. In the corresponding SPT edge theory, this kind of model would give an example of a *disordered* DQCP.

2.2.10 Acknowledgements

2.3   Supplemental Material

2.3.1 Field theory description of deconfined quantum critical line

In this section, we present a field-theoretic description of the deconfined quantum critical line that separates the two symmetry breaking phases of the SPT edge theory. The exactly solvable DQCP presented in the main text corresponds to a particular point along this line, as we explain below.

We begin with a field theory description of the SPT edge theory. This field theory consists of two bosonic fields θ, ϕ with the commutation relation

$$\big[\theta(x'), \partial_x \phi(x)\big] = 2\pi i \delta(x - x'), \tag{2.20}$$

where the fundamental local operators in the SPT edge theory are $e^{\pm i\theta}, e^{\pm i\phi}$. The $\mathbb{Z}_{2a} \times \mathbb{Z}_{2b}$

symmetries act on θ and ϕ as follows:

$$U_a : \phi \to \phi + \pi \qquad \theta \to \theta$$
$$U_b : \phi \to \phi \qquad \theta \to \theta + \pi. \tag{2.21}$$

(To see that Eq. (2.21) describes the desired mixed anomaly between $\mathbb{Z}_{2a}$ and $\mathbb{Z}_{2b}$, observe that the symmetry actions U_a and U_b are not anomalous as individual $\mathbb{Z}_2$ symmetries, while the product $U_b \cdot U_a$ *is* anomalous[63, 45]. This also holds for the lattice model in the main text and is characteristic of the mixed anomaly for $\mathbb{Z}_{2a} \times \mathbb{Z}_{2b}$).

Next, observe that we can realize the $\mathbb{Z}_{2a}$ broken ($\mathbb{Z}_{2b}$ unbroken) phase of the SPT edge theory with the following edge Hamiltonian:

$$\mathcal{H} = \frac{1}{8\pi} \left[K \left(\partial_x \theta \right)^2 + \frac{4}{K} \left(\partial_x \phi \right)^2 \right] + A_\phi \cos(2\phi), \tag{2.22}$$

Here, K is the Luttinger parameter, A_ϕ is a real coefficient, and we work in units where the edge velocity v is set to $v = 1$. The above Hamiltonian breaks the $\mathbb{Z}_{2a}$ symmetry spontaneously in a regime where the term $A_\phi \cos(2\phi)$ is relevant. In this case, ϕ becomes fixed to one of the two minima of the cosine potential leading to an expectation value for $e^{i\phi}$, which is odd under U_a. Likewise, we can realize the $\mathbb{Z}_{2b}$ broken ($\mathbb{Z}_{2a}$ unbroken) phase using the edge Hamiltonian

$$\mathcal{H} = \frac{1}{8\pi} \left[K \left(\partial_x \theta \right)^2 + \frac{4}{K} \left(\partial_x \phi \right)^2 \right] + A_\theta \cos(2\theta), \tag{2.23}$$

As before, if we are in regime where $A_\theta \cos(2\theta)$ is relevant, then $e^{i\theta}$ acquires an expectation value, spontaneously breaking the $\mathbb{Z}_{2b}$ symmetry.

The above considerations suggest a natural field theory for the deconfined quantum crit-
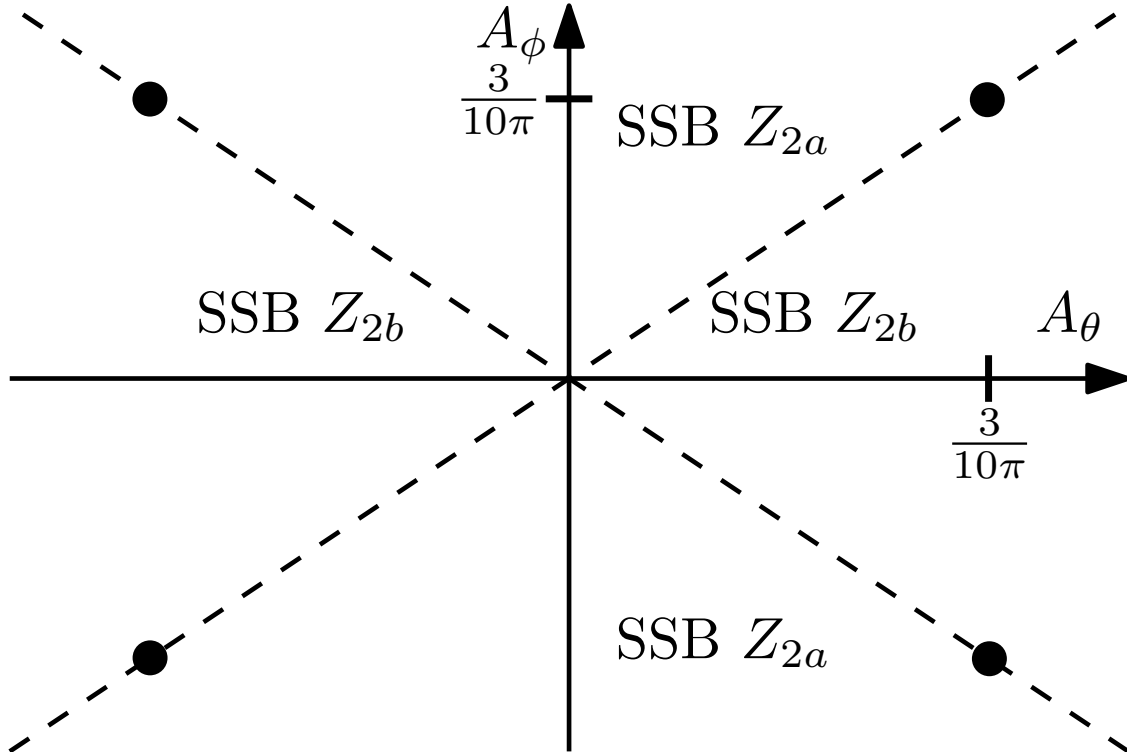
Figure 2.5: Phase diagram for the Hamiltonian in (2.24) for $K = 2$. The dotted lines are critical lines, with continuously varying exponents. The black dots at $(A_\theta, A_\phi) = \left(\pm\frac{3}{10\pi}, \pm\frac{3}{10\pi}\right)$ indicate points along the critical lines described by the exactly solvable critical points from the main text.

ical line separating the two symmetry breaking phases:

$$\mathcal{H} = \frac{1}{8\pi}\left[K\left(\partial_x\theta\right)^2 + \frac{4}{K}\left(\partial_x\phi\right)^2\right] + A_\theta\cos(2\theta) + A_\phi\cos(2\phi), \tag{2.24}$$

Only one of the two cosine operators is relevant for a given value of K: the scaling dimension of $\cos(2\phi)$ is K while the scaling dimension of $\cos(2\theta)$ is $\frac{4}{K}$. Therefore, $\cos(2\phi)$ is relevant for $K < 2$ and $\cos(2\theta)$ is relevant for $K > 2$. At $K = 2$, both cosines are marginal. For this value of K, the two marginal operators $\cos(2\phi)$ and $\cos(2\theta)$ compete, and the fate of the theory depends on the magnitudes of the coefficients A_ϕ, A_θ (see Fig. 2.5). In particular, if $|A_\phi| > |A_\theta|$ then the $\mathbb{Z}_{2a}$ symmetry is spontaneously broken, while if $|A_\phi| < |A_\theta|$ then the $\mathbb{Z}_{2b}$ symmetry is spontaneously broken. The deconfined quantum critical line(s) occur when

$A_\phi = \pm A_\theta$.

A few comments about (2.24): first, we note that the field theory (2.24) has been used in various contexts in the literature (see e.g. Ref [53] and references therein), and is similar to the field theory of the 1D DQCP discussed in Ref. [39]. We also note that if we define $\theta' = 2\theta$ and $\phi' = \phi/2$, the resulting field theory for θ' and ϕ' is precisely the field theory that describes the $\mathbb{Z}_4$ spontaneous symmetry breaking critical line[64]. This mapping to the $\mathbb{Z}_4$ symmetry breaking transition is the field theory analog of the lattice mapping discussed in the main text.

We now review how to derive the properties of the critical lines with $A_\phi = \pm A_\theta$. To do this, we fix $K = 2$ and reparameterize the two cosines in (2.24) in symmetric and anti-symmetric combinations:

$$A_\theta \cos(2\theta) + A_\phi \cos(2\phi) = g_+[\cos(2\theta) + \cos(2\phi)]$$
$$+ g_-[\cos(2\theta) - \cos(2\phi)] \tag{2.25}$$

The critical lines occur when either $g_+ = 0$ or $g_- = 0$. For concreteness, consider the critical line with $g_- = 0$. The key to analyzing this line is to utilize the hidden $SU(2)$ symmetry in this model. In particular, there exists an $SU(2)$ rotation that maps

$$\cos(2\theta) + \cos(2\phi) \rightarrow \frac{1}{2}[(\partial_x\theta)^2 - (\partial_x\phi)^2] \tag{2.26}$$

and leaves $\cos(2\theta) - \cos(2\phi)$ and $(\partial_x\theta)^2 + (\partial_x\phi)^2$ invariant. After this (unitary) $SU(2)$ transformation, our Hamiltonian becomes

$$\mathcal{H} \rightarrow \frac{\tilde{v}}{8\pi}\left[\tilde{K}\,(\partial_x\theta)^2 + \frac{4}{\tilde{K}}\,(\partial_x\phi)^2\right]$$
$$+ g_-[\cos(2\theta) - \cos(2\phi)] \tag{2.27}$$

23

where

$$\tilde{K}^2 = 4\frac{1 + 2\pi g_+}{1 - 2\pi g_+} \qquad \tilde{v}^2 = 1 - 4\pi^2 g_+^2. \tag{2.28}$$

Crucially, along the critical line $g_- = 0$, the $SU(2)$ rotated Hamiltonian (2.27) is *Gaussian*. As a result, critical exponents can be computed straightforwardly. These critical exponents vary continuously along the critical line due to the continuously varying Luttinger parameter $\tilde{K}$.

To complete this discussion, we now work out which point(s) along these critical lines correspond to the exactly solvable lattice model given in Eq. 15. To this end, recall that in the main text, we mapped our solvable lattice model onto two decoupled Ising models. This mapping implies that the operator that drives the transition is the sum of the energy fields of the two Ising models, which has a scaling dimension 1. In comparison, in the field theory (2.27), the operator that drives the transition is $[\cos(2\theta) - \cos(2\phi)]$ which has a scaling dimension of $\min(\frac{4}{\tilde{K}}, \tilde{K})$ (since the scaling dimensions of $\cos(2\theta)$ and $\cos(2\phi)$ are $\frac{4}{\tilde{K}}$ and $\tilde{K}$, respectively). Setting $\frac{4}{\tilde{K}} = 1$ and $\tilde{K} = 1$, we see that our exactly solvable lattice model corresponds to the two points $g_+ = \pm\frac{3}{10\pi}$ for the critical line with $g_- = 0$. Similarly, along the other critical line with $g_+ = 0$, the solvable model corresponds to the two points with $g_- = \pm\frac{3}{10\pi}$. These points are marked in the phase diagram shown in Fig. 2.5.

2.3.2 Chiral perturbations

In the main text, we mentioned that, if we don't impose time reversal and parity symmetry, then there exist chiral perturbations that can destroy our exactly solvable DQCP and drive the system into a gapless phase. In this section, we analyze these chiral perturbations using the field theory (2.24) and we identify the regions of the critical lines where these perturbations are relevant/irrelevant. In the regions where they are relevant (such as in our exactly solvable lattice model), we need time reversal and parity symmetry to stabilize the direct transition, while in the regions where they are irrelevant, we do not need any

24

additional symmetries.

In the field theory (2.24), the chiral perturbations correspond to $\partial_x \phi$ and $\partial_x \theta$. Note that these operators are invariant under U_a and U_b, but they break either time reversal or parity symmetry, if we define

$$
\begin{aligned}
T : \phi \to \phi \qquad \theta \to -\theta \\
P : \phi \to -\phi \qquad \theta \to \theta
\end{aligned}
\tag{2.29}
$$

To determine when the chiral perturbations are relevant and when they are not, we must perform the same $SU(2)$ transformation as we described in the previous section on these operators. It is easiest to first take linear combinations of the two chiral perturbations, given by $\partial_x(\phi + \theta)$ and $\partial_x(\phi - \theta)$. The $SU(2)$ rotation maps $\partial_x(\phi + \theta)$ and $\partial_x(\phi - \theta)$ to $\cos(\phi + \theta)$ and $\cos(\phi - \theta)$ respectively. The scaling dimension of $\cos(\phi + \theta)$ and $\cos(\phi - \theta)$, which we call Δ_c, is given by

$$
\Delta_c = \frac{1}{\tilde{K}} + \frac{\tilde{K}}{4}
\tag{2.30}
$$

The chiral perturbation is relevant when $\Delta_c < 2$, which corresponds to

$$
(4 - 2\sqrt{3}) < \tilde{K} < (4 + 2\sqrt{3})
\tag{2.31}
$$

In this range, we must require time reversal symmetry and parity symmetry in order to exclude these perturbations and stabilize the direct transition. Outside of this range, the chiral perturbations are irrelevant, so we do not need to impose these extra symmetries.

2.3.3   Duality transformation

In this section, we explain how the duality transformation U_c (which is also a unitary symmetry) acts on the different operators in the SPT edge theory. Our strategy will be to first work out how U_c acts on the operators in the $\mathbb{Z}_4$ spin chain; we will then translate this over

to the SPT edge theory.

To understand how U_c acts on the $\mathbb{Z}_4$ spin chain variables, it is convenient to use the gauge theory language where we think of the $\mathbb{Z}_4$ spin chain as coupled to a $\mathbb{Z}_2$ gauge field. As we mentioned in the main text, the gauge theory language is an alternative way to describe the sector structure of the $\mathbb{Z}_4$ spin chain. To use the gauge theory language, we introduce a $\mathbb{Z}_2$ gauge field $\{\nu_{j+1/2}\}$ on the links of the lattice, and we impose the gauge constraint $\nu^x_{j-1/2}\nu^x_{j+1/2} = S^2_j$. The local gauge invariant operators in the $\mathbb{Z}_4$ spin chain are $\{C^\dagger_j \nu^z_{j+1/2} C_{j+1}, S_j, C^2_j, \nu^x_{j+1/2}\}$. All other gauge invariant operators can be built from these operators, so it suffices to understand how U_c acts on these operators.

The action of the duality transformation U_c on the first two operators, $\{C^\dagger_j \nu^z_{j+1/2} C_{j+1}, S_j\}$ is similar to standard Kramers-Wannier duality:

$$
\begin{aligned}
U^\dagger_c C^\dagger_j \nu^z_{j+1/2} C_{j+1} U_c &= S_{j+1} \\
U^\dagger_c S_j U_c &= C^\dagger_j \nu^z_{j+1/2} C_{j+1}.
\end{aligned}
\tag{2.32}
$$

To figure out the action of U_c on the other two gauge invariant operators, $\{C^2_j, \nu^x_{j+1/2}\}$, we use the Gauss law constraint $\nu^x_{j-1/2}\nu^x_{j+1/2} = S^2_j$ to deduce that

$$
\begin{aligned}
U^\dagger_c C^2_j C^2_{j+1} U_c &= S^2_{j+1} = \nu^x_{j+1/2}\nu^x_{j+3/2} \\
U^\dagger_c \nu^x_{j-1/2}\nu^x_{j+1/2} U_c &= U^\dagger_c S^2_j U_c = C^2_j C^2_{j+1}.
\end{aligned}
\tag{2.33}
$$

In order for U_c to be locality preserving and satisfy (2.33), it must have the following action on C^2_j and $\nu^x_{j+1/2}$:

$$
\begin{aligned}
U^\dagger_c C^2_j U_c &= \nu^x_{j+1/2} \\
U^\dagger_c \nu^x_{j+1/2} U_c &= C^2_{j+1}.
\end{aligned}
\tag{2.34}
$$

(As an aside, note that the above formulas imply that U^2_c acts like a unit translation on the

$\mathbb{Z}_4$ spin chain).

Now that we have figured out how U_c acts on the operators in the (gauged) $\mathbb{Z}_4$ spin chain, we can translate this action to the SPT edge theory using our mapping. More specifically, we will need the mapping between the *gauged* spin chain and the SPT edge theory. This mapping is essentially identical to the one described in Eqs. (5-6) in the main text, but with the replacement $C_j^\dagger C_{j+1} \to C_j^\dagger \nu_{j+1/2}^z C_{j+1}$:

$$
\begin{aligned}
C_j^\dagger \nu_{j+1/2}^z C_{j+1} &\leftrightarrow \tau_{j+1/2}^x i^{(1-\sigma_j^z \sigma_{j+1}^z)/2} \\
S_j &\leftrightarrow \sigma_j^x \left[\left(\frac{1+\sigma_{j-1}^z \sigma_j^z}{2} \right) + \left(\frac{1-\sigma_{j-1}^z \sigma_j^z}{2} \right) \tau_{j-1/2}^z \right] \\
&\times \left[\left(\frac{1+\sigma_j^z \sigma_{j+1}^z}{2} \right) \tau_{j+1/2}^z + \left(\frac{1-\sigma_j^z \sigma_{j+1}^z}{2} \right) \right]
\end{aligned}
\tag{2.35}
$$

We can also derive how the mapping acts on C_j^2 and $\nu_{j+1/2}^x$, by squaring the two equations in (2.35) and using the constraint $\nu_{j-1/2}^x \nu_{j+1/2}^x = S_j^2$:

$$
C_j^2 \leftrightarrow \sigma_j^z, \qquad \nu_{j+1/2}^x \leftrightarrow \tau_{j+1/2}^z.
\tag{2.36}
$$

We are now ready to work out how the duality transformation U_c acts on the operators in the SPT edge theory. It suffices to work out the action of U_c on $\{\sigma_j^z, \tau_{j+1/2}^z, \sigma_j^x, \tau_{j+1/2}^x\}$ since all other operators can be built out of these. For the first two operators, $\{\sigma_j^z, \tau_{j+1/2}^z\}$, we can work out the action of U_c using Eqs. (2.32), (2.34) and (2.36):

$$
\begin{aligned}
U_c^\dagger \sigma_j^z U_c &= \tau_{j+1/2}^z \\
U_c^\dagger \tau_{j+1/2}^z U_c &= \sigma_{j+1}^z.
\end{aligned}
\tag{2.37}
$$

Thus, U_c exchanges the $\mathbb{Z}_{2a}$ and $\mathbb{Z}_{2b}$ order parameters – as we mentioned in the main text.

The duality transformation U_c has a more complicated action on σ_j^x and $\tau_{j+1/2}^x$. To obtain

27

the action of U_c on σ_j^x, we first solve for σ_j^x in terms of gauged $\mathbb{Z}_4$ spin chain operators. From (2.35), we have

$$
\sigma_j^x \leftrightarrow \left[\left(\frac{1 + \sigma_{j-1}^z \sigma_j^z}{2} \right) + \left(\frac{1 - \sigma_{j-1}^z \sigma_j^z}{2} \right) \tau_{j-1/2}^z \right]
$$
$$
\times \left[\left(\frac{1 + \sigma_j^z \sigma_{j+1}^z}{2} \right) \tau_{j+1/2}^z + \left(\frac{1 - \sigma_j^z \sigma_{j+1}^z}{2} \right) \right] S_j^\dagger.
$$

(2.38)

Writing the right hand side in terms of gauged spin chain operators, we get

$$
\sigma_j^x \leftrightarrow \left[\left(\frac{1 + C_{j-1}^2 C_j^2}{2} \right) + \left(\frac{1 - C_{j-1}^2 C_j^2}{2} \right) \nu_{j-1/2}^x \right]
$$
$$
\times \left[\left(\frac{1 + C_j^2 C_{j+1}^2}{2} \right) \nu_{j+1/2}^x + \left(\frac{1 - C_j^2 C_{j+1}^2}{2} \right) \right] S_j^\dagger.
$$

(2.39)

Then using the action of U_c on the gauged spin chain operators (2.32-2.33) and translating back into the SPT edge theory degrees of freedom using (2.35-2.36), we get

$$
U_c^\dagger \sigma_j^x U_c = \left[\left(\frac{1 + \tau_{j-1/2}^z \tau_{j+1/2}^z}{2} \right) + \left(\frac{1 - \tau_{j-1/2}^z \tau_{j+1/2}^z}{2} \right) \sigma_j^z \right]
$$
$$
\times \left[\left(\frac{1 + \tau_{j+1/2}^z \tau_{j+3/2}^z}{2} \right) \sigma_{j+1}^z + \left(\frac{1 - \tau_{j+1/2}^z \tau_{j+3/2}^z}{2} \right) \right]
$$
$$
\times (-i)^{(1 - \sigma_j^z \sigma_{j+1}^z)/2} \tau_{j+1/2}^x.
$$

(2.40)

Similarly, solving for $\tau_{j+1/2}^x$, gives

$$
\tau_{j+1/2}^x = i^{(1 - \sigma_j^z \sigma_{j+1}^z)/2} C_{j+1}^\dagger \nu_{j+1/2}^z C_j
$$
$$
= i^{(1 - C_j^2 C_{j+1}^2)/2} C_{j+1}^\dagger \nu_{j+1/2}^z C_j.
$$

(2.41)

Again using the transformation laws for the spin chiain (2.32-2.33) and translating back

28

into the SPT edge theory degrees of freedom using (2.35-2.36), we obtain

$$U_c^\dagger \tau_{j+1/2}^x U_c = i^{(1-\tau_{j+1/2}^z \tau_{j+3/2}^z)/2}$$
$$\times \left[\left(\frac{1 + \sigma_j^z \sigma_{j+1}^z}{2} \right) + \left(\frac{1 - \sigma_j^z \sigma_{j+1}^z}{2} \right) \tau_{j+1/2}^z \right] \quad (2.42)$$
$$\times \left[\left(\frac{1 + \sigma_{j+1}^z \sigma_{j+2}^z}{2} \right) \tau_{j+3/2}^z + \left(\frac{1 - \sigma_{j+1}^z \sigma_{j+2}^z}{2} \right) \right] \sigma_{j+1}^x.$$

Eqs. (2.37), (2.40), and (2.42) completely define the action of U_c on all operators in the SPT edge theory.

2.4   Additional results

We now provide two additional results to the main paper and its supplemental materials. First, we rederive the above story using dualities of the twisted discrete gauge theory obtained by gauging the $(2+1)D$ bulk $\mathbb{Z}_2 \times \mathbb{Z}_2$ SPT. Second, we provide a proof that the story can be generalized to any primitive mixed anomaly between cyclic groups. Both of these results were obtained in collaboration with Michael Levin.

2.4.1   Derivation from $(2+1)D$ topological order

The above results can be rederived using dualities of gauge theories. First, consider twisted $\mathbb{Z}_2 \times \mathbb{Z}_2$ obtained by gauging the $\mathbb{Z}_2 \times \mathbb{Z}_2$ SPT with anomaly given above. This gauge theory has anyons generated by

$$\{m_1, e_1, m_2, e_2\}. \quad (2.43)$$

The mixed anomaly means that m_1 and m_2 have nontrivial mutual statistics $e^{i\theta_{m_1,m_2}}$. Specifically, according to Ref. [59], the phase obtained by braiding m_1 fully around m_2 $\gcd(2,2) = 2$ times is given by

$$e^{i2\theta_{m_1,m_2}} = -1, \quad (2.44)$$

29

which in turn equals $e^{i\theta_{m_1,m_2^2}}$. According to these braiding statistics, we can identify

$$m_2^2 = e_1 \qquad m_1^2 = e_2. \tag{2.45}$$

Upon a relabeling of the anyon labels, this is simply (untwisted) $\mathbb{Z}_4$ gauge theory. $\mathbb{Z}_4$ gauge theory has anyons generated by $\{m, e\}$ with $m^4 = e^4 = 1$ and $e^{i\theta_{e,m}} = i$. Specifically, we can identify

$$m_1 \leftrightarrow m \qquad e_2 \leftrightarrow m^2$$
$$m_2 \leftrightarrow e \qquad e_1 \leftrightarrow e^2, \tag{2.46}$$

which is an exact duality between the two gauge theories.

$\mathbb{Z}_4$ gauge theory has three distinct gapped boundaries, corresponding to the three different phases of the $\mathbb{Z}_4$ spin chain. These gapped boundaries are labeled by three lagrangian subgroups:

$$\mathcal{L}_1 = \{\mathbb{1}, e, e^2, e^3\} \leftrightarrow \text{SSB } \mathbb{Z}_4 \to \mathbb{Z}_1$$
$$\mathcal{L}_2 = \{\mathbb{1}, m, m^2, m^3\} \leftrightarrow \text{symmetric} \tag{2.47}$$
$$\mathcal{L}_3 = \{\mathbb{1}, e^2, m^2, e^2 m^2\} \leftrightarrow \text{SSB } \mathbb{Z}_4 \to \mathbb{Z}_2.$$

Using the duality in (2.46), we map $\mathcal{L}_1 \to \{1, m_2, e_1, m_2 e_1\}$ which is the phase in the SPT edge theory that spontaneously breaks $\mathbb{Z}_{2a}$ and respects $\mathbb{Z}_{2b}$. Similarly we map $\mathcal{L}_2 \to \{1, m_1, e_2, m_1 e_2\}$ which is the phase that spontaneously breaks $\mathbb{Z}_{2b}$ and respects $\mathbb{Z}_{2a}$. Finally, we map $\mathcal{L}_3 \to \{1, e_1, e_2, e_1 e_2\}$ which is the phase in the SPT edge theory where the full symmetry spontaneously broken. This recovers the results derived in the main paper. Note that we can also rederive the exact operator mapping between the microscopic lattice models, by mapping the string operators of the two gauge theories.

2.4.2 General mixed anomalies between cyclic groups

We will now show that a twisted $\mathbb{Z}_{N_1} \times \mathbb{Z}_{N_2}$ gauge theory with anomaly given by a nontrivial $e^{i\Theta_{12}}$, with trivial $e^{i\Theta_1}, e^{i\Theta_2}$ (note that by construction, $e^{i\Theta_{ijk}}$ must also be trivial), can be mapped to an untwisted $\mathbb{Z}_{N_1 N_2}$ gauge theory if and only if $e^{i\Theta_{12}}$ is a primitive N_{12}th root of unity, where $N_{12} = \gcd(N_1, N_2)$ (here we use the notation of Ref. [59]). This generalizes the mapping used in the main paper to general mixed anomalies of cyclic groups.

Let the anyons of the $\mathbb{Z}_{N_1} \times \mathbb{Z}_{N_2}$ gauge theory be generated by e_1, m_1 and e_2, m_2 respectively. We use the fact that $e^{i\Theta_{12}}$ is defined as

$$e^{i\Theta_{12}} = e^{iN^{12}\theta_{m_1,m_2}}, \tag{2.48}$$

where $N^{12} = \text{lcm}(N_1, N_2)$ and $e^{i\theta_{m_1,m_2}}$ is the braiding phase between m_1 and m_2. $e^{i\Theta_{12}}$ can be written as

$$e^{i\Theta_{12}} = e^{\frac{2\pi i k}{N_{12}}}, \tag{2.49}$$

where $k \in [0, N_{12})$, so we have

$$e^{i\theta_{m_1,m_2}} = e^{\frac{2\pi i k}{N_{12}N^{12}}} = e^{\frac{2\pi i k}{N_1 N_2}}. \tag{2.50}$$

This means that

$$e^{i\theta}_{e_2^n m_1^r, e_1^l m_2^m} = e^{\frac{2\pi i r m k}{N_1 N_2} + \frac{2\pi i n m}{N_2} + \frac{2\pi i r l}{N_1}}. \tag{2.51}$$

We want $e_2^n m_1^r$ and $e_1^l m_2^m$ to generate the two $\mathbb{Z}_{N_1 N_2}$ symmetries. This means that

$$rmk + nmN_1 + rlN_2 = 1 \mod N_1 N_2. \tag{2.52}$$

We will show that we can do even better, and find a solution to

$$rmk + nmN_1 + rlN_2 = 1. \tag{2.53}$$

We need to show that given any N_1 and N_2 and k satisfying $\gcd(k, N_{12}) = 1$, we can always solve (2.53).

We first group the terms in (2.53) to get

$$r(mk + lN_2) + nmN_1 = 1 \bmod N_1 N_2. \tag{2.54}$$

Suppose instead that there is no solution to (2.53). This means that there is no solution to the following similar equation:

$$r(k + lN_{12}) + nN_1 = 1. \tag{2.55}$$

To see why this is the case, notice that if there exists a solution to (2.55), then we can use the fact that there always exists a and b satisfying

$$N_{12} = aN_1 + bN_2, \tag{2.56}$$

according to Bezout's identity. This gives

$$r(k + l'N_2) + n'N_1 = 1, \tag{2.57}$$

where $l' = lb$ and $n' = la + n$.

If there is no solution to (2.55), then there is also no solution to

$$r(k + lN_{12}) + nN_3 = 1, \tag{2.58}$$

32

where $N_3 = N_1/N_{12}$. This is because of the following. If (2.55) has no solution, then this means that there exists an integer p that divides both $(k + lN_{12})$ and N_1. However, if p divides N_{12}, then it cannot divide k, because $\gcd(k, N_{12}) = 1$. In this case, p cannot divide $(k + lN_{12})$. This means that p cannot divide N_{12}, so in order for p to divide N_1, it must divide N_1/N_{12}. But if it divides N_1/N_{12}, then there is no solution to (2.58). Next we have

$$r(k + lN_{3,12}) + nN_3 = 1, \tag{2.59}$$

again due to Bezout's identity, and

$$r(k + lN_{3,12}) + nN_4 = 1, \tag{2.60}$$

where $N_4 = N_3/N_{3,12}$. Let us describe this sequence of equations by (x_n, y_n), where $x_{n+1} = \gcd(x_n, y_n)$ and $y_{n+1} = y_n/x_{n+1}$. Then eventually, for some n, either $x_n = 1$ or $y_n = 1$. In either case, we can just choose $l = n = 0, k = r = 1$. Then from this solution and working backward, we can obtain a solution to (2.53). This results in a contradiction, so there must be a solution to (2.53).

Surprisingly, this result means that we can have a DQCP in a $(1 + 1)D$ system without any anomaly at all, as long as N_1 and N_2 are coprime. In this case, $N_{12} = k = 1$, so the DQCP can be mapped to a SSB transition in a $\mathbb{Z}_{N_1 N_2}$ spin chain. For $N_1 N_2 > 4$, we can use strong disorder to ensure a continuous phase transition[62].

CHAPTER 3

STORY 2: QUANTUM DYNAMICS AND ENTANGLEMENT TRANSITIONS

3.1 Introduction: Entanglement transitions

There are two basic tools for manipulating quantum states: unitary time evolution and measurement. As discussed in Sec. 1.3, entanglement transitions occur due to competition between these two processes. To understand why this transition might occur, let us consider two limiting cases. In the limit of no measurement and only unitary time evolution, a generic state becomes *volume-law entangled* in the long-time limit. In 1D, this means that the entanglement entropy between a subsystem of size ℓ and its complement scales as

$$S(\ell) = a\ell + \cdots \tag{3.1}$$

where a is a constant and $(\cdots)$ refer to subleading terms. In the other limit, of no unitary time evolution and only commuting single-site measurements, the long-time steady-state would be *area-law entangled*, which in 1D means that

$$S(\ell) = \text{const} + \cdots \tag{3.2}$$

Therefore, the competition results in a transition between steady states that are distinguished by their entanglement properties.

Note that unitary time evolution is a locality-preserving operation: time evolution (with local interactions) over a time t can only create correlations over a linear distance proportional to t, because correlations grow within a light-cone by Lieb-Robinson bounds. On the other hand, measurement is *not* locality-preserving: a local measurement can destroy correlations that are arbitrarily far apart in space. It may therefore seem that measurements

have an unfair advantage: correlations created by time evolution for arbitrarily long times can be destroyed instantaneously by a local projective measurement. Therefore, any finite amount of measurement might completely win over unitary time evolution.

As was first confirmed in Refs. [23, 24, 25, 26], this is not actually the case. In interacting systems, it has now been shown through both numerical and analytical methods that measurement-induced phase transitions (MIPTs) occur in a variety of settings. The typical setting for an MIPT is in a chain of qubits, where random two-site gates are interspersed with rate p of projective on-site measurements weighted according to the Born probability. In this setting, the Hartley (zeroth) entanglement entropy $S_0(\ell)$ for a subsystem ℓ, which is the logarithm of the rank of the reduced density matrix, was studied using a mapping to classical bond percolation[25]. This mapping gave the critical exponent $\nu_0 = \frac{4}{3}$ at the MIPT, defined by $S_0(\ell) \sim (p_c - p)^{\nu_0}$, which was confirmed with numerics. The critical exponents ν_n for $n > 0$ have not been determined analytically.

While MIPTs for interacting systems are very common (albeit still not analytically understood), MIPTs for a simpler, more analytically tractable *Gaussian* circuits are much more rare. Gaussian circuits are circuits in which the unitary time evolution consists only of fermion bilinears, and measurements are restricted to fermion occupation number. In fact, it was proven in Ref. [65] that the volume-law phase is unstable to any nonzero rate of projective measurement in Gaussian systems. A process related to projective measurement is weak measurement, given by imaginary time evolution $U(i\lambda) = e^{\lambda O}$ where O is an operator. In the limit $\lambda \to \infty$, $U(i\lambda)$ is simply a projector onto the eigenstate of O with the largest eigenvalue, but $U(i\lambda)$ is not a projector for any finite λ. Weak measurements can be implemented by coupling the system to an ancilla, measuring the ancilla, and postselecting, as explained in Sec. 3.3.1. Gaussian circuits with weak measurement rather than projective measurements are also known simply as Gaussian non-unitary circuits, because they contain gates that are not unitary. Such circuits also demonstrated an absence of the volume-law

phase for any amount of non-unitarity[66].

In our model, we alternate between translation-invariant unitary time evolution and weak measurement on all of the sites. It is not obvious that weak measurement on all the sites would be any less destructive than projective measurement on a single site. However, we show that in this model, we *can* obtain a (finely-tuned) MIPT, despite the circuit being Gaussian. Furthermore, we can compute the critical exponents $\{\nu_n\}$ describing this critical point exactly.

3.2 Volume-law to area-law entanglement transition in a non-unitary periodic Gaussian circuit

This chapter is reprinted with permission from:

Etienne Granet, Carolyn Zhang, and Henrik Dreyer. Volume-law to area-law entanglement transition in a non-unitary periodic Gaussian circuit. arXiv preprint arXiv:2212.10584.

Abstract

We consider Gaussian quantum circuits that alternate unitary gates and post-selected weak measurements, with spatial translation symmetry and time periodicity. We show analytically that such models can host different kinds of measurement-induced phase transitions detected by entanglement entropy, by mapping the unitary gates and weak measurements onto Möbius transformations. We demonstrate the existence of a log-law to area-law transition, as well as a volume-law to area-law transition at a finite measurement amplitude. For the latter, we compute the critical exponent ν for the Hartley, von Neumann and Rényi entropies exactly.

3.2.1 Introduction

In recent years, there has been an immense amount of work on dynamical phase transitions driven by competition between unitary time evolution and projective measurements, called measurement-induced phase transitions (MIPTs). Although generic unitary time evolution leads to volume-law entangled states in the long-time limit, interspersing the unitary evolution with local measurements can stabilize area-law entangled steady states [25, 23, 24, 26]. These MIPTs have been studied in various setups, mostly through numerical methods [67, 68, 69, 70, 71, 72, 73, 74, 75, 76, 77, 78, 79, 80, 81, 82, 83, 84, 85, 86, 87, 88, 89, 90, 91, 92, 93]. A subclass of circuits called Gaussian circuits allows for analytical calculations because they only involve unitaries and measurements built out of fermion bilinears. However, though the volume-law to area-law MIPT was observed for interacting circuits, it has not yet been observed in Gaussian circuits [94, 95, 96, 97, 66, 65, 98, 99].

In this work, we analytically study Gaussian non-unitary circuits with spatial translation symmetry and discrete time translation symmetry. They consist of Gaussian unitary gates and weak measurements, obtained by coupling the system to ancillas, measuring the ancillas, and post-selecting (see Sec. 3.3). We show that these non-unitary circuits can demonstrate MIPTs between different entanglement phases as we tune the measurement amplitude, which is related to the ancilla coupling. Surprisingly, for specific parameters, we find a volume-law to area-law transition at a finite measurement amplitude. We derive the exact critical measurement amplitude and the correlation length exponents $\{\nu_n\}$ for the Hartley ($n = 0$), von Neumann ($n = 1$) and Rényi ($n > 1$) entanglement entropies. To our knowledge, this is the first example of a volume-law to area-law transition in a Gaussian non-unitary circuit, and of an analytical computation of all $\{\nu_n\}$ at a MIPT.
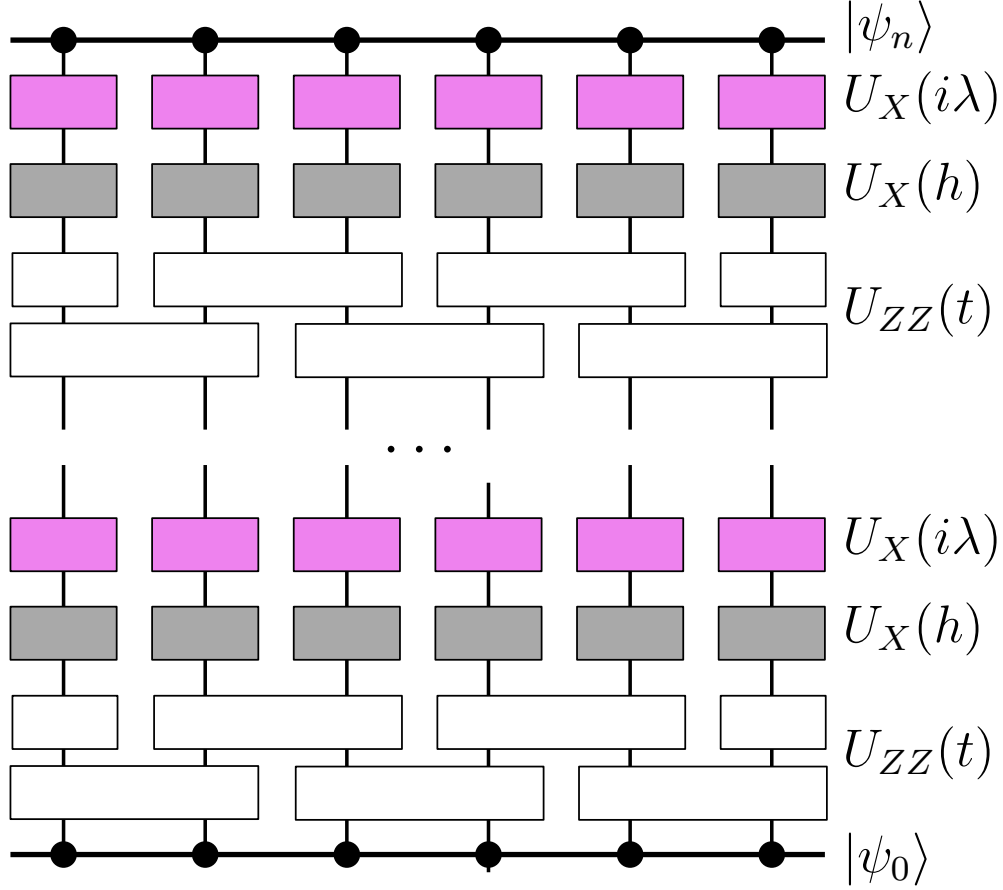
Figure 3.1: A schematic of n applications of the round described by (3.5), with $p = 1$. $|\psi_n\rangle$ is the normalized final state.

3.2.2 Setup

We study non-unitary circuits built out of the following translation-invariant 1D layers [100, 101]:

$$U_{ZZ}(t) = e^{-it \sum_{j=1}^{L} \sigma_j^z \sigma_{j+1}^z}$$

$$U_{YY}(t) = e^{-it \sum_{j=1}^{L} \sigma_j^y \sigma_{j+1}^y} \tag{3.3}$$

$$U_X(t) = e^{-it \sum_{j=1}^{L} \sigma_j^x}$$

where $\sigma_j^{x,y,z}$ are Pauli matrices, and periodic boundary conditions $L + 1 \equiv 1$ are assumed. These layers can be written as free fermion evolution using the standard Jordan-Wigner
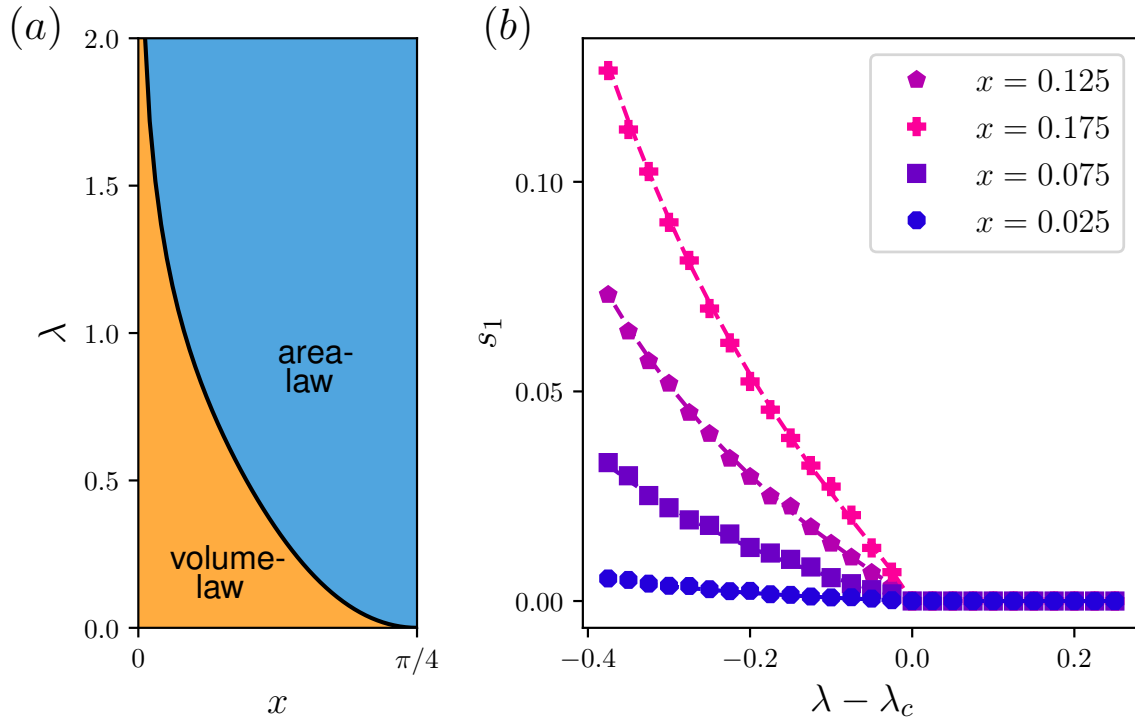
Figure 3.2: (a) Phase diagram for the non-unitary circuit described in (3.15), with x and λ as defined in (3.16) and (3.4) respectively. The phase boundary is given by (3.20). (b) Scaling of the von-Neumann entropy. Markers denote the slope of the best linear fits to the exact entropy $S_1(\ell) \sim s_1 \ell + b$ after 500 cycles on subsystem sizes up to $\ell = 100$. Dashed lines denote the closed form expression (3.31).

transformation $\sigma_j^x = 1 - 2c_j^\dagger c_j$ and $\sigma_j^z = (c_j + c_j^\dagger) \prod_{\ell=1}^{j-1}(1 - 2c_\ell^\dagger c_\ell)$, where $c_j^\dagger, c_j$ are fermion creation and annihilation operators. Non-unitarity is introduced by allowing t to be complex, which corresponds to weak measurement or dynamics in open quantum systems [102].

We will focus on circuits built out of the following elementary cycle of layers

$$U(t, h, \lambda) = U_X(i\lambda)U_X(h)U_{ZZ}(t)\,, \qquad (3.4)$$

for t, h, λ real parameters. We can use this cycle to build more complicated rounds described by $\mathcal{U}$:

$$\mathcal{U} = U(t_p, h_p, \lambda_p)...U(t_1, h_1, \lambda_1)\,, \qquad (3.5)$$

39

with $t_r, h_r, \lambda_r, r \in \{1, ..., p\}$ fixed real parameters. We will study the entanglement properties of a subsystem of large size ℓ after $n \to \infty$ identical rounds $\mathcal{U}$, in the thermodynamic limit $L \to \infty$, with $\ell \ll n \ll L$. This kind of setup, for $p = 1$, is illustrated in Fig. 3.1. Because each round is identical, our models have discrete time translation symmetry. While we use the particular structure of cycle and round defined in (3.4) and (3.5), we note that our methods can be applied to any round built out of (3.3).

3.2.3 *Time evolution via Möbius transformations.*

The actions of the layers in (3.3) are particularly simple on coherent states [100]. These are states of the form

$$|\psi(\mathcal{A}, f(k))\rangle = \mathcal{A} \prod_{k \in K_L^+} \left[1 + f(k)c^\dagger(-k)c^\dagger(k)\right] |0\rangle, \tag{3.6}$$

where $K_L = \frac{2\pi}{L}\left\{-\frac{L}{2} + \frac{1}{2}, \cdots, \frac{L}{2} - \frac{1}{2}\right\}$ and $K_L^+ \subset K_L$ contains all the positive momenta, and $|0\rangle$ the tensor product of $+1$ eigenstates of σ_j^x at each site. Here, $\mathcal{A}$ normalizes the state and contains a phase, and $f(k)$ is an amplitude for fermions at momenta $k, -k$.

The crucial observation of Ref. [100] was that a coherent state remains a coherent state after the application of any of the layers in (3.3), but with modified $\mathcal{A}$ and $f(k)$. In particular, each of the layers in (3.3) transforms $f(k)$ by a Möbius transformation:

$$U_g(t)|\psi(\mathcal{A}, f(k))\rangle = |\psi(\tilde{\mathcal{A}}, \tilde{f}(k))\rangle, \tag{3.7}$$

where $g = ZZ, YY, X$ and

$$\tilde{f}(k) = F(f) = \frac{af(k) + b}{cf(k) + d}, \tag{3.8}$$

where $a, b, c,$ and d are complex functions of t and k. We provide their explicit forms for the three kinds of layers in Sec. 3.3. The transformation on $\mathcal{A}$ will not be needed in this work.

40

Because the composition of Möbius transformations is a Möbius transformation, the action of $U(t, h, \lambda)$ and $\mathcal{U}$ can also be written as (3.8). It follows that $\mathcal{U}^n |\psi(\mathcal{A}, f(k))\rangle$ also produces a coherent state for any n. Like any Möbius transformation, the transformation associated with $\mathcal{U}$ can be packaged into a 2×2 matrix

$$\mathcal{M}_k = \begin{pmatrix} a & b \\ c & d \end{pmatrix} \tag{3.9}$$

acting on the vector $\begin{pmatrix} f(k) \\ 1 \end{pmatrix}$: the new value $\tilde{f}(k)$ is given by the ratio of the two components of the resulting vector. The matrix of the Möbius transformation associated with $\mathcal{U}^n$ is then simply obtained by repeated matrix multiplications $\mathcal{M}_k^n$. Therefore, in order to obtain the behaviour at large n of $\mathcal{U}^n |0\rangle$, we need to study the fixed points of the Möbius transformation $\mathcal{M}_k$ associated with $\mathcal{U}$ and their stability. Note that the initial state can be any coherent state, and therefore any free fermion state with zero total momentum, as well as some non-zero momentum states by applying with $c^\dagger(k_0)$ operators on the coherent state [103].

Let us denote the normalized state after n rounds by $|\psi(\mathcal{A}_n, f_n(k))\rangle$. The fixed points of the Möbius transformation are the two solutions to the quadratic equation

$$f_\infty(k) = \frac{a f_\infty(k) + b}{c f_\infty(k) + d}. \tag{3.10}$$

We label these fixed points by $f_\infty^-(k)$ and $f_\infty^+(k)$ for each k. The stability of these fixed points are given by $|F'(f)|$: if $|F'(f)|_{f=f_\infty^-(k)} < 1$, then $f_\infty^-(k)$ is a stable fixed point. Since a Möbius transformation can have at most only one stable fixed point, any choice of initial state $f_0(k) \neq f_\infty^+(k)$ will be attracted to $f_\infty^-(k)$ as $n \to \infty$, for that particular value of k. It can be shown that

$$|F'(f)|_{f=f_\infty^-} = \frac{1}{|F'(f)|_{f=f_\infty^+}} = \frac{|\mu_-(k)|}{|\mu_+(k)|}, \tag{3.11}$$

where $\mu_-(k)$ and $\mu_+(k)$ with $|\mu_-(k)| \leq |\mu_+(k)|$ are the two eigenvalues of $\mathcal{M}_k$. So for

41

$|\mu_-(k)| \neq |\mu_+(k)|$, there is a unique stable fixed point given by $f_\infty^-(k)$, while $f_\infty^+(k)$ is an unstable fixed point. On the contrary, if $|\mu_-(k)| = |\mu_+(k)|$, then there are no stable fixed points and $f_n(k)$ will not converge as $n \to \infty$ whenever $f_0(k) \neq f_\infty^\pm(k)$.

These two alternatives completely determine the steady state entanglement properties. Let us call the values of k for which $|\mu_-(k)| = |\mu_+(k)|$ "critical". We will only need to consider $k \in [0, \pi]$ because $f(k)$ must be an antisymmetric function for (3.6) to be consistent. If there are no critical $k \in [0, \pi]$, we will show that the steady state has area-law entanglement, which in 1D means that in the thermodynamic limit $S_m(\ell)$ saturates to a finite value when $\ell \to \infty$. If there is a finite number of critical k, then the steady state generically has log-law entanglement: $S_m(\ell) \sim \log(\ell)$. Finally, if there is a whole interval of critical k, then the steady state has volume-law entanglement: $S_m(\ell) \sim \ell$.

In order to determine analytically whether such critical k exist for a given Möbius transformation, we use that $|\mu_-(k)| = |\mu_+(k)|$ if and only if the following two conditions are satisfied:

$$(i) \quad \Im \frac{\mathrm{Tr}(\mathcal{M}_k)}{\sqrt{\det(\mathcal{M}_k)}} = 0 \qquad (ii) \quad \left| \Re \frac{\mathrm{Tr}(\mathcal{M}_k)}{\sqrt{\det(\mathcal{M}_k)}} \right| \leq 2 \,. \tag{3.12}$$

We prove this in Sec. 3.3. We will now give two examples of non-unitary circuits and show that, by studying their corresponding Möbius transformations, we can obtain their phase diagrams exactly.

3.2.4 Log-law to area-law transition.

We will now show that a log-law to area-law transition can occur in a simple circuit containing only one cycle (3.4), i.e. $p = 1$ in (3.5). For this circuit, we have

$$
\mathcal{M}_k = \begin{pmatrix} z_{k,t} e^{-2\lambda + 2ih} & e^{-2\lambda + 2ih} \\ -e^{2\lambda - 2ih} & z^*_{k,t} e^{2\lambda - 2ih} \end{pmatrix}, \tag{3.13}
$$

where

$$
z_{k,t} = \frac{e^{2it} \tan(k/2) + \frac{e^{-2it}}{\tan(k/2)}}{2 \sin(2t)}. \tag{3.14}
$$

To investigate the entanglement properties of this circuit, we study the conditions (3.12) for the existence of critical k, as detailed in Sec. 3.3. We find that if $\lambda = 0$, both conditions in (3.12) are satisfied for all k. Because there is a whole interval of critical k (in fact, the entire range of k), the steady state exhibits volume-law entanglement, as expected in absence of measurements. For $\lambda > 0$, the phase of the system depends on the condition $|\tan(2h)| > |\tan(2t)|$. If this condition holds, then the steady-state always demonstrates area-law entanglement. Otherwise, there is a critical value λ_c such that for $0 < \lambda < \lambda_c$ there is a unique critical k given by $k = \arccos\left[\frac{\tan(2h)}{\tan(2t)}\right]$ for which both conditions of (3.12) hold, implying a log-law entanglement. For $\lambda > \lambda_c$ there are no critical k, indicating area-law entanglement. $\lambda_c(t, h)$ can be computed exactly and is given in Sec. 3.3. Therefore, when $|\tan(2h)| < |\tan(2t)|$, the system demonstrates a log-law to area-law transition at $\lambda = \lambda_c$. Such transitions are well-known in free fermionic non-unitary circuits [97, 104, 95, 105].

Let us finally mention the case $h = t = \pi/4$. Here we find for any λ an interval $[k_c, \pi - k_c]$ of critical k, with $0 < k_c < \pi/2$ depending on λ. This yields a volume law phase, but without any transition to an area-law behaviour at any finite λ, consistent with Ref. [106].

3.2.5 Volume-law to area-law transition

We now consider a round with two cycles:

$$\mathcal{U} = U(t_2, h_2, \lambda)U(t_1, h_1, \lambda). \tag{3.15}$$

For generic values of the parameters, such circuits do not have volume-law to area-law MIPTs in λ. However, for

$$t_1 = h_1 = \frac{\pi}{4} - x \qquad t_2 = h_2 = \frac{\pi}{4} + x, \tag{3.16}$$

where $x \in [0, \pi/4]$, we will show that there exists an x-dependent λ_c such that the steady state demonstrates volume-law entanglement for $\lambda < \lambda_c$ and area-law entanglement for $\lambda > \lambda_c$.

From the definition of $z_{k,t}$ in (3.14), we have $z_{k,t_1} = -z_{k,t_2}^*$. Therefore, $\mathcal{M}_k$ for (3.15) simplifies to

$$\mathcal{M}_k = \begin{pmatrix} |z_{k,t_1}|^2 e^{-4\lambda} - e^{4ix} & z_{k,t_1}^*(e^{-4\lambda} + e^{4ix}) \\ -z_{k,t_1}(e^{4\lambda} + e^{-4ix}) & |z_{k,t_1}|^2 e^{4\lambda} - e^{-4ix} \end{pmatrix}. \tag{3.17}$$

To determine the critical k, we compute

$$\frac{\mathrm{Tr}(\mathcal{M}_k)}{\sqrt{\det(\mathcal{M}_k)}} = 2\frac{|z_{k,t_1}|^2 \cosh(4\lambda) - \cos(4x)}{1 + |z_{k,t_1}|^2}. \tag{3.18}$$

This quantity is always real, so condition (i) of (3.12) is satisfied for all k. Condition (ii) can be written as

$$\tan^2(k/2) + \frac{1}{\tan^2(k/2)} \leq \frac{4\cos^4(2x)}{\sinh^2(2\lambda)} + 2\cos(4x). \tag{3.19}$$

For this to hold for at least one value of k, we need it to be true for $k = \frac{\pi}{2}$, which

44

minimizes the left-hand side. Plugging in $k = \frac{\pi}{2}$, we find that the interval of critical k disappears when $\lambda > \lambda_c$ where

$$\lambda_c = \frac{1}{2}\text{arcsinh}\left[\frac{\cos^2(2x)}{\sin(2x)}\right]. \tag{3.20}$$

Therefore, the steady state demonstrates area-law entanglement for $\lambda > \lambda_c$. For $\lambda < \lambda_c$, (3.19) is satisfied for $k \in [k_c, \pi - k_c]$, with k_c obeying (3.19) with equality. Within this interval, $f_n(k)$ does not converge to a stable fixed point, and we will now show that this leads to volume-law entanglement.

3.2.6 Behavior of entanglement entropy

Given a state $|\psi\rangle$ on a spin chain of size L, the reduced density matrix ρ_ℓ on $[1, \ell]$ is given by

$$\rho_\ell = \text{Tr}_{\ell+1,\dots,L}\left(|\psi\rangle\langle\psi|\right). \tag{3.21}$$

We define the entanglement entropies $S_m(\ell)$ as

$$
\begin{aligned}
S_0(\ell) &= \log \text{rank}[\rho]\,, &\quad& \text{Hartley} \\
S_1(\ell) &= -\text{Tr}[\rho \log \rho]\,, &\quad& \text{von Neumann} \\
S_m(\ell) &= \frac{\log \text{Tr}[\rho^m]}{1-m}\,, &\quad& m \geq 2\,, \quad \text{Rényi}\,.
\end{aligned}
\tag{3.22}
$$

While it is difficult to obtain the exact behavior of $S_m(\ell)$ at intermediate times, we can compute the coefficient of the volume-law ($\mathcal{O}(\ell)$) contribution to $S_m(\ell)$ in the $n \to \infty$ limit. To that end, we introduce the correlation matrix Γ on the subsystem $[1, 2, \dots \ell]$, given by

$$\langle\psi| \begin{pmatrix} a_{2j-1} \\ a_{2j} \end{pmatrix} \cdot \begin{pmatrix} a_{2k-1} & a_{2k} \end{pmatrix} |\psi\rangle = \delta_{j,k} + i\Gamma_{jk}, \tag{3.23}$$

45

with the Majorana fermions $a_{2j-1} = c_j + c_j^\dagger$ and $a_{2j} = i(c_j - c_j^\dagger)$. Γ has a block-Toeplitz structure:

$$\Gamma = \left(\Pi_{j-i}\right)_{i,j=1,\dots,\ell} \quad \Pi_j = \begin{pmatrix} -\varphi_j & \psi_j \\ -\psi_{-j} & \varphi_j \end{pmatrix}, \tag{3.24}$$

where from (3.6), φ_j and ψ_j are computed to be

$$\begin{aligned} \varphi_j &= \frac{i}{2\pi} \int_{-\pi}^{\pi} dk e^{-ikj} \frac{f_n(k) + f_n(k)^*}{1 + |f_n(k)|^2} \\ \psi_j &= \frac{1}{2\pi} \int_{-\pi}^{\pi} dk e^{-ikj} \frac{f_n(k) - f_n(k)^* + |f_n(k)|^2 - 1}{1 + |f_n(k)|^2}. \end{aligned} \tag{3.25}$$

We find that φ_j and ψ_j converge to some $\bar{\varphi}_j$ and $\bar{\psi}_j$ respectively as $n \to \infty$, and we define $\hat{\varphi}(k)$ and $\hat{\psi}(k)$ through $\bar{\varphi}_j = \frac{1}{2\pi} \int_{-\pi}^{\pi} dk e^{-ikj} \hat{\varphi}(k)$ and $\bar{\psi}_j = \frac{1}{2\pi} \int_{-\pi}^{\pi} dk e^{-ikj} \hat{\psi}(k)$. When $f_n(k)$ converges to a stable fixed point, we can replace $f_n(k)$ in (3.25) by $f_\infty^-(k)$. Notice that if there is a critical value of k, then $f_\infty^-(k)$ generically fails to be smooth because it jumps between the two fixed points of the Möbius transformation. This leads to power-law decay of correlations of Majorana fermions in real-space according to (3.25), implying log-law entanglement. On the other hand, if there are no critical k, $f_\infty^-(k)$ is smooth and real-space correlations decay exponentially, implying area-law entanglement for pure states [107, 108].

If $k \in [k_c, \pi - k_c]$ is critical, then $f_n(k)$ in this momentum range does not converge and depends on both the initial state $f_0(k)$ and the cycle number n. We choose the initial state $f_0(k) = 0$ for all k which, in the spin language, means all spins in the $+1$ eigenstate of σ_j^x. For this initial state, we have $f_n(k) = x_n(k)/y_n(k)$ with

$$\begin{pmatrix} x_n(k) \\ y_n(k) \end{pmatrix} = \mathcal{M}_k^n \cdot \begin{pmatrix} 0 \\ 1 \end{pmatrix}. \tag{3.26}$$

46

Since $|\mu_-(k)| = |\mu_+(k)|$, we can write $\mu_+(k)/\mu_-(k) = e^{2i\theta_k}$ for $k \in [k_c, \pi - k_c]$, where

$$\theta_k = \arccos \left[\frac{|z_{k,t_1}|^2 \cosh(4\lambda) - \cos(4x)}{1 + |z_{k,t_1}|^2} \right] . \tag{3.27}$$

Diagonalizing $\mathcal{M}_k$, we find

$$f_n(k) = \frac{b(k) \sin(n\theta_k)}{(-a(k) + \cos\theta_k) \sin(n\theta_k) + \sin(\theta_k) \cos(n\theta_k)}, \tag{3.28}$$

where a and b are matrix elements of $\mathcal{M}_k/\sqrt{\det \mathcal{M}_k}$ as in (3.9), and we have indicated their k dependence explicitly. We see that in this case, $f_n(k)$ does not converge to a stable fixed point as $n \to \infty$ and instead keeps oscillating. To compute $\hat{\varphi}(k)$ and $\hat{\psi}(k)$, we separate the slowly varying and quickly oscillating parts of $f_n(k)$ by defining

$$\mathfrak{f}(k, u) = \frac{b(k) \sin u}{(-a(k) + \cos\theta_k) \sin u + \sin\theta_k \cos u} . \tag{3.29}$$

As shown in Sec. 3.3, we compute $\hat{\varphi}(k)$ and $\hat{\psi}(k)$ by averaging over the fast oscillations:

$$\begin{aligned}
\hat{\varphi}(k) &= \frac{i}{2\pi} \int_0^{2\pi} du \frac{\mathfrak{f}(k, u) + \mathfrak{f}(k, u)^*}{1 + |\mathfrak{f}(k, u)|^2} \\
\hat{\psi}(k) &= \frac{1}{2\pi} \int_0^{2\pi} du \frac{\mathfrak{f}(k, u) - \mathfrak{f}(k, u)^* + |\mathfrak{f}(k, u)|^2 - 1}{1 + |\mathfrak{f}(k, u)|^2} .
\end{aligned} \tag{3.30}$$

We now follow Ref. [109] to compute the entanglement entropy. Repeating the calculations therein, we find the following leading behavior when $\ell \to \infty$:

$$S_m(\ell) = \frac{\ell}{2\pi} \int_{-\pi}^{\pi} dk H_m \left(\sqrt{|\hat{\varphi}(k)|^2 + |\hat{\psi}(k)|^2} \right) , \tag{3.31}$$

with $\mathcal{O}(\log \ell)$ corrections, and with $H_m(x)$ given by

$$
\begin{aligned}
H_0(x) &= \mathbb{1}_{x \in (-1,1)} \\
H_1(x) &= -\frac{1+x}{2} \log \frac{1+x}{2} - \frac{1-x}{2} \log \frac{1-x}{2} \\
H_m(x) &= \frac{1}{1-m} \log \left[\left(\frac{1+x}{2} \right)^m + \left(\frac{1-x}{2} \right)^m \right],
\end{aligned}
\tag{3.32}
$$

for $m \geq 2$. When $f_n(k)$ converges to a stable fixed point, we plug $f_\infty^-(k)$ into the definition of $\hat{\varphi}(k)$ and $\hat{\psi}(k)$, and obtain

$$
|\hat{\varphi}(k)|^2 + |\hat{\psi}(k)|^2 = 1.
\tag{3.33}
$$

Since $H_m(1) = 0$, these momenta do not contribute to the volume law term $\mathcal{O}(\ell)$, nor to the $\mathcal{O}(\log \ell)$ term [110]. On the other hand, when $f_n(k)$ does not converge to a stable fixed point, we can show from (3.58) that

$$
|\hat{\varphi}(k)|^2 + |\hat{\psi}(k)|^2 < 1.
\tag{3.34}
$$

Therefore, these momenta do contribute to the $\mathcal{O}(\ell)$ term. We obtain

$$
S_m(\ell) =
\begin{cases}
s_m(\lambda)\ell, & \text{if } \lambda < \lambda_c \\
\mathcal{O}(\ell^0), & \text{if } \lambda > \lambda_c,
\end{cases}
\tag{3.35}
$$

with $s_m(\lambda)$ a coefficient computable from (3.31) (see Sec. 3.3). We compare these exact calculations with numerical computations of entanglement entropies in Fig. 3.2. In the limit $\lambda \to \lambda_c$, we define the critical exponent ν by the leading behaviour of $s_m(\lambda)$ when $\lambda \to \lambda_c$:

$$
s_m(\lambda) = a_m (\lambda_c - \lambda)^\nu + \mathcal{O}((\lambda_c - \lambda)^{\nu'}),
\tag{3.36}
$$

48

where $\nu' > \nu$. We obtain analytically

$$s_0(\lambda_c - \lambda) \sim (\lambda_c - \lambda)^{1/2}$$

$$s_1(\lambda_c - \lambda) \sim (\lambda_c - \lambda)\log(\lambda_c - \lambda) \qquad (3.37)$$

$$s_m(\lambda_c - \lambda) \sim (\lambda_c - \lambda) \,,$$

with coefficients given in Sec. 3.3 and subleading terms $\sim (\lambda_c - \lambda)^{3/2}$. Therefore, $\nu = \frac{1}{2}$ for $S_0(\ell)$ and $\nu = 1$ for $S_m(\ell)$, where $m \geq 1$, with marginal logarithmic corrections at $m = 1$ [111, 112]. At the critical point $\lambda = \lambda_c$, the only critical k is $k = \frac{\pi}{2}$, but $\theta_{\frac{\pi}{2}} = 0$ according to (3.27). So $f_n(\frac{\pi}{2})$ converges to a stationary value, and the $\mathcal{O}(\log \ell)$ coefficients vanish, yielding a central charge $c = 0$, consistent with Ref. [105, 97].

3.2.7 Discussion

We presented a general framework for obtaining exact results on steady-states of clean Gaussian non-unitary circuits with discrete time translation symmetry using Möbius transformations. A few comments are in order. First, it was shown in Ref. [70, 65] that entanglement transitions are also purification transitions. This can also be seen in our analysis: if a Möbius transformation has a single stable fixed point for all k, the steady state is independent of the initial state. Therefore, the corresponding circuit would map mixed states to the pure state given by $f_\infty^-(k)$, as $n \to \infty$. On the other hand, when there is a region of critical k, $f_n(k)$ in this interval always retains its dependence on the initial state, and a mixed state remains mixed even as $n \to \infty$.

Second, we note that the distinction governed by conditions (3.12) is equivalent to a statement on the reality of the single-particle energies $\{\epsilon_k\}$ of the effective Hamiltonian H defined by $\mathcal{U} = e^{iH}$: ϵ_k is real if and only if k is critical. Therefore, increasing the non-unitarity of the model through λ has a similar effect as in the continuous-time model of Ref. [93].

49

While we only studied steady states of two simple kinds of rounds, the general framework of Möbius transformations can be used to study any other circuit built out of the layers in (3.3) and their intermediate time dynamics. Note that these MIPTs can be detected directly by either measuring two-point correlation functions in the steady state or by measuring correlations between mode occupation numbers $c^\dagger(k)c(k)$. For the latter, the measurement outcome depends on the criticality of k. Therefore, while difficult to implement due to the mid-circuit postselection, they are easy to detect.

3.2.8   Acknowledgements

3.3   Supplemental Material

3.3.1   Realization of the weak measurement

The non-unitary operator $e^{\lambda\sigma_j^x}$ can be realized (up to an unimportant normalization factor) with an ancilla spin and a post-selection. Namely we have, with σ_j^x acting on the spin in the spin chain and σ_a^y acting on the ancilla,

$$e^{\lambda\sigma_j^x} \propto {}_a\langle 0|e^{i\left(\frac{\theta+\theta'}{2}+\frac{\theta-\theta'}{2}\sigma_j^x\right)\sigma_a^y}|0\rangle_a \,, \qquad \text{with } e^{2\lambda} = \frac{\cos\theta}{\cos\theta'} \,. \tag{3.38}$$

Notice that we post-select the ancilla to be in the $+1$ eigenstate of σ_a^y. We must perform this post-selection after every cycle and at each site.

3.3.2 Möbius transformations

The Möbius transformations for the layers in Eq. (1) of the main text were derived in Ref. [100] (with a different convention $t \to -t$). We list them here for convenience:

$$
\begin{aligned}
U_{ZZ}(t) : \tilde{f}(k) &= \frac{[1 + \tan^2(k/2)e^{4it}]f(k) + i\tan(k/2)(1 - e^{4it})}{-i\tan(k/2)(1 - e^{4it})f(k) + \tan^2(k/2) + e^{4it}} \\
U_{YY}(t) : \tilde{f}(k) &= \frac{[1 + \tan^2(k/2)e^{4it}]f(k) - i\tan(k/2)(1 - e^{4it})}{i\tan(k/2)(1 - e^{4it})f(k) + \tan^2(k/2) + e^{4it}} \\
U_X(t) : \tilde{f}(k) &= e^{4it}f(k) .
\end{aligned}
\tag{3.39}
$$

3.3.3 Proof of Eq. (10)

We now prove that the two eigenvalues $\mu_-(k)$ and $\mu_+(k)$ of $\mathcal{M}_k$ have equal magnitude if and only if

$$
\begin{aligned}
(i) \quad & \Im\left(\frac{\mathrm{Tr}(\mathcal{M}_k)}{\sqrt{\det(\mathcal{M}_k)}}\right) = 0 \\
(ii) \quad & \left|\Re\left(\frac{\mathrm{Tr}(\mathcal{M}_k)}{\sqrt{\det(\mathcal{M}_k)}}\right)\right| \leq 2 .
\end{aligned}
\tag{3.40}
$$

Let $K = \frac{\mu_-(k)}{\mu_+(k)}$. We use the fact that

$$
\sqrt{K} + \frac{1}{\sqrt{K}} = \frac{\mathrm{Tr}(\mathcal{M}_k)}{\sqrt{\det(\mathcal{M}_k)}}.
\tag{3.41}
$$

Now setting $K = \kappa e^{i\alpha}$ with $\kappa > 0$, the two eigenvalues have equal magnitude if and only if $\kappa = 1$, and we have

$$
\Im\left(\frac{\mathrm{Tr}(\mathcal{M}_k)}{\sqrt{\det(\mathcal{M}_k)}}\right) = \left(\sqrt{\kappa} - \frac{1}{\sqrt{\kappa}}\right)\sin\frac{\alpha}{2} .
\tag{3.42}
$$

The above quantity is zero if and only if $\kappa = 1$ or $\sin(\alpha/2) = 0$. Similarly, we have

$$\Re\left(\frac{\operatorname{Tr}(\mathcal{M}_k)}{\sqrt{\det(\mathcal{M}_k)}}\right) = \left(\sqrt{\kappa} + \frac{1}{\sqrt{\kappa}}\right)\cos\frac{\alpha}{2}. \tag{3.43}$$

If $\kappa = 1$, then the right-hand side is smaller than or equal to 2 in absolute value. This proves that $\kappa = 1$ implies (3.40). If now $\kappa \neq 1$ but $\sin(\alpha/2) = 0$, then $\cos(\alpha/2) = \pm 1$ and the right-hand side is strictly larger than 2 in absolute value. Hence if $\kappa \neq 1$, at least one of the two conditions in (3.40) is not satisfied, which proves the equivalence.

3.3.4   Log-law to area-law transition

We consider here the setup given by the matrix in Eq. (11). Defining

$$z_{k,t} = \rho e^{i\phi}, \qquad \rho > 0, \tag{3.44}$$

we have
$$\begin{aligned}
\operatorname{Im}\frac{\operatorname{tr}\mathcal{M}_k}{\sqrt{\det\mathcal{M}_k}} &= -\frac{2\rho\sin(\phi+2h)\sinh(2\lambda)}{\sqrt{1+\rho^2}}\\
\operatorname{Re}\frac{\operatorname{tr}\mathcal{M}_k}{\sqrt{\det\mathcal{M}_k}} &= \frac{2\rho\cos(\phi+2h)\cosh(2\lambda)}{\sqrt{1+\rho^2}}.
\end{aligned} \tag{3.45}$$

From the definition of $z_{k,t}$, we have

$$\rho^2 = \frac{\tan^2(k/2) + \tan^{-2}(k/2) + 2\cos(4t)}{4\sin^2(2t)}, \tag{3.46}$$

and

$$\tan\phi = -\cos k \tan(2t). \tag{3.47}$$

The condition $\sin(\phi + 2h) = 0$ is equivalent to $\tan\phi = -\tan(2h)$, which thus gives the equation

$$\cos k = \frac{\tan(2h)}{\tan(2t)}. \tag{3.48}$$

For this to have a solution one needs $|\tan(2h)| \le |\tan(2t)|$. Hence for $\lambda \ne 0$, the condition (i) of (3.40) is only satisfied for $k_c = \pm \arccos \frac{\tan(2h)}{\tan(2t)}$ when $|\tan(2h)| \le |\tan(2t)|$. Then the condition (ii) of (3.40) yields at $k = k_c$

$$\frac{\rho^2}{1 + \rho^2} \cosh^2(2\lambda) \le 1 \,. \tag{3.49}$$

Using the expression for ρ^2 and

$$\tan^2(k_c/2) = \frac{\tan(2t) - \tan(2h)}{\tan(2t) + \tan(2h)} \,, \tag{3.50}$$

one finds then that it is equivalent to $\lambda \le \lambda_c$ with the critical value of λ given by

$$\lambda_c = \frac{1}{2} \text{arcsinh} \left[\sqrt{\frac{2 \sin^2(2t)}{\cos(4t) + \frac{\tan^2(2t) + \tan^2(2h)}{\tan^2(2t) - \tan^2(2h)}}} \right] . \tag{3.51}$$

3.3.5   Proof of Eq. (30)

In this appendix, we prove Eq. (30) in the main text, where we obtain $\hat{\phi}(k)$ and $\hat{\psi}(k)$ by averaging over u:

$$\hat{\varphi}(k) = \frac{i}{2\pi} \int_0^{2\pi} du \frac{\mathfrak{f}(k, u) + \mathfrak{f}(k, u)^*}{1 + |\mathfrak{f}(k, u)|^2}$$

$$\hat{\psi}(k) = \frac{1}{2\pi} \int_0^{2\pi} du \frac{\mathfrak{f}(k, u) - \mathfrak{f}(k, u)^* + |\mathfrak{f}(k, u)|^2 - 1}{1 + |\mathfrak{f}(k, u)|^2} \,. \tag{3.52}$$

For a smooth bounded function $F(k, u)$ that is 2π periodic in u, we can decompose for $\epsilon > 0$

$$
\int_{-\pi}^{\pi} F(k, n\theta_k)\mathrm{d}k = \sum_{m=0}^{2\pi/\epsilon} \int_{-\pi+m\epsilon}^{-\pi+(m+1)\epsilon} \mathrm{d}k F(k, n\theta_k)
$$

$$
= \sum_{m=0}^{2\pi/\epsilon} \int_{-\pi+m\epsilon}^{-\pi+(m+1)\epsilon} \mathrm{d}k F(-\pi + m\epsilon, n\theta_k) + \mathcal{O}(\epsilon) \tag{3.53}
$$

$$
= \sum_{m=0}^{2\pi/\epsilon} \frac{1}{n\theta'_{-\pi+m\epsilon}} \int_{n\theta_{-\pi+m\epsilon}}^{n\theta_{-\pi+(m+1)\epsilon}} \mathrm{d}u F(-\pi + m\epsilon, u) + \mathcal{O}(\epsilon).
$$

Importantly, the $\mathcal{O}(\epsilon)$ can be bounded independently of n from the assumptions on F. Each of these terms in the sum has a limit when $n \to \infty$ given by

$$
\lim_{n\to\infty} \frac{1}{n\theta'_{-\pi+m\epsilon}} \int_{n\theta_{-\pi+m\epsilon}}^{n\theta_{-\pi+(m+1)\epsilon}} \mathrm{d}u F(-\pi+m\epsilon, u) = \frac{\theta_{-\pi+(m+1)\epsilon} - \theta_{-\pi+m\epsilon}}{2\pi\theta'_{\pi+m\epsilon}} \int_0^{2\pi} \mathrm{d}u F(-\pi+m\epsilon, u).
$$
$$
\tag{3.54}
$$

Hence we obtain

$$
\int_{-\pi}^{\pi} F(k, n\theta_k)\mathrm{d}k = \sum_{m=0}^{2\pi/\epsilon} \frac{\theta_{-\pi+(m+1)\epsilon} - \theta_{-\pi+m\epsilon}}{2\pi\theta'_{\pi+m\epsilon}} \int_0^{2\pi} \mathrm{d}u F(-\pi + m\epsilon, u) + \mathcal{O}(\epsilon) + \mathcal{O}(1/n)
$$

$$
= \frac{\epsilon}{2\pi} \sum_{m=0}^{2\pi/\epsilon} \int_0^{2\pi} \mathrm{d}u F(-\pi + m\epsilon, u) + \mathcal{O}(\epsilon) + \mathcal{O}(1/n)
$$

$$
= \frac{1}{2\pi} \int_{-\pi}^{\pi} \mathrm{d}k \int_0^{2\pi} \mathrm{d}u F(k, u) + \mathcal{O}(\epsilon) + \mathcal{O}(1/n).
$$
$$
\tag{3.55}
$$

We can now apply this to φ_j and ψ_j with $f_n(k)$ given in Eq. (28) of the main text:

$$
f_n(k) = \frac{b(k)\sin(n\theta_k)}{(-a(k) + \cos\theta_k)\sin(n\theta_k) + \sin(\theta_k)\cos(n\theta_k)}, \tag{3.56}
$$

For example for φ_j we would choose

$$
F(k, u) = ie^{-ikj} \frac{\mathfrak{f}(k, u) + \mathfrak{f}(k, u)^*}{1 + |\mathfrak{f}(k, u)|^2}, \tag{3.57}
$$

with the definition

$$\mathfrak{f}(k, u) = \frac{b(k) \sin u}{(-a(k) + \cos \theta_k) \sin u + \sin \theta_k \cos u}, \tag{3.58}$$

and we see that $F(k, u)$ is indeed smooth and bounded in absolute value by 1. Hence we obtain that φ_j and ψ_j converge when $n \to \infty$ to $\bar{\varphi}_j$ and $\bar{\psi}_j$ with $\hat{\varphi}(k)$ and $\hat{\psi}(k)$ given by (3.52).

3.3.6   Proof of Eq. (31)

We follow Ref.[109] to prove Eq. (31) in the main text. Denoting $\pm i\nu_p$ the eigenvalues of Γ, the entanglement entropies $S_m(\ell)$ are

$$S_m(\ell) = \sum_{p=1}^{\ell} H_m(\nu_p). \tag{3.59}$$

Defining

$$D(\lambda) = \det[i\lambda \operatorname{Id}_{2\ell} - \Gamma], \tag{3.60}$$

we have $D(\lambda) = \prod_{p=1}^{\ell}(\lambda^2 - \nu_p^2)$, and so $S_m(\ell)$ can be written as a contour integral in the upper-half plane of $\partial_\lambda \log D(\lambda)$ multiplied by $H_m(\lambda)$, since each ν_p is a simple pole of $\partial_\lambda \log D(\lambda)$. Let us introduce the 2×2 matrices $\hat{\Pi}(k)$ by

$$\bar{\Pi}_j = \frac{1}{2\pi} \int_{-\pi}^{\pi} dk e^{-ikj} \hat{\Pi}(k), \tag{3.61}$$

where $\bar{\Pi}_j$ denotes the limit $n \to \infty$ of Π_j. It reads

$$\hat{\Pi}(k) = \begin{pmatrix} -\hat{\varphi}(k) & \hat{\psi}(k) \\ -\hat{\psi}(-k)^* & \hat{\varphi}(k) \end{pmatrix}. \tag{3.62}$$

Now, using Szego's lemma, we have when $\ell \to \infty$

$$\log D(\lambda) = \frac{\ell}{2\pi} \int_0^{2\pi} \mathrm{d}k \, \log \det[i\lambda \, \mathrm{Id}_2 - \hat{\Pi}(k)] + \mathcal{O}(\log \ell) \,. \tag{3.63}$$

We find, using $\hat{\psi}(-k) = \hat{\psi}(k)^*$

$$\det[i\lambda \, \mathrm{Id}_2 - \hat{\Pi}(k)] = |\hat{\psi}(k)|^2 + |\hat{\varphi}(k)|^2 - \lambda^2 \,. \tag{3.64}$$

Hence $\partial_\lambda \log D(\lambda)$ has simple poles at

$$\lambda = \pm\sqrt{|\hat{\psi}(k)|^2 + |\hat{\varphi}(k)|^2} \,. \tag{3.65}$$

Hence, carrying the contour integral yields Eq. (31) of the main text.

3.3.7 Proof of Eq. (34)

In this appendix, we prove the statement in the main text that

$$|\hat{\varphi}(k)|^2 + |\hat{\psi}(k)|^2 < 1 \tag{3.66}$$

when k is critical. Since $x \to x^2$ is a strictly convex function, we have for any function $F(u)$

$$\left(\frac{1}{2\pi} \int_0^{2\pi} \mathrm{d}u F(u) \right)^2 \leq \frac{1}{2\pi} \int_0^{2\pi} \mathrm{d}u F(u)^2 \,, \tag{3.67}$$

with equality if and only if $F(u)$ is constant. We then write

$$|\hat{\varphi}(k)|^2 + |\hat{\psi}(k)|^2 = \left(\frac{1}{2\pi} \int_0^{2\pi} \mathrm{d}u \frac{2\Re\mathfrak{f}(k,u)}{1 + |\mathfrak{f}(k,u)|^2} \right)^2 + \left(\frac{1}{2\pi} \int_0^{2\pi} \mathrm{d}u \frac{|\mathfrak{f}(k,u)|^2 - 1}{1 + |\mathfrak{f}(k,u)|^2} \right)^2$$
$$+ \left(\frac{1}{2\pi} \int_0^{2\pi} \mathrm{d}u \frac{2\Im\mathfrak{f}(k,u)}{1 + |\mathfrak{f}(k,u)|^2} \right)^2 \,. \tag{3.68}$$

56

Since $\mathfrak{f}(k, u)$ is not constant in u, we have

$$|\hat{\varphi}(k)|^2+|\hat{\psi}(k)|^2 < \frac{1}{2\pi} \int_0^{2\pi} du \left[\left(\frac{2\Re\mathfrak{f}(k, u)}{1 + |\mathfrak{f}(k, u)|^2} \right)^2 + \left(\frac{2\Im\mathfrak{f}(k, u)}{1 + |\mathfrak{f}(k, u)|^2} \right)^2 + \left(\frac{|\mathfrak{f}(k, u)|^2 - 1}{1 + |\mathfrak{f}(k, u)|^2} \right)^2 \right].$$

(3.69)

The integrand simplifies to 1, yielding (3.66).

3.3.8 Critical exponents

The entanglement entropy is given by

$$S_m(\ell) = \frac{\ell}{2\pi} \int_{-\pi}^{\pi} dk H_m \left(\sqrt{|\hat{\varphi}(k)|^2 + |\hat{\psi}(k)|^2} \right) + \mathcal{O}(\log \ell).$$

(3.70)

Since $|\hat{\varphi}(k)|^2 + |\hat{\psi}(k)|^2 = 1$ when k is not critical, and since $H_m(1) = 0$, only the critical values of k contribute to the volume law scaling. Hence we have

$$S_m(\ell) = \frac{\ell}{\pi} \int_{k_c}^{\pi - k_c} dk H_m \left(\sqrt{|\hat{\varphi}(k)|^2 + |\hat{\psi}(k)|^2} \right) + \mathcal{O}(\log \ell).$$

(3.71)

where k_c satisfies

$$\tan(k_c/2)^2 + \tan(k_c/2)^{-2} = \frac{4\cos^4(2x)}{\sinh^2(2\lambda)} + 2\cos(4x).$$

(3.72)

Recall that the entanglement entropy $S_m(\ell)$ has the following behaviour at large ℓ

$$S_m(\ell) = \begin{cases} s_m(\lambda)\ell, & \text{if } \lambda < \lambda_c \\ \mathcal{O}(\ell^0), & \text{if } \lambda > \lambda_c, \end{cases}$$

(3.73)

with $s_m(\lambda)$ some coefficient. We define the critical exponent ν by the leading behaviour of $s_m(\lambda)$ when $\lambda \to \lambda_c$

$$s_m(\lambda) = a_m(\lambda_c - \lambda)^\nu + \mathcal{O}((\lambda_c - \lambda)^{\nu'}),$$

(3.74)

57

where $\nu' > \nu$. This critical behaviour can be studied performing an expansion of (3.71) when $\lambda \to \lambda_c$. To that end, we need the dominant expression of k_c and θ_k when $\lambda \to \lambda_c$. Firstly, from (3.72) we find

$$k_c = \frac{\pi}{2} - \frac{2\sin(2x)}{\sqrt{\tanh(2\lambda_c)}}\sqrt{\lambda_c - \lambda} + \mathcal{O}(\lambda_c - \lambda).$$ (3.75)

We now perform an expansion of θ_k for $k \in [k_c, \pi - k_c]$. We note that as $\lambda \to \lambda_c$, we have $k_c \to \pi/2$, so the values of $k \in [k_c, \pi - k_c]$ also come close to $\pi/2$. This requires thus an expansion of θ_k in $(k - \pi/2)^2$ and $\lambda_c - \lambda$. We find

$$\theta_k = \sqrt{8\sin^2(2x)\sinh(4\lambda_c)(\lambda_c - \lambda) - 2\cos^2(2x)[\cosh(4\lambda_c) + \cos(4x)](k - \tfrac{\pi}{2})^2}$$
$$+ \mathcal{O}(\lambda_c - \lambda) + \mathcal{O}(k - \tfrac{\pi}{2})^2.$$ (3.76)

We then need the behaviour of $\hat{\varphi}, \hat{\psi}$ perturbatively in $\lambda_c - \lambda$. For a, b, c, d, e, f constants and $\theta \to 0$ we have the expansion

$$\frac{1}{2\pi} \int_0^{2\pi} \mathrm{d}u \frac{a\sin^2 u + b\theta \sin u \cos u + c\theta^2}{d\sin^2 u + e\theta \sin u \cos u + f\theta^2}$$
$$= \frac{a}{d} + \frac{2|\theta|}{\pi} \int_0^\infty \frac{(dc - fa - eb + \frac{e^2 a}{d})u^2 + fc - \frac{f^2 a}{d}}{d^2 u^4 + (2df - e^2)u^2 + f^2} \mathrm{d}u + \mathcal{O}(\theta^2),$$ (3.77)

To prove this, we write

$$\int_0^{2\pi} \mathrm{d}u \frac{a\sin^2 u + b\theta \sin u \cos u + c\theta^2}{d\sin^2 u + e\theta \sin u \cos u + f\theta^2} = 2\pi\frac{a}{d} + \int_{-\pi}^\pi \mathrm{d}u \frac{(b - \frac{ea}{d})\theta \sin u \cos u + (c - \frac{fa}{d})\theta^2}{d\sin^2 u + e\theta \sin u \cos u + f\theta^2}.$$ (3.78)

Then we decompose the integral into the intervals $[-\epsilon, \epsilon]$, $[\pi - \epsilon, \pi]$, $[-\pi, -\pi + \epsilon]$ and the rest denoted I, for some $\epsilon > 0$. The limit $\theta \to 0$ can be taken directly on I, and using the change of variable $u \to -u$ one finds $I = \mathcal{O}(\theta^2)$. On $[-\epsilon, \epsilon]$, provided ϵ is small enough we can replace $\sin u$ by u and $\cos u$ by 1. Then we perform the change of variable $u = \theta v$ and

take the limit $\theta \to 0$. With a similar process on the other intervals, we obtain (3.77).

Using (3.77), we find

$$\sqrt{|\hat{\varphi}(k)|^2 + |\hat{\psi}(k)|^2} = 1 - \gamma|\theta_k| + \mathcal{O}(\theta_k^2) \,, \tag{3.79}$$

with after some algebra

$$\gamma = \frac{4}{\pi} \int_0^\infty du \frac{|b|^2 u^2 + \frac{|b|^2}{|b|^2+|1-a|^2}}{(|b|^2 + |1-a|^2)^2 u^4 + 2[|b|^2 + |1-a|^2 - 2(\Re(1-a))^2]u^2 + 1} \,, \tag{3.80}$$

where the coefficients $a(k), b(k)$ are evaluated at $k = \pi/2$, and that we recall are defined as the coefficients of the matrix $\mathcal{M}_k/\sqrt{\det \mathcal{M}_k}$ in Eq. (16) of the main text, as in Eq. (7). Explicitly

$$a(\pi/2) = \sin^2(2x)e^{-4\lambda_c} - \cos^2(2x)e^{4ix} \,, \qquad b(\pi/2) = \sin(2x)\cos(2x)(e^{-4\lambda_c} + e^{4ix}) \,. \tag{3.81}$$

From (3.71) we have then for $m \geq 2$

$$\begin{aligned}
s_m(\lambda) &= \frac{2}{\pi} \int_{k_c}^{\pi/2} dk H_m\left(\sqrt{|\hat{\varphi}(k)|^2 + |\hat{\psi}(k)|^2}\right) \\
&= -\frac{2\gamma H_m'(1)}{\pi} \int_{k_c}^{\pi/2} dk\theta_k + \mathcal{O}((\lambda_c - \lambda)^{3/2}) \,.
\end{aligned} \tag{3.82}$$

Using (3.76) and (3.75) we find

$$\begin{aligned}
\int_{k_c}^{\pi/2} dk\theta_k &= 8\sin^2(2x)\cosh(2\lambda_c)(\lambda_c - \lambda) \int_0^1 dy\sqrt{1-y^2} + \mathcal{O}((\lambda_c - \lambda)^{3/2}) \\
&= 2\pi \sin^2(2x)\cosh(2\lambda_c)(\lambda_c - \lambda) + \mathcal{O}((\lambda_c - \lambda)^{3/2}) \,.
\end{aligned} \tag{3.83}$$

59

Hence we obtain the following behaviour for $m \geq 2$

$$s_m(\lambda) = 2\gamma \sin^2(2x) \cosh(2\lambda_c) \frac{m}{m-1}(\lambda_c - \lambda) + \mathcal{O}((\lambda_c - \lambda)^{3/2}), \tag{3.84}$$

and all the Rényi entropies have the critical exponent

$$\nu = 1. \tag{3.85}$$

As for the von Neumann entropy, we have

$$H_1(1 - \epsilon) = \frac{\epsilon}{2}\left(1 - \log\frac{\epsilon}{2}\right) + \mathcal{O}(\epsilon^2). \tag{3.86}$$

Hence it displays a marginally corrected critical behaviour as

$$s_1(\lambda) = \gamma \sin^2(2x) \cosh(2\lambda_c) \frac{(1 - 2\log 2)}{2}(\lambda_c - \lambda) \log(\lambda_c - \lambda) + \mathcal{O}(\lambda_c - \lambda). \tag{3.87}$$

As for the Hartley entropy, we have

$$s_0(\lambda) = \frac{2}{\pi} \int_{k_c}^{\pi/2} \mathrm{d}k, \tag{3.88}$$

so

$$s_0(\lambda) = \frac{4\sin(2x)}{\pi\sqrt{\tanh(2\lambda_c)}}\sqrt{\lambda_c - \lambda} + \mathcal{O}(\lambda_c - \lambda), \tag{3.89}$$

yielding the critical exponent

$$\nu = \frac{1}{2}. \tag{3.90}$$

3.4 Additional results

Here we study the quasi-periodic circuit of Ref. [106] and recover the volume-law to log-law transition by studying Möbius transformations. This section was inspired by conversations with Peter Lu, Tarun Grover, and Etienne Granet.

3.4.1 Quasi-periodic circuit

The non-unitary circuit in Ref. [106] is given by

$$V(T) = \prod_{t=1}^{T} e^{i\tilde{h} \sum_r \sigma_r^x} e^{i\tilde{J}_t \sum_r \sigma_r^z \sigma_{r+1}^z}. \tag{3.91}$$

For ease of analysis, we will switch the two terms, and study the circuit

$$V(T) = \prod_{t=1}^{T} e^{i\tilde{J}_t \sum_r \sigma_r^x} e^{i\tilde{h} \sum_r \sigma_r^z \sigma_{r+1}^z}, \tag{3.92}$$

so that the quasi-periodicity is in the σ_r^x term. We found that for a single round, the Mobius transformation is

$$M_k(t) = \begin{pmatrix} e^{4i\tilde{J}_t} \left(e^{4i\tilde{h}} + \frac{1}{\tan^2(k/2)} \right) & e^{4i\tilde{J}_t}(1 - e^{4i\tilde{h}})\frac{i}{\tan(k/2)} \\ -(1 - e^{4i\tilde{h}})\frac{i}{\tan(k/2)} & 1 + e^{4i\tilde{h}}\frac{1}{\tan^2(k/2)} \end{pmatrix} \tag{3.93}$$

For the quasi-periodic circuit, Ref. [106] defined

$$\begin{aligned} \tilde{J}_t &= -\frac{\pi}{4} + \frac{i}{2} \log \tan(h_t) \\ \tilde{h} &= \arctan(-i e^{-2iJ}), \end{aligned} \tag{3.94}$$

where

$$h_t = h + \lambda \cos(2\pi Q t + \delta), \tag{3.95}$$

and Q is irrational. Simplifying (3.94), we get

$$
\begin{aligned}
\tilde{J}_t &= -\left(-\frac{\pi}{4} + \frac{\pi}{2}\frac{1}{2}\left(1 - \mathrm{sgn}(\tan(h_t)))\right)\right) + \frac{i}{2}\log|\tan(h_t)| \\
\tilde{h} &= -\frac{\pi}{4} + \frac{1}{2}\log\tan(J)i.
\end{aligned}
\tag{3.96}
$$

M_k simplifies to

$$
M_k(t) = \begin{pmatrix}
-\frac{1}{\tan^2(h_t)}\left(-\frac{1}{\tan^2(J)} + \frac{1}{\tan^2(k/2)}\right) & -\frac{1}{\tan^2(h_t)}\left(1 + \frac{1}{\tan^2(J)}\right)\frac{i}{\tan(k/2)} \\
-\left(1 + \frac{1}{\tan^2(J)}\right)\frac{i}{\tan(k/2)} & 1 - \frac{1}{\tan^2(J)}\frac{1}{\tan^2(k/2)}
\end{pmatrix}.
\tag{3.97}
$$

We must now check whether or not $M_k(t)$ satisfies (3.12), to determine whether or not k is critical. To check whether or not $M_k(t)$ satisfies the first condition, we must check whether $\det(M_k(t))$ is positive or negative. We have

$$
\begin{aligned}
\det(M_k(t)) \sim &\left(\frac{1}{\tan^2(J)} - \frac{1}{\tan^2(k/2)}\right)\left(1 - \frac{1}{\tan^2(J)\tan^2(k/2)}\right) \\
&+ \left(1 + \frac{1}{\tan^2(J)}\right)^2 \frac{1}{\tan^2(k/2)}.
\end{aligned}
\tag{3.98}
$$

This quantity is positive for all k, so $M_k(t)$ satisfies the first condition for all h_t. Next, we need to check if $M_k(t)$ satisfies the second condition. We evaluate

$$
\left|\frac{-\frac{1}{\tan(h_t)}\left(-\frac{1}{\tan^2(J)} + \frac{1}{\tan^2(k/2)}\right) + \tan(h_t)\left(1 - \frac{1}{\tan^2(J)}\frac{1}{\tan^2(k/2)}\right)}{\sqrt{\left(\left(\frac{1}{\tan^2(J)} - \frac{1}{\tan^2(k/2)}\right)\left(1 - \frac{1}{\tan^2(J)\tan^2(k/2)}\right) + \left(1 + \frac{1}{\tan^2(J)}\right)^2\frac{1}{\tan^2(k/2)}\right)}}\right| \leq 2.
\tag{3.99}
$$

One can check that this is always satisfied for a region of k as long as $\tan(h_t) \neq 0 (h_t \neq 0, \pi)$ and $\tan(h_t) \neq \infty \left(h_t \neq \pm\frac{\pi}{2}\right)$, as expected of a non-unitary circuit with a dual that is unitary.

Now if we have a quasiperiodic circuit with $\lambda > \lambda_c$, then in the limit of infinite time, there will be time steps where h_t gets arbitrarily close to π. Notice that in the periodic case,

h_t can also hit π for $\lambda > \lambda_c$, but one must finely tune δ. Therefore, there should also be a volume-law to log-law transition with appropriately tuned δ. In the quasi-periodic case, this does not depend on δ. Suppose that this happens at $t = t_n$. Then

$$M_k(t_n, \ldots t_1) = M_k(t_n)M_k(t_{n-1}, \ldots t_1). \tag{3.100}$$

For $h_t \to \pi$, we have

$$\left| \frac{\text{Tr}(M_k(t_n, \ldots t_1))}{\sqrt{\det(M_k(t_n, \ldots t_1))}} \right| \sim \frac{1}{\tan(h_t)} \to \infty. \tag{3.101}$$

This violates the second condition, so in the infinite time limit, there is no finite range of critical k. The physical intuition for this is the same as in Ref. [106], that transition comes from there being a projective measurement on all the sites, for $\lambda > \lambda_c$.

CHAPTER 4

STORY 3: TOPOLOGICAL PHASES AND GAPLESS EDGES

4.1   Introduction: Models for topological phases

A local commuting projector Hamiltonian (LCPH) is a Hamiltonian defined on a lattice Λ, that takes the form

$$H = \sum_{r \in \Lambda} H_r, \tag{4.1}$$

where each term H_r is supported within a bounded distance ξ of the site r, up to exponential tails. The defining features of a LCPH are that (1) the local terms are projectors and (2) they all commute with each other:

$$[H_r, H_{r'}] = 0 \qquad H_r^2 = H_r = H_r^{\dagger} \qquad \forall r, r' \in \Lambda. \tag{4.2}$$

These models are exactly solvable despite being strongly interacting. Specifically, their ground states and excited states can be obtained by finding simultaneous eigenstates of the local Hamiltonian terms. For example, the ground state is explicitly given by

$$P_{\mathrm{GS}} = \prod_{r \in \Lambda} \left(\frac{1 - H_r}{2} \right), \tag{4.3}$$

and excited states can be obtained by violating local projectors.

LCPHs have contributed greatly to our understanding of gapped phases of matter. Gapped phases of matter are phases where a set of degenerate ground states are separated from the excited states by a gap Δ that does not vanish in the thermodynamic limit. In particular, LCPHs can be constructed for broad classes of topological phases[13, 44, 14, 113, 15, 16, 114]. For example, the toric code[11] and many other two-dimensional topological orders have a corresponding string-net model[13], which is a LCPH.

Given the broad applicability of LCPHs, it is important to study their limitations: what phases *cannot* be realized by LCPHs? In two spatial dimensions, it is hypothesized that any topological order that does not admit a gapped boundary cannot be realized by a LCPH. There are some partial proofs of this hypothesis. For example, if a topological phase has a nonzero chiral central charge c_-, then it does not admit a gapped edge, and does not have any LCPH realization. To see why this is the case, note that the chiral central charge is proportional to energy current at the edge[12]:

$$I = \frac{\pi}{12}c_- T^2,$$
(4.4)

where T is the temperature. However, the energy current from A to B is given by[12, 115]

$$I_{AB} = \sum_{a \in A} \sum_{b \in B} \langle -i[H_a, H_b] \rangle,$$
(4.5)

where the expectation value is taken in the thermal state $\rho \sim e^{-\beta H}$. It follows that for a commuting projector Hamiltonian, c_- must be zero. Some topological phases have $c_- = 0$ but have a nonzero *electric* Hall conductance[116]. It was shown in Ref. [30] that these phases also cannot be realized by commuting projector Hamiltonians. However, the proof in Ref. [30] relies on abstract methods in algebraic geometry, that do not give much physical intuition for the result. Instead, we use a flux insertion argument, based on a real-space formula for the Hall conductance, to prove the the result in a physically intuitive way. This proof not only clarifies the physical reason for the result, but it also shows why there are certain loopholes, such as using infinite-dimensional local Hilbert spaces. In additional, while the proof in Ref. [30] is restricted to the case where the local terms $\{H_r\}$ are strictly local, our proof also applies to $\{H_r\}$ with exponentially decaying tails. This allows us to use our proof to show that any system of non-interacting electrons with exponentially localized Wannier functions has a vanishing Hall conductance.

4.2 Vanishing Hall conductance for commuting Hamiltonians

This chapter is reprinted with permission from:

Carolyn Zhang and Michael Levin. Vanishing Hall conductance for commuting Hamiltonians.

Phys. Rev. B 105, L081103, Feb 2022.

© 2020 American Physical Society

Abstract

We consider the process of flux insertion for ground states of almost local commuting projector Hamiltonians in two spatial dimensions. In the case of finite dimensional local Hilbert spaces, we prove that this process cannot pump any charge and we conclude that the Hall conductance must vanish.

4.2.1 Introduction

A local commuting projector Hamiltonian (LCPH) is a special kind of quantum lattice model of the form $H = \sum_r H_r$, where each H_r is a projection operator supported on a finite collection of nearby lattice sites, and where the different H_r's commute with one another. Lattice models of this kind, such as the toric code model[11], have proven to be powerful tools for studying interacting topological phases of matter. Given the many applications of these models[13, 44, 15, 16, 18], it is important to understand their limitations: that is, what phases *cannot* be realized by LCPHs? In two dimensions, it is known[1] that one class of such phases are those with a nonzero thermal Hall conductance[117]. In this work, we show that another class of such phases are those with a nonzero *electric* Hall conductance ν. This claim was first proved in Ref. [30] using algebraic geometry. Here, we give a simple and physically motivated proof based on the idea of flux insertion. Our techniques are closely related to

---

1. To see why the thermal Hall conductance must vanish for commuting Hamiltonians, note that the energy current $f_{jk} = 0$ in Eq. (154) of Ref. [117], and hence one can choose $h_{jkl} = 0$ in Eq. (159), which leads to a vanishing thermal Hall conductance in Eq. (160).

those of Refs. [118, 119, 120]. Our argument has the additional advantage that it extends to *almost* local CPHs (ALCPHs), a generalization of LCPHs that includes Hamiltonians with interactions that decay faster than any power.

4.2.2 Physical argument.

We first present an intuitive, but non-rigorous, argument for our no-go result. This argument is similar to our main argument, but not as general, since it applies only to *strictly* local commuting projector Hamiltonians. It also assumes the "local topological quantum order" (LTQO) property (4.11), which is stronger than the property (4.12) used in the main argument.

Imagine starting in a ground state $|\Omega\rangle$ of a two dimensional LCPH and then adiabatically inserting $\pm 2\pi$ flux at two punctures. This process can be implemented by a string operator U localized along a line between the two punctures, as illustrated in Fig. 4.1. By the Laughlin argument [121, 122], the amount of charge pumped by this process from one puncture to the other is equal to $2\pi\nu$. Let B be a region surrounding one of the two punctures, and let Q_B be the operator that measures the total charge in region B. The charge pumped by the flux insertion is then $\langle\Omega|U^\dagger Q_B U - Q_B|\Omega\rangle$, so the Hall conductance is

$$\nu = \frac{1}{2\pi}\langle\Omega|U^\dagger Q_B U - Q_B|\Omega\rangle, \tag{4.6}$$

Since the system is charge conserving and the current flows only along the string, the operator $T \equiv U^\dagger Q_B U - Q_B$ is localized near the point where the string intersects the boundary of B, as indicated in Fig. 4.1.

Now consider the charge pumped by inserting many units of flux, written as a telescoping sum:

$$\langle\Omega|U^{\dagger n}Q_B U^n - Q_B|\Omega\rangle = \sum_{k=0}^{n-1}\langle\Omega|U^{\dagger k}T U^k|\Omega\rangle. \tag{4.7}$$

67
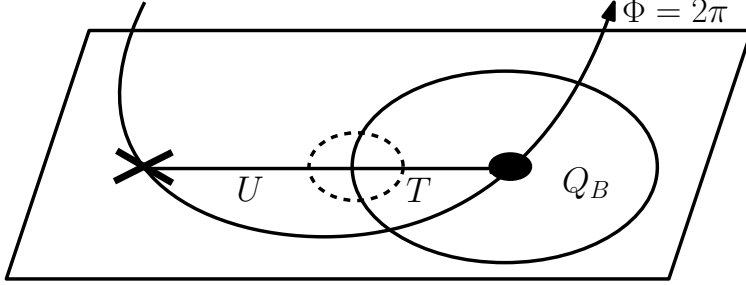
Figure 4.1: Setup for physical argument. A string operator U inserts $\pm 2\pi$ flux at its end-points. This operation pumps charge from one puncture to the other, increasing the total charge Q_B within region B (solid circle). The operator $T = U^\dagger Q_B U - Q_B$ measuring the change in Q_B is supported in the small dotted circle. For an LCPH, U commutes exactly with all Hamiltonian terms that are supported away from the two punctures.

Crucially, for an LCPH, the operator U commutes exactly with all H_r terms away from the two punctures (we justify this claim below). This means, in particular, that $U^k|\Omega\rangle$ does not contain any excitations away from the two punctures, i.e. it is a "local ground state" in this region. Then, assuming that the Hamiltonian obeys the local TQO condition (4.11), we deduce that $U^k|\Omega\rangle$ must have the same expectation values as $|\Omega\rangle$ for any local observable supported away from the punctures. In particular, specializing to the observable T, we deduce that $\langle\Omega|U^{k\dagger}TU^k|\Omega\rangle = \langle\Omega|T|\Omega\rangle$. We conclude that all of the terms in the sum in (4.7) give the same quantity $2\pi\nu$, so the right hand side evaluates to $2\pi n\nu$.

At the same time, the absolute value of the left hand side of (4.7) is bounded by $|q_{\max} - q_{\min}|$ where $q_{\max}$ and $q_{\min}$ are the largest and smallest eigenvalues of Q_B. Hence, we have the bound $2\pi n|\nu| \leq |q_{\max} - q_{\min}|$. Since n can be made arbitrarily large, we conclude that $\nu = 0$.

To complete the argument, we now explain why U commutes with all the H_r terms away from the two punctures. The key point is that all the H_r terms that are supported away from the two punctures remain commuting projectors throughout the flux insertion process[30]. Therefore, if the system starts in an eigenspace of some H_r away from the punctures, it will stay in this eigenspace throughout the flux insertion, since all the terms in the Hamiltonian commute with $H_r(t)$ at all times, and the process is adiabatic. In particular, the system

is in the same eigenspace at the end of the process as at the beginning, implying that U commutes with H_r.

This behavior should be contrasted with that of non-commuting Hamiltonians: in that case, U does not commute with H_r, so there is no reason that $U^k|\Omega\rangle$ has to be in a ground state away from the two punctures for arbitrarily large k. Instead, every time we apply U, we create additional (possibly charged) excitations, that spread outward from the two punctures as k increases. When k is large enough, the excited region in $U^k|\Omega\rangle$ reaches the support of T and the total pumped charge stops growing linearly. Hence ν can be nonzero without contradiction.

An important loophole in the above no-go argument is that it assumes that Q_B has a bounded spectrum. This assumption can break down if the Hilbert space on each lattice site is infinite dimensional. This explains how the LCPH in Ref. [123] can realize a state with $\nu \neq 0$: the example given there uses a system built out of infinite dimensional rotor degrees of freedom. In such a system, a finite region B can absorb an infinite amount of charge, so ν can be nonzero.

We now turn to a rigorous version of this argument based on *infinitesimal* flux insertion. This argument applies to a more general class of almost local commuting projector Hamiltonians (ALCPHs).

4.2.3 Setup

We consider a sequence of two dimensional lattice spin systems of increasing linear size L, defined on a torus geometry. We denote the lattice by $\Lambda = \{-L/2 + 1, \cdots, L/2 - 1, L/2\}^2$ where we take L to be even for convenience. Each site $r \in \Lambda$ corresponds to a finite dimensional local Hilbert space, where the dimension is fixed and does not depend on L. In the following, all constants are uniform in the system size; the notation $\mathcal{O}(L^{-\infty})$ means $\leq C_k L^{-k}$ for all k, for some constant C_k.

We consider Hamiltonians that are sums of commuting projectors of the form

$$H = \sum_{r \in \Lambda} H_r, \quad [H_r, H_{r'}] = 0, \quad H_r^2 = H_r = H_r^\dagger. \tag{4.8}$$

Each projector H_r is "almost local" in the sense that H_r commutes with operators $O_{r'}$, supported on a single site r', up to error superpolynomially small in the distance $|r - r'|$:

$$\|[H_r, O_{r'}]\| \leq \|O_{r'}\| \cdot \mathcal{O}(|r - r'|^{-\infty}). \tag{4.9}$$

We also assume each H_r is charge conserving:

$$[H_r, Q_\Lambda] = 0 \qquad \forall r \in \Lambda, \tag{4.10}$$

where $Q_\Lambda = \sum_{r \in \Lambda} q_r$ is a sum of Hermitian charge operators q_r, each supported on site r, with an integer spectrum and a uniformly bounded norm. In addition, we assume that the number of ground states of H remains bounded as $L \to \infty$ and that these ground states are simultaneous eigenstates of the projectors $\{H_r : r \in \Lambda\}$ with eigenvalue 0 (i.e. H is frustration-free).

To state our final assumption, we first need to introduce some notation. For any region R, we define the corresponding "local ground state subspace" V_R to be the set of all states that are annihilated by the projectors $\{H_r : r \in R\}$. We denote the projector onto V_R by P_R, and we denote the expectation value of an observable O, averaged over V_R, by $\langle O \rangle_R = \frac{1}{\text{Tr}(P_R)} \text{Tr}(P_R O)$. We use the abbreviation $P \equiv P_\Lambda$ to denote the projector onto the global ground state subspace, and likewise we use the notation $\langle O \rangle \equiv \langle O \rangle_\Lambda$ to denote the average over the global ground state subspace.

Our final assumption is a weaker version of the local topological order (LTQO) condition of Refs. [124, 125]. The usual LTQO condition states that for any region R, and any local

observable $O_{\tilde{R}}$ supported in a smaller region $\tilde{R} \subset R$, the expectation value of $O_{\tilde{R}}$ in (any) local ground state $|\Psi_R\rangle \in V_R$ is approximately the same as the expectation value in (any) global ground state $|\Omega\rangle$:

$$\langle\Psi_R|O_{\tilde{R}}|\Psi_R\rangle = \langle\Omega|O_{\tilde{R}}|\Omega\rangle + \|O_{\tilde{R}}\| \cdot \mathcal{O}(\mathrm{dist}(\tilde{R}, R^c)^{-\infty}), \tag{4.11}$$

where R^c is the complement of R in Λ. In this paper, we will only need the weaker property that the *average* expectation value of $O_{\tilde{R}}$ over the local ground state subspace V_R is approximately equal to the average expectation value of $O_{\tilde{R}}$ over the global ground state subspace:

$$\langle O_{\tilde{R}}\rangle_R = \langle O_{\tilde{R}}\rangle + \|O_{\tilde{R}}\| \cdot \mathcal{O}(\mathrm{dist}(\tilde{R}, R^c)^{-\infty}). \tag{4.12}$$

Note that (4.12), unlike (4.11), does not require local indistinguishability of ground states. Rather, it can be interpreted as a local response condition: it says that local observables $O_{\tilde{R}}$ have approximately the same (zero temperature) expectation values in the full system as they do in a subsystem $R \supset \tilde{R}$. One difference between (4.12) and the usual LTQO condition (4.11) is that (4.12) can be satisfied by systems with spontaneous symmetry breaking, while such systems generally violate (4.11).

4.2.4 Hall conductance

To define the Hall conductance within this setting, we consider a geometry consisting of two overlapping disks A and B of radius $\frac{L}{4}$, centered at $(-\frac{L}{8}, 0)$ and $(\frac{L}{8}, 0)$ respectively (see Fig. 4.2).

Our definition involves a string operator K_A^- that runs along the lower half boundary of A and that inserts an infinitesimal flux into the center of B. To construct K_A^-, we assume
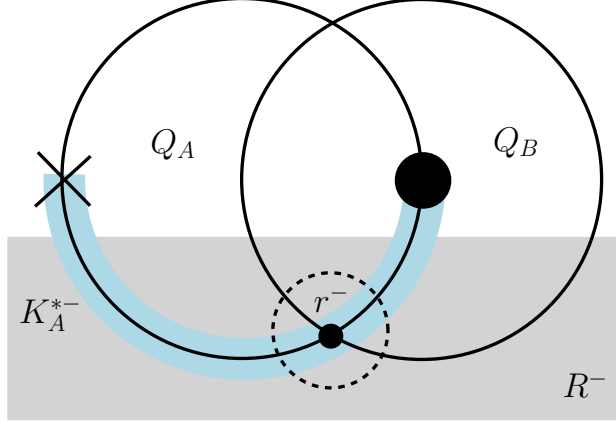
Figure 4.2: Geometry of main argument. Two disks A, B with charge Q_A, Q_B, intersect in the lower half torus at point r^-. The operators K_A^{*-} and $[K_A^{*-}, Q_B]$ are supported in the blue strip and the dotted circle respectively. The operator $Q_A - K_A^{*-}$ commutes (up to $\mathcal{O}(L^{-\infty})$) with P_{R^-}, the projector into the local ground state subspace of the (shaded) region R^-.

the existence of an operator K_A with two properties. First, K_A satisfies

$$[Q_A - K_A, P] = 0. \tag{4.13}$$

Second, K_A is supported "near" the boundary of A. More precisely, K_A can be approximated, up to $\mathcal{O}(L^{-\infty})$, by a sum of terms of the form

$$K_A = \sum_{r \in \partial_{\alpha L} A} \overline{K}_{r,A} + \mathcal{O}(L^{-\infty}) \tag{4.14}$$

where $\partial_{\alpha L} A = \{r \in \Lambda : \max(\operatorname{dist}(r, A), \operatorname{dist}(r, A_c)) \leq \alpha L\}$ is a strip of width $2\alpha L$ along the boundary of A, with $0 < \alpha \leq \frac{1}{32}$. Here, each $\overline{K}_{r,A}$ is a strictly local charge conserving operator, with a uniformly bounded norm, supported in $D_{\alpha L}(r)$, a disk of radius αL centered at r. It has been shown that an operator K_A with these two properties can be constructed for all gapped, charge conserving Hamiltonians[126, 118].

Given a K_A with these properties, we construct a corresponding string operator K_A^- by restricting the sum in (4.14) to sites in the lower half torus, which we denote by $\Lambda^- = \{r \in$

$\Lambda : r_y \leq 0\}$:

$$K_A^- = \sum_{r \in (\partial_{\alpha L} A) \cap \Lambda^-} \overline{K}_{r,A}. \tag{4.15}$$

To see why K_A^- inserts an infinitesimal flux, note that for $\theta \ll 1$, the operator $e^{i\theta K_A}$ has the same action on ground states as the gauge transformation $e^{i\theta Q_A}$ by (4.13); likewise, the restricted operator $e^{i\theta K_A^-}$ acts like a gauge transformation along the lower boundary of A but acts trivially along the upper boundary of A, exactly as one expects for an infinitesimal flux insertion operator.

With these preliminaries, we can now define the Hall conductance in a form that is most convenient for our purposes:

$$\nu = -i \lim_{L \to \infty} \langle [K_A^-, Q_B] \rangle. \tag{4.16}$$

This expression can be interpreted as the charge pumped into B by an infinitesimal flux insertion.

Note that (4.16) can be related to the more familiar Kubo formula for the Hall conductance. Using (4.13) but with B instead of A, we see that $\langle [K_A^-, Q_B] \rangle = \langle [K_A^-, K_B] \rangle$ by cyclicity of the trace. K_B can then be replaced by K_B^-, up to $\mathcal{O}(L^{-\infty})$, giving $\nu = -i \lim_{L \to \infty} \langle [K_A^-, K_B^-] \rangle$. This is the adiabatic curvature [126, 127], which is well-known [128] to express the Kubo linear response coefficient in the QHE.

Importantly, *any* K_A satisfying (4.13) and (4.14) is valid for computing ν. We will leverage this non-uniqueness of K_A in this work, by constructing a K_A with special properties.

4.2.5   Main result

We now use (4.16) to compute the Hall conductance for ALCPHs. Our main result is the following: Let H be a charge conserving ALCPH. There is a choice of K_A, which we call K_A^*, satisfying (4.13,4.14) such that the corresponding operator K_A^{*-}, defined as in (4.15),

obeys

$$\langle[K_A^{*-}, Q_B]\rangle = \mathcal{O}(L^{-\infty}). \tag{4.17}$$

In particular, $\nu = 0$.

Proof. Let K_A^* be defined by

$$K_A^* = Q_A - \int \mathcal{D}_\Lambda[\theta] e^{i(\theta, H)} Q_A e^{-i(\theta, H)}, \tag{4.18}$$

where $\mathcal{D}_\Lambda[\theta] = \prod_{r \in \Lambda} \frac{d\theta_r}{2\pi}$, $(\theta, H) = \sum_{r \in \Lambda} \theta_r H_r$, and we integrate over $\{0 \le \theta_r \le 2\pi\}$. With this definition, the operator $Q_A - K_A^*$ is simply an *average* of $U Q_A U^\dagger$ over all unitary operators $U = e^{i(\theta, H)}$ generated by the commuting projectors, H_r. Therefore, by construction, $Q_A - K_A^*$ commutes with every unitary operator $e^{i(\theta, H)}$, and hence it also commutes with the generators, H_r:

$$[Q_A - K_A^*, H_r] = 0, \quad (r \in \Lambda) \tag{4.19}$$

This ensures that K_A^* satisfies (4.13).

In fact, K_A^* also satisfies (4.14), i.e. it can be approximated by a sum of local terms supported along the boundary of A. Intuitively, this is because the above averaging procedure only modifies Q_A near its boundary since the Hamiltonian is commuting and charge conserving. This claim is encapsulated in the following lemma: K_A^* can be approximated, up to $\mathcal{O}(L^{-\infty})$, by a sum of the form

$$K_A^* = \sum_{r \in \partial_{\alpha L} A} \overline{K}_{r,A}^* + \mathcal{O}(L^{-\infty}) \tag{4.20}$$

where $\overline{K}_{r,A}^*$ is a strictly local charge conserving operator, with a uniformly bounded norm, supported in $D_{\alpha L}(r)$.

The proof of Lemma 4.2.5 is particularly simple for the special case of strictly local commuting projector Hamiltonians. In fact, in this case, Eq. (4.20) holds without any error

terms. To see this, notice that in (4.18) we only need to include H_r within a finite distance of the boundary of A because all other H_r's commute with Q_A exactly. We can then write K_A^* as $K_A^* = \sum_{r \in A} K_{r,A}^*$ where $K_{r,A}^*$ is defined just like K_A^* in (4.18) except with Q_A replaced by q_r and with the averaging restricted to H_r's within a finite distance of the boundary of A. Eq. (4.20) then follows immediately since $K_{r,A}^*$ vanishes exactly except for r within a finite distance of the boundary of A. A similar proof holds in the more general case of *almost* local commuting projector Hamiltonians; see Sec. 4.3 for details[2].

We now assume Lemma 4.2.5 and proceed with the proof of the theorem. First, we define K_A^{*-} as in (4.15):

$$K_A^{*-} = \sum_{r \in (\partial_{\alpha L} A) \cap \Lambda^-} \overline{K}_{r,A}^*. \tag{4.21}$$

We then make two observations. The first observation, which follows immediately from the definition (4.21) and charge conservation, is that

$$\mathrm{supp}([K_A^{*-}, Q_B]) \subset D_{2\alpha L}(r^-), \tag{4.22}$$

where r^- is the point in the lower half torus where the boundaries of A and B intersect (see Fig. 4.2).

The second observation is that

$$[Q_A - K_A^{*-}, P_{R^-}] = \mathcal{O}(L^{-\infty}), \tag{4.23}$$

where $R^- = \{r \in \Lambda : r_y < -2\alpha L\}$. To see this, it suffices to show that $[Q_A - K_A^{*-}, H_r] = \mathcal{O}(L^{-\infty})$ for any $r \in R^-$ since $P_{R^-} = \prod_{r \in R^-}(1 - H_r)$. From (4.19),

$$[Q_A - K_A^{*-}, H_r] = [K_A^* - K_A^{*-}, H_r].$$

_____

2. See Sec. 4.3 for the proof of Lemma 4.2.5 for ALCPHs.

75

The right hand side is $\mathcal{O}(L^{-\infty})$. Indeed, $K_A^* - K_A^{*-}$ can be approximated, up to $\mathcal{O}(L^{-\infty})$, by a sum of local terms $\overline{K}_{r,A}^*$ strictly supported in $\{r \in \Lambda : r_y \geq -\alpha L\}$, and each of these $\mathcal{O}(L)$ terms commutes with the almost local terms H_r up to $\mathcal{O}(L^{-\infty})$ according to (4.9).

We now use (4.22,4.23) to complete the proof. First, by cyclicity of the trace,

$$\langle [Q_A - K_A^{*-}, Q_B] \rangle_{R^-} = \langle \{Q_B, [P_{R^-}, Q_A - K_A^{*-}]\} \rangle_{R^-}, \tag{4.24}$$

where $\{\cdot, \cdot\}$ denotes the anticommutator. By (4.23), the right hand side is $\mathcal{O}(L^{-\infty})$; therefore since $[Q_A, Q_B] = 0$, we deduce that

$$\langle [K_A^{*-}, Q_B] \rangle_{R^-} = \mathcal{O}(L^{-\infty}). \tag{4.25}$$

At the same time, using (4.12) together with (4.22) and the fact that the distance from $D_{2\alpha L}(r^-)$ to the complement of R^- is proportional to L, we have

$$\langle [K_A^{*-}, Q_B] \rangle = \langle [K_A^{*-}, Q_B] \rangle_{R^-} + \mathcal{O}(L^{-\infty}). \tag{4.26}$$

Theorem 4.2.5 then follows immediately from (4.25,4.26).

It is instructive to compare this proof with the physical argument we presented earlier. To make this comparison, we think of $Q_A - K_A^{*-}$ as the infinitesimal analog of the flux insertion operator U. Specifically, we note that the unitary U corresponding to a 2π flux insertion is given by $U = e^{-2\pi i(Q_A - K_A^{*-})}$[118]. We can then see that the two observations (4.22, 4.23) that underlie our proof have close parallels with the physical argument. In particular, (4.22) is analogous to our previous claim that $U^\dagger Q_B U - Q_B$ is localized near the point where the support of U intersects B. Likewise, (4.23) is analogous to our claim that U preserves the ground state away from the punctures. One difference between the two arguments is that the above argument requires that the site Hilbert space is finite dimensional, e.g. when we cyclically permute the trace in (4.24), while the physical argument only uses the weaker

assumption that Q_B has a bounded spectrum.

4.2.6 Discussion

While we have focused on Hamiltonians built out of commuting *projectors*, our results apply to a broader class of commuting Hamiltonians. For example, we can replace the projector assumption with a weaker gap assumption: the lowest eigenvalue of H_r is 0 and it is isolated from the rest of its spectrum by a local gap $g_r \geq g > 0$ with g independent of r, L. To see why our results apply in this case, note that we can pick a smooth function χ_g such that $\chi_g(E) = 0$ if $E \leq 0$ and $\chi_g(E) = 1$ if $E \geq g$. We can then spectrally flatten H_r to the projector $\chi_g(H_r)$. Smoothness of χ_g translates to a rapid decay in real space and so $\chi_g(H_r)$ remains almost local. It follows that $\tilde{H} = \sum_r \chi_g(H_r)$ is an ALCPH with the same ground state space as H. Hence, the Hall conductance vanishes for ground states of such almost local, locally gapped, commuting Hamiltonians.

Our results can also be readily extended to *fermionic* systems. Indeed, while the setup for our proof was explicitly bosonic, all results continue to hold in the fermionic setting, provided that we restrict to operators with even fermion parity. This restriction ensures that the locality expressed by (almost) commutation continues to hold in the fermionic setting.

One application of our results is that they provide a short proof that any system of non-interacting electrons with localized Wannier functions has a vanishing Hall conductance. To prove this, let the projector into the lowest band be $P = \sum_{r,\mu} |\psi_{r,\mu}\rangle\langle\psi_{r,\mu}|$ and let the projector into the other bands be $1 - P = \sum_{r,\mu'} |\tilde{\psi}_{r,\mu'}\rangle\langle\tilde{\psi}_{r,\mu'}|$. Here, $\{|\psi_{r,\mu}\rangle\}$ and $\{|\tilde{\psi}_{r,\mu'}\rangle\}$ are pairwise orthogonal, superpolynomially localized Wannier functions. A parent Hamiltonian with lowest band projector P is given by $H = \sum_{r,\mu} a(\psi_{r,\mu})a^\dagger(\psi_{r,\mu}) + \sum_{r,\mu'} a^\dagger(\tilde{\psi}_{r,\mu'})a(\tilde{\psi}_{r,\mu'})$, where $a^\dagger(\psi_{r,\mu})$ creates a $\psi_{r,\mu}$ excitation from the Fock vacuum. It is clearly a commuting projector Hamiltonian, and the decay of the Wannier functions implies that the terms are

almost localized. Hence H is an ALCPH and our theorem implies that the Hall conductance vanishes. In fact, Ref. [129] already proved a stronger version of this result, but our proof has the advantage of applying to a much larger class of interacting systems.

One direction for future work is to investigate which two dimensional topological phases can be realized by ALCPHs in the *absence* of any symmetries. In this case, a reasonable conjecture is that ALCPHs can realize precisely those topological phases that support gapped boundaries. Assuming this conjecture, it is particularly interesting to consider topological phases that have a vanishing thermal Hall conductance, but do not support gapped boundaries [130]. These phases presumably do not have an ALCPH realization, but there is no direct proof of this, to our knowledge.

4.2.7   Acknowledgements

4.3   Supplemental Material

In this Supplemental Material, we prove Lemma 1 from the main text. First, we introduce some notation. For any operator O and any subset S of lattice sites, we define a corresponding "averaged" operator $\mathbb{E}_S(O)$ by averaging O over the unitaries generated by $\{H_r : r \in S\}$:

$$\mathbb{E}_S(O) = \int \mathcal{D}_S[\theta] e^{i(\theta,H)_S} O e^{-i(\theta,H)_S}. \tag{4.27}$$

where $\mathcal{D}_S[\theta] = \prod_{r \in S} \frac{d\theta_r}{2\pi}$, $(\theta, H)_S = \sum_{r \in S} \theta_r H_r$, and we integrate over $\{0 \leq \theta_r \leq 2\pi\}$. In this notation, K_A^* can be written as

$$K_A^* = Q_A - \mathbb{E}_\Lambda(Q_A) \tag{4.28}$$

The averaging operation $\mathbb{E}_S$ has several important properties that we will use below. We note first of all that $\mathbb{E}_S$ is a contraction, i.e. $\|\mathbb{E}_S(O)\| \leq \|O\|$, and second of all that, since the Hamiltonian is commuting, $\mathbb{E}_S = \mathbb{E}_{S \setminus S'} \circ \mathbb{E}_{S'} = \mathbb{E}_{S'} \circ \mathbb{E}_{S \setminus S'}$ for any $S' \subset S$ where $S \setminus S'$ is the complement of S' in S. It follows in particular that

$$\|\mathbb{E}_S(O) - \mathbb{E}_{S'}(O)\| \leq \|\mathbb{E}_{S \setminus S'}(O) - O\|. \tag{4.29}$$

Another useful bound is that

$$\|e^{i(\theta,H)_S} O e^{-i(\theta,H)_S} - O\| \leq 2\pi \sum_{r \in S} \|[H_r, O]\| . \tag{4.30}$$

This bound follows from the fact that

$$\left\| \frac{d}{dt} (e^{-it(\theta,H)_S} O e^{it(\theta,H)_S}) \right\| \leq 2\pi \sum_{r \in S} \|[H_r, O]\| ,$$

together with the fundamental theorem of calculus. Integrating (4.30) over all θ_r's gives yet another property of $\mathbb{E}_S$:

$$\|\mathbb{E}_S(O) - O\| \leq 2\pi \sum_{r \in S} \|[H_r, O]\|. \tag{4.31}$$

Finally, combining (4.29, 4.31), we deduce the bound

$$\|\mathbb{E}_S(O) - \mathbb{E}_{S'}(O)\| \leq 2\pi \sum_{r \in S \setminus S'} \|[H_r, O]\|. \tag{4.32}$$

We now apply the above bound (4.32) to the case $O = Q_A$. In that case, charge conservation guarantees that $[H_r, Q_A] = -[H_r, Q_{A^c}]$ and therefore, by the almost locality of H_r,

$$[H_r, Q_A] = \mathcal{O}\left(\max(\text{dist}(r, A), \text{dist}(r, A^c))^{-\infty}\right). \tag{4.33}$$

In other words, only H_r with r near the edge of A fail to commute with Q_A. Combining this with (4.32), we see that we can restrict the average in (4.28) to a strip along the boundary of A with superpolynomially small error:

$$K_A^* = Q_A - \mathbb{E}_{\partial_{\alpha L/2} A}(Q_A) + \mathcal{O}(L^{-\infty}). \tag{4.34}$$

Next, we split $Q_A = \sum_{r \in A} q_r$ in two contributions, Q_{bdry} and Q_{int}, according to to whether $r \in \partial_{\alpha L} A$ or not. From (4.31), we can see that the contribution to K_A^* from Q_{int} is $\mathcal{O}(L^{-\infty})$ since the distance between $\partial_{\alpha L/2} A$ and Q_{int} is proportional to L. Therefore, we can replace Q_A by Q_{bdry} in (4.34):

$$K_A^* = Q_{\text{bdry}} - \mathbb{E}_{\partial_{\alpha L/2} A}(Q_{\text{bdry}}) + \mathcal{O}(L^{-\infty}).$$

To proceed further, we write Q_{bdry} as a sum of q_r's and we use (4.32) to approximate $\mathbb{E}_{\partial_{\alpha L/2} A}(q_r) = \mathbb{E}_{\tilde{D}_{\alpha L/2}(r)}(q_r) + \mathcal{O}(L^{-\infty})$ where $\tilde{D}_{\alpha L/2}(r) = D_{\alpha L/2}(r) \cap \partial_{\alpha L/2} A$. In this way, we derive

$$K_A^* = \sum_{r \in (\partial_{\alpha L} A) \cap A} K_{r,A}^* + \mathcal{O}(L^{-\infty})$$

where

$$K_{r,A}^* = q_r - \mathbb{E}_{\tilde{D}_{\alpha L/2}(r)}(q_r) \tag{4.35}$$

All that remains is to show that $K_{r,A}^*$ can be approximated by a strictly local, uniformly bounded, charge conserving operator $\overline{K}_{r,A}^*$ supported within $D_{\alpha L}(r)$. To show this, we need

80

one more property of $\mathbb{E}_S$, namely the inequality

$$\|[\mathbb{E}_S(O_1), O_2]\| \le 4\pi \|O_1\| \cdot \sum_{r \in S} \|[H_r, O_2]\| \tag{4.36}$$

which holds for any two operators O_1, O_2 with $[O_1, O_2] = 0$. To derive this inequality, note that

$$\|[\mathbb{E}_S(O_1), O_2]\| \le \int \mathcal{D}_S[\theta] \; \|[O_1, e^{-i(\theta, H)_S} O_2 e^{i(\theta, H)_S}]\| \tag{4.37}$$

Combining (4.30, 4.37) and using $[O_1, O_2] = 0$ gives (4.36).

We are now ready to complete the argument and show that $K_{r,A}^*$ is localized near r. To do this, we consider the commutator $[K_{r,A}^*, O_x]$ where O_x is an operator supported on some site x outside of $D_{\alpha L}(r)$. Using the above inequality (4.36) with $O_1 = q_r$ and $O_2 = O_x$, and $S = \tilde{D}_{\alpha L/2}(r)$, we deduce that

$$\|[K_{r,A}^*, O_x]\| \le 4\pi \|q_r\| \cdot \sum_{r \in \tilde{D}_{\alpha L/2}(r)} \|[H_r, O_x]\|$$

$$\le \|O_x\| \cdot \mathcal{O}(L^{-\infty}) \tag{4.38}$$

where the last line follows from the almost locality of H_r. Since O_x is an arbitrary single site operator supported outside of $D_{\alpha L}(r)$, the bound (4.38) implies our claim: $K_{r,A}^*$ can be approximated up to $\mathcal{O}(L^{-\infty})$ by an observable, $\overline{K}_{r,A}^*$, that is strictly supported inside of $D_{\alpha L}(r)$. [For example, $\overline{K}_{r,A}^*$ can be defined by simply taking the partial trace of $K_{r,A}^*$ over all the lattice sites outside of $D_{\alpha L}(r)$]. It is also clear by construction that these $\overline{K}_{r,A}^*$ operators are charge conserving, and they are uniformly bounded because the norm of $K_{r,A}^*$ is bounded by $2\|q_r\|$ by (4.35). This completes the proof of Lemma 1 from the main text.

CHAPTER 5

OUTLOOK

In this thesis we showed how simply toy models can lead to new insights in various disparate topics in condensed matter theory. Many questions remain, and we highlight a few of them here.

5.1 Quantum criticality

A natural next step following our work in Ch. 2 is to obtain an analytically tractable model for a DQCP in 2D. Evidence has been mounting that the original VBS to Néel DQCP in 2D is actually weakly first order[35, 36, 37, 38], but there may be other 2D lattice models that give genuine DQCPs. The model presented in Ch. 2 describes the 1D edge of a 2D SPT, so one place to look for such a 2D DQCP is at the boundary of a 3D SPT. An important aspect of our 1D model was that charge and domain walls in 1D are both point-like. This allows for our mapping to the $\mathbb{Z}_4$ spin chain. In 2D, charge is pointlike but domain walls are line-like, so there may not be an exact mapping like that in Ch. 2. One possible solution is to consider mixed anomalies of continuous symmetries, where the charges and vortices are both point-like. Another possibility is to consider vortices with interesting structures formed at the junctions of domain walls, similar to the C_4 vortices of the VBS-Néel transition.

5.2 Quantum dynamics

In Ch. 3, we obtained a volume-law to area-law transition in a Gaussian non-unitary circuit, but it was fine-tuned with respect to certain parameters in the circuit. One direction for future work is to understand whether or not this is generic, i.e. whether any such entanglement transition in a Gaussian circuit has to be fine-tuned. In particular, Ref. [65] proved that the volume-law phase in Gaussian circuits is unstable to any amount of projective measurement.

It would be interesting to better understand to what extent similar rigorous results can be obtained for Gaussian non-unitary circuits, with weak rather than projective measurements.

One motivation for the project presented in Ch. 3 was the question of whether or not disorder and randomness affects the nature of the entanglement transition. From the mapping of random non-unitary Gaussian circuits onto Chalker-Coddington models[66] and the observation that disorder is a relevant perturbation in these models[131], it seems that disorder would affect the universality class of the transition. It remains to be seen whether or not there exists a volume-law to area-law entanglement transition in Gaussian circuits in the presence of randomness in the gates or in the weak measurements. The latter would occur if we do not postselect on the ancilla (see Sec. 3.3.1). We hypothesize that the transition does not exist in the presence of randomness, but we do not have a proof. One possible approach for this problem is studying perturbative disorder in Gaussian circuits. In interacting systems, the role of disorder on the universality class of the transition is also not clear.

Another future direction is studying interacting but integrable non-unitary circuits, which may realize entanglement transitions distinct from both Gaussian circuits and generic interacting circuits. In forthcoming work[132], we study one particular such model[133]. In addition to being integrable, the model has an antiunitary symmetry playing a similar role to parity-time (PT) symmetry. As shown in Ref. [75], there is an interesting connection between entanglement transitions and (generalized) PT symmetry breaking in generic interacting non-unitary circuits. The integrable nature of the model we study allows for more analytic results, and we find that its antiunitary symmetry breaking transition has entanglement behavior different from that in generic interacting models. Many questions remain along this line of research: how generic is the entanglement behavior we find for other integrable non-unitary circuits with antiunitary symmetry? Can critical properties be determined analytically? How can the non-unitary gates be implemented in a physical setting?

5.3 Topological phases

There are many open questions related to models for topological phases. We will begin with some directions for future work that are related to the results presented in Ch. 4, and then we will mention some more general problems.

As mentioned in Ch. 4, it is believed that commuting projector Hamiltonians in 2D can only realize phases with gapped boundaries. However, there is no proof of this, except in the special cases discussed in Ch. 4. Recently, the property that a topological order admits a gapped edge has been reformulated in terms of a set of topological invariants that generalize the chiral central charge. The so-called "higher central charges" can be computed from the anyon data[134, 135, 136], and can also be extracted from the ground state wavefunction[137]. We highlight two interesting questions regarding the higher central charges. First, can higher central charge be related to transport properties of the edge, like how chiral central charge is related to the thermal Hall conductance? Relatedly, does higher central charge have a bulk formula via bulk-boundary correspondence, like chiral central charge[115]? Second, can one prove that the higher central charges must vanish for any commuting projector Hamiltonian? For the chiral central charge, this follows directly from the formula for the energy current, as discussed in Ch. 4. Therefore, an answer to the first question might help answer the second question.

If phases that do not admit a gapped boundary do not have a commuting projector description, then it would be important to understand how to construct more general models for them[138]. While these models may not be exactly solvable, they may still be partially solvable, like Kitaev's honeycomb model for Ising topological order[12]. For fermionic topological phases, such lattice models would allow for explicit gauging of fermion parity, by coupling the fermions to gauge fields and applying a gauge constraint. In principle, one can then explicitly derive the minimal modular extensions of the fermionic topological order, which are the smallest bosonic topological orders that contain the anyons of the fermionic

topological order. In turn, the minimal modular extensions would allow for computation of the chiral central charge of the fermionic topological order modulo 1/2.

A technically challenging problem related to existing models of topological phases is constructing microscopic lattice models for condensation of general non-abelian anyons. To put this question in context, note that for abelian topological phases, we can drive an anyon condensation transition by adding short string operators $H_{r,a}$ where r denotes the lattice site and a denotes the anyon, to the string-net Hamiltonian H_{SN}:

$$H(\lambda) = H_{SN} - \lambda \sum_{r,a} H_{r,a} \tag{5.1}$$

This would lead to condensation of the a anyons at large λ. The analogous microscopic procedure for condensing non-abelian anyons is not understood. A related problem is how to construct a string-net model with a boundary given a general Lagrangian algebra: a Lagrangian algebra specifies a gapped boundary of a topological order via abstract data describing how anyons are absorbed by the boundary, but it is not clear how to translate it into a microscopic model.

There are some interesting questions at the intersection of condensed matter and quantum information. For example, there is a hierarchy of complexity of topological orders given by abelian, nilpotent, solvable, non-solvable but weakly integral, and not weakly integral. It is hypothesized that only the latter kind of topological order can perform universal quantum computation by braiding alone[139], and some of the other kinds of topological orders can perform universal quantum computation upon supplementing the braiding with additional operations[140, 141]. There is a related hierarchy of complexity for preparation of these topological phases[142]. For example, there are recipes for preparing "solvable" topological orders using sequences of finite time evolution, measurement, and feedforward (i.e. using the measurement results to correct errors). However, for some of these topological orders, the details of some of these steps (i.e. the actual unitary for the finite time evolution) are

not fully developed. It is hypothesized, but not proven, that non-solvable topological orders cannot be prepared using a finite sequence of the above three steps. It would be interesting to rigorously study the limitations of different preparation protocols and their relations to universal quantum computation, possibly using constraints on the string operators of the resulting topological order[143] and their braiding properties.

The main theme of this thesis is toy models in condensed matter physics. However, toy models may have limited applicability in realistic physical systems. Exactly solvable models tend to be simple in terms of ground state structure, but complex in terms of interactions. For example, the exactly solvable model for the 2D $\mathbb{Z}_2$ SPT contains 7-body interactions[63]. For experimental realization, it would be crucial to simplify the interactions. Currently, beyond quantum hall pseud-potential constructions[7] and coupled wire constructions[144, 145], there are few frameworks for constructing realistic models of topological phases. One approach for obtaining more realistic models is using exactly solvable models as a starting point, and adding modifications while staying in the same phase. Much of the work in this direction is inevitably numerical[146, 147, 148], with surprising new findings that beg for better physical understanding.

To close, we share an image of the sunrise observed from a short distance below the peak of Grand Teton. This image serves as a symbol for the vast landscape of open questions and hope for the future.

REFERENCES

[1] Michael Levin and T. Senthil. Deconfined quantum criticality and néel order via dimer disorder. *Phys. Rev. B*, 70:220403, Dec 2004.

[2] Ernst Ising. *Beitrag zur theorie des ferro-und paramagnetismus*. PhD thesis, Grefe & Tiedemann Hamburg, 1924.

[3] Lars Onsager. Crystal statistics. i. a two-dimensional model with an order-disorder transition. *Phys. Rev.*, 65:117–149, Feb 1944.

[4] F. D. M. Haldane. Model for a quantum hall effect without landau levels: Condensed-matter realization of the "parity anomaly". *Phys. Rev. Lett.*, 61:2015–2018, Oct 1988.

[5] A Yu Kitaev. Unpaired majorana fermions in quantum wires. *Physics-uspekhi*, 44(10S):131, 2001.

[6] Xiao-Liang Qi and Shou-Cheng Zhang. Topological insulators and superconductors. *Rev. Mod. Phys.*, 83:1057–1110, Oct 2011.

[7] F Duncan M Haldane. Continuum dynamics of the 1-d heisenberg antiferromagnet: Identification with the o (3) nonlinear sigma model. *Physics letters a*, 93(9):464–468, 1983.

[8] Ian Affleck, Tom Kennedy, Elliott H Lieb, and Hal Tasaki. Rigorous results on valence-bond ground states in antiferromagnets. *Condensed Matter Physics and Exactly Soluble Models: Selecta of Elliott H. Lieb*, pages 249–252, 2004.

[9] Subir Sachdev and Jinwu Ye. Gapless spin-fluid ground state in a random quantum heisenberg magnet. *Phys. Rev. Lett.*, 70:3339–3342, May 1993.

[10] Alexei Kitaev. A simple model of quantum holography (part 2). *Entanglement in Strongly-Correlated Quantum Matter*, page 38, 2015.

[11] A Yu Kitaev. Fault-tolerant quantum computation by anyons. *Annals of Physics*, 303(1):2–30, 2003.

[12] Alexei Kitaev. Anyons in an exactly solved model and beyond. *Annals of Physics*, 321(1):2–111, 2006.

[13] Michael A. Levin and Xiao-Gang Wen. String-net condensation: A physical mechanism for topological phases. *Phys. Rev. B*, 71:045110, Jan 2005.

[14] Chien-Hung Lin, Michael Levin, and Fiona J. Burnell. Generalized string-net models: A thorough exposition. *Phys. Rev. B*, 103:195155, May 2021.

[15] Chris Heinrich, Fiona Burnell, Lukasz Fidkowski, and Michael Levin. Symmetry-enriched string nets: Exactly solvable models for set phases. *Phys. Rev. B*, 94:235136, Dec 2016.

[16] Meng Cheng, Zheng-Cheng Gu, Shenghan Jiang, and Yang Qi. Exactly solvable models for symmetry-enriched topological phases. *Phys. Rev. B*, 96:115107, Sep 2017.

[17] Claudio Chamon. Quantum glassiness in strongly correlated clean systems: An example of topological overprotection. *Phys. Rev. Lett.*, 94:040402, Jan 2005.

[18] Jeongwan Haah. Local stabilizer codes in three dimensions without string logical operators. *Phys. Rev. A*, 83:042330, Apr 2011.

[19] Sagar Vijay, Jeongwan Haah, and Liang Fu. Fracton topological order, generalized lattice gauge theory, and duality. *Phys. Rev. B*, 94:235157, Dec 2016.

[20] Rahul M Nandkishore and Michael Hermele. Fractons. *Annual Review of Condensed Matter Physics*, 10:295–313, 2019.

[21] Lev Davidovich Landau. On the theory of phase transitions. i. *Zh. Eksp. Teor. Fiz.*, 11:19, 1937.

[22] John Cardy. *Scaling and renormalization in statistical physics*, volume 5. Cambridge university press, 1996.

[23] Yaodong Li, Xiao Chen, and Matthew P. A. Fisher. Quantum zeno effect and the many-body entanglement transition. *Phys. Rev. B*, 98:205136, Nov 2018.

[24] Yaodong Li, Xiao Chen, and Matthew P. A. Fisher. Measurement-driven entanglement transition in hybrid quantum circuits. *Phys. Rev. B*, 100:134306, Oct 2019.

[25] Brian Skinner, Jonathan Ruhman, and Adam Nahum. Measurement-induced phase transitions in the dynamics of entanglement. *Phys. Rev. X*, 9:031009, Jul 2019.

[26] Amos Chan, Rahul M. Nandkishore, Michael Pretko, and Graeme Smith. Unitary-projective entanglement dynamics. *Phys. Rev. B*, 99:224307, Jun 2019.

[27] Xiao-Gang Wen. Colloquium: Zoo of quantum-topological phases of matter. *Rev. Mod. Phys.*, 89:041004, Dec 2017.

[28] Marvin E Cage, Kv Klitzing, AM Chang, F Duncan, M Haldane, Robert B Laughlin, AMM Pruisken, and DJ Thouless. *The quantum Hall effect.* Springer Science & Business Media, 2012.

[29] K. v. Klitzing, G. Dorda, and M. Pepper. New method for high-accuracy determination of the fine-structure constant based on quantized hall resistance. *Phys. Rev. Lett.*, 45:494–497, Aug 1980.

[30] Anton Kapustin and Lukasz Fidkowski. Local commuting projector hamiltonians and the quantum hall effect. *Commun. Math. Phys.*, 373(2):763–769, 2020.

[31] T. Senthil, Leon Balents, Subir Sachdev, Ashvin Vishwanath, and Matthew P. A. Fisher. Quantum criticality beyond the landau-ginzburg-wilson paradigm. *Phys. Rev. B*, 70:144407, Oct 2004.

[32] Todadri Senthil, Ashvin Vishwanath, Leon Balents, Subir Sachdev, and Matthew PA Fisher. Deconfined quantum critical points. *Science*, 303(5663):1490–1494, 2004.

[33] Anders W. Sandvik. Evidence for deconfined quantum criticality in a two-dimensional heisenberg model with four-spin interactions. *Phys. Rev. Lett.*, 98:227202, Jun 2007.

[34] Roger G. Melko and Ribhu K. Kaul. Scaling in the fan of an unconventional quantum critical point. *Phys. Rev. Lett.*, 100:017203, Jan 2008.

[35] Adam Nahum, J. T. Chalker, P. Serna, M. Ortuño, and A. M. Somoza. Deconfined quantum criticality, scaling violations, and classical loop models. *Phys. Rev. X*, 5:041048, Dec 2015.

[36] Yu Nakayama and Tomoki Ohtsuki. Necessary condition for emergent symmetry from the conformal bootstrap. *Phys. Rev. Lett.*, 117:131601, Sep 2016.

[37] David Poland, Slava Rychkov, and Alessandro Vichi. The conformal bootstrap: Theory, numerical techniques, and applications. *Rev. Mod. Phys.*, 91:015002, Jan 2019.

[38] Jiarui Zhao, Yan-Cheng Wang, Zheng Yan, Meng Cheng, and Zi Yang Meng. Scaling of entanglement entropy at deconfined quantum criticality. *Phys. Rev. Lett.*, 128:010601, Jan 2022.

[39] Shenghan Jiang and Olexei Motrunich. Ising ferromagnet to valence bond solid transition in a one-dimensional spin chain: Analogies to deconfined quantum critical points. *Phys. Rev. B*, 99:075103, Feb 2019.

[40] Brenden Roberts, Shenghan Jiang, and Olexei I. Motrunich. Deconfined quantum critical point in one dimension. *Phys. Rev. B*, 99:165143, Apr 2019.

[41] Rui-Zhen Huang, Da-Chuan Lu, Yi-Zhuang You, Zi Yang Meng, and Tao Xiang. Emergent symmetry and conserved current at a one-dimensional incarnation of deconfined quantum critical point. *Phys. Rev. B*, 100:125137, Sep 2019.

[42] Christopher Mudry, Akira Furusaki, Takahiro Morimoto, and Toshiya Hikihara. Quantum phase transitions beyond landau-ginzburg theory in one-dimensional space revisited. *Phys. Rev. B*, 99:205153, May 2019.

[43] Wayne Zheng, D. N. Sheng, and Yuan-Ming Lu. Unconventional quantum phase transitions in a one-dimensional lieb-schultz-mattis system. *Phys. Rev. B*, 105:075147, Feb 2022.

[44] Xie Chen, Zheng-Cheng Gu, Zheng-Xin Liu, and Xiao-Gang Wen. Symmetry protected topological orders and the group cohomology of their symmetry group. *Phys. Rev. B*, 87:155114, Apr 2013.

[45] Dominic V. Else and Chetan Nayak. Classifying symmetry-protected topological phases through the anomalous action of the symmetry on the edge. *Phys. Rev. B*, 90:235137, Dec 2014.

[46] Xiao-Liang Qi, Taylor L Hughes, and Shou-Cheng Zhang. Fractional charge and quantized current in the quantum spin hall state. *Nature Physics*, 4(4):273–276, 2008.

[47] Michael P. Zaletel. Detecting two-dimensional symmetry-protected topological order in a ground-state wave function. *Phys. Rev. B*, 90:235113, Dec 2014.

[48] Juven C. Wang, Luiz H. Santos, and Xiao-Gang Wen. Bosonic anomalies, induced fractional quantum numbers, and degenerate zero modes: The anomalous edge physics of symmetry-protected topological states. *Phys. Rev. B*, 91:195134, May 2015.

[49] Arkya Chatterjee and Xiao-Gang Wen. Algebra of local symmetric operators and braided fusion n-category–symmetry is a shadow of topological order. *arXiv preprint arXiv:2203.03596*, 2022.

[50] Jorge V. José, Leo P. Kadanoff, Scott Kirkpatrick, and David R. Nelson. Renormalization, vortices, and symmetry-breaking perturbations in the two-dimensional planar model. *Phys. Rev. B*, 16:1217–1241, Aug 1977.

[51] Robbert Dijkgraaf, Cumrun Vafa, Erik Verlinde, and Herman Verlinde. The operator algebra of orbifold models. *Communications in Mathematical Physics*, 123(3):485–526, 1989.

[52] Mahito Kohmoto, Marcel den Nijs, and Leo P. Kadanoff. Hamiltonian studies of the $d = 2$ ashkin-teller model. *Phys. Rev. B*, 24:5229–5241, Nov 1981.

[53] P Lecheminant, Alexander O Gogolin, and Alexander A Nersesyan. Criticality in self-dual sine-gordon models. *Nuclear Physics B*, 639(3):502–523, 2002.

[54] H. J. Schulz. Phase transitions in monolayers adsorbed on uniaxial substrates. *Phys. Rev. B*, 28:2746–2749, Sep 1983.

[55] David A. Huse and Michael E. Fisher. Commensurate melting, domain walls, and dislocations. *Phys. Rev. B*, 29:239–270, Jan 1984.

[56] Samuel Nyckees and Frédéric Mila. Commensurate-incommensurate transition in the chiral ashkin-teller model. *Phys. Rev. Research*, 4:013093, Feb 2022.

[57] Seth Whitsitt, Rhine Samajdar, and Subir Sachdev. Quantum field theory for the chiral clock transition in one spatial dimension. *Phys. Rev. B*, 98:205118, Nov 2018.

[58] Chong Wang, Adam Nahum, Max A. Metlitski, Cenke Xu, and T. Senthil. Deconfined quantum critical points: Symmetries and dualities. *Phys. Rev. X*, 7:031051, Sep 2017.

[59] Chenjie Wang and Michael Levin. Topological invariants for gauge theories and symmetry-protected topological phases. *Phys. Rev. B*, 91:165119, Apr 2015.

[60] Daniel S. Fisher. Random transverse field ising spin chains. *Phys. Rev. Lett.*, 69:534–537, Jul 1992.

[61] Daniel S. Fisher. Critical behavior of random transverse-field ising spin chains. *Phys. Rev. B*, 51:6411–6461, Mar 1995.

[62] T. Senthil and Satya N. Majumdar. Critical properties of random quantum potts and clock models. *Phys. Rev. Lett.*, 76:3001–3004, Apr 1996.

[63] Michael Levin and Zheng-Cheng Gu. Braiding statistics approach to symmetry-protected topological phases. *Phys. Rev. B*, 86:115109, Sep 2012.

[64] Xiao-Gang Wen. *Quantum field theory of many-body systems: from the origin of sound to an origin of light and electrons*. OUP Oxford, 2004.

[65] Lukasz Fidkowski, Jeongwan Haah, and Matthew B Hastings. How dynamical quantum memories forget. *Quantum*, 5:382, 2021.

[66] Chao-Ming Jian, Bela Bauer, Anna Keselman, and Andreas W. W. Ludwig. Criticality and entanglement in nonunitary quantum circuits and tensor networks of noninteracting fermions. *Phys. Rev. B*, 106:134206, Oct 2022.

[67] Marcin Szyniszewski, Alessandro Romito, and Henning Schomerus. Entanglement transition from variable-strength weak measurements. *Physical Review B*, 100(6):064204, 2019.

[68] Aidan Zabalo, Michael J. Gullans, Justin H. Wilson, Sarang Gopalakrishnan, David A. Huse, and J. H. Pixley. Critical properties of the measurement-induced transition in random quantum circuits. *Phys. Rev. B*, 101:060301, Feb 2020.

[69] Soonwon Choi, Yimu Bao, Xiao-Liang Qi, and Ehud Altman. Quantum error correction in scrambling dynamics and measurement-induced phase transition. *Phys. Rev. Lett.*, 125:030505, 2020.

[70] Michael J. Gullans and David A. Huse. Dynamical purification phase transition induced by quantum measurements. *Phys. Rev. X*, 10:041020, Oct 2020.

[71] Shao-Kai Jian, Chunxiao Liu, Xiao Chen, Brian Swingle, and Pengfei Zhang. Measurement-induced phase transition in the monitored sachdev-ye-kitaev model. *Physical Review Letters*, 127(14):140601, 2021.

[72] Adam Nahum, Sthitadhi Roy, Brian Skinner, and Jonathan Ruhman. Measurement and entanglement phase transitions in all-to-all quantum circuits, on quantum trees, and in landau-ginsburg theory. *PRX Quantum*, 2(1):010352, 2021.

[73] M Buchhold, Y Minoguchi, A Altland, and S Diehl. Effective theory for the measurement-induced phase transition of dirac fermions. *Physical Review X*, 11(4):041004, 2021.

[74] Qicheng Tang and W Zhu. Measurement-induced phase transition: A case study in the nonintegrable model by density-matrix renormalization group calculations. *Physical Review Research*, 2(1):013022, 2020.

[75] Sarang Gopalakrishnan and Michael J Gullans. Entanglement and purification transitions in non-hermitian quantum mechanics. *Physical review letters*, 126(17):170503, 2021.

[76] Xhek Turkeshi, Rosario Fazio, and Marcello Dalmonte. Measurement-induced criticality in (2+ 1)-dimensional hybrid quantum circuits. *Physical Review B*, 102(1):014315, 2020.

[77] Maxwell Block, Yimu Bao, Soonwon Choi, Ehud Altman, and Norman Y Yao. Measurement-induced transition in long-range interacting quantum circuits. *Physical Review Letters*, 128(1):010604, 2022.

[78] Utkarsh Agrawal, Aidan Zabalo, Kun Chen, Justin H Wilson, Andrew C Potter, JH Pixley, Sarang Gopalakrishnan, and Romain Vasseur. Entanglement and charge-sharpening transitions in u (1) symmetric monitored quantum circuits. *Physical Review X*, 12(4):041002, 2022.

[79] Shengqi Sang, Yaodong Li, Tianci Zhou, Xiao Chen, Timothy H Hsieh, and Matthew PA Fisher. Entanglement negativity at measurement-induced criticality. *PRX Quantum*, 2(3):030313, 2021.

[80] Marcin Szyniszewski, Alessandro Romito, and Henning Schomerus. Universality of entanglement transitions from stroboscopic to continuous measurements. *Physical review letters*, 125(21):210602, 2020.

[81] Shimpei Goto and Ippei Danshita. Measurement-induced transitions of the entanglement scaling law in ultracold gases with controllable dissipation. *Physical Review A*, 102(3):033316, 2020.

[82] Oliver Lunt and Arijeet Pal. Measurement-induced entanglement transitions in many-body localized systems. *Physical Review Research*, 2(4):043072, 2020.

[83] Thomas Botzung, Sebastian Diehl, and Markus Müller. Engineered dissipation induced entanglement transition in quantum spin chains: from logarithmic growth to area law. *Physical Review B*, 104(18):184422, 2021.

[84] Javier Lopez-Piqueres, Brayden Ware, and Romain Vasseur. Mean-field entanglement transitions in random tree tensor networks. *Physical Review B*, 102(6):064202, 2020.

[85] Crystal Noel, Pradeep Niroula, Daiwei Zhu, Andrew Risinger, Laird Egan, Debopriyo Biswas, Marko Cetina, Alexey V Gorshkov, Michael J Gullans, David A Huse, et al. Measurement-induced quantum phases realized in a trapped-ion quantum computer. *Nature Physics*, pages 1–5, 2022.

[86] Jason Iaconis, Andrew Lucas, and Xiao Chen. Measurement-induced phase transitions in quantum automaton circuits. *Physical Review B*, 102(22):224311, 2020.

[87] Zhi-Cheng Yang, Yaodong Li, Matthew PA Fisher, and Xiao Chen. Entanglement phase transitions in random stabilizer tensor networks. *Physical Review B*, 105(10):104306, 2022.

[88] Yimu Bao, Soonwon Choi, and Ehud Altman. Theory of the phase transition in random unitary circuits with measurements. *Physical Review B*, 101(10):104301, 2020.

[89] Chao-Ming Jian, Yi-Zhuang You, Romain Vasseur, and Andreas WW Ludwig. Measurement-induced criticality in random quantum circuits. *Physical Review B*, 101(10):104302, 2020.

[90] Bruno Bertini and Lorenzo Piroli. Scrambling in random unitary circuits: Exact results. *Physical Review B*, 102(6):064305, 2020.

[91] Tsung-Cheng Lu and Tarun Grover. Spacetime duality between localization transitions and measurement-induced transitions. *PRX Quantum*, 2:040319, Oct 2021.

[92] Katja Klobas and Bruno Bertini. Entanglement dynamics in rule 54: Exact results and quasiparticle picture. *SciPost Physics*, 11(6):107, 2021.

[93] Youenn Le Gal, Xhek Turkeshi, and Marco Schiro. Volume-to-area law entanglement transition in a non-hermitian free fermionic chain. *arXiv:2210.11937*, Oct 2022.

[94] Xiangyu Cao, Antoine Tilloy, and Andrea De Luca. Entanglement in a fermion chain under continuous monitoring. *SciPost Physics*, 7(2):024, 2019.

[95] Xiao Chen, Yaodong Li, Matthew P. A. Fisher, and Andrew Lucas. Emergent conformal symmetry in nonunitary random dynamics of free fermions. *Phys. Rev. Research*, 2:033017, Jul 2020.

[96] Adam Nahum and Brian Skinner. Entanglement and dynamics of diffusion-annihilation processes with majorana defects. *Phys. Rev. Research*, 2:023288, Jun 2020.

[97] O. Alberton, M. Buchhold, and S. Diehl. Entanglement transition in a monitored free-fermion chain: From extended criticality to area law. *Phys. Rev. Lett.*, 126:170602, Apr 2021.

[98] Federico Carollo and Vincenzo Alba. Entangled multiplets and spreading of quantum correlations in a continuously monitored tight-binding chain. *Phys. Rev. B*, 106:L220304, Dec 2022.

[99] Pengfei Zhang, Shao-Kai Jian, Chunxiao Liu, and Xiao Chen. Emergent replica conformal symmetry in non-hermitian syk _2 chains. *Quantum*, 5:579, 2021.

[100] Henrik Dreyer, Mircea Bejan, and Etienne Granet. Quantum computing critical exponents. *Phys. Rev. A*, 104:062614, Dec 2021.

[101] Etienne Granet, Henrik Dreyer, and Fabian H.L. Essler. Out-of-equilibrium dynamics of the xy spin chain from form factor expansion. *SciPost Phys.*, 12:019, 2022.

[102] A. McDonald, R. Hanai, and A. A. Clerk. Nonequilibrium stationary states of quantum non-hermitian lattice models. *Phys. Rev. B*, 105:064302, Feb 2022.

[103] Etienne Granet. Exact mean-field solution of a spin chain with short-range and long-range interactions. *arXiv preprint arXiv:2209.08756*, 2022.

[104] Matteo Ippoliti, Tibor Rakovszky, and Vedika Khemani. Fractal, logarithmic, and volume-law entangled nonthermal steady states via spacetime duality. *Physical Review X*, 12(1):011045, 2022.

[105] Xhek Turkeshi, Alberto Biella, Rosario Fazio, Marcello Dalmonte, and Marco Schiró. Measurement-induced entanglement transitions in the quantum ising chain: From infinite to zero clicks. *Phys. Rev. B*, 103:224210, Jun 2021.

[106] Tsung-Cheng Lu and Tarun Grover. Spacetime duality between localization transitions and measurement-induced transitions. *PRX Quantum*, 2:040319, 2021.

[107] Matthew B Hastings. An area law for one-dimensional quantum systems. *Journal of statistical mechanics: theory and experiment*, 2007(08):P08024, 2007.

[108] Fernando GSL Brandao and Michał Horodecki. Exponential decay of correlations implies area law. *Communications in mathematical physics*, 333(2):761–798, 2015.

[109] Pasquale Calabrese and John Cardy. Evolution of entanglement entropy in one-dimensional systems. *Journal of Statistical Mechanics: Theory and Experiment*, 2005(04):P04010, 2005.

[110] Filiberto Ares, José G Esteve, Fernando Falceto, and Zoltán Zimborás. Sublogarithmic behaviour of the entanglement entropy in fermionic chains. *Journal of Statistical Mechanics: Theory and Experiment*, 2019(9):093105, 2019.

[111] I Affleck, D Gepner, H J Schulz, and T Ziman. Critical behaviour of spin-s heisenberg antiferromagnetic chains: analytic and numerical results. *J. Phys. A: Math. Gen.*, 22:511, 1989.

[112] Sebastian Eggert. Numerical evidence for multiplicative logarithmic corrections from marginal operators. *Phys.Rev. B*, 54:9612, 1996.

[113] Nicolas Tarantino and Lukasz Fidkowski. Discrete spin structures and commuting projector models for two-dimensional fermionic symmetry-protected topological phases. *Phys. Rev. B*, 94:115115, Sep 2016.

[114] Nathanan Tantivasadakarn and Ashvin Vishwanath. Full commuting projector hamiltonians of interacting symmetry-protected topological phases of fermions. *Phys. Rev. B*, 98:165104, Oct 2018.

[115] Anton Kapustin and Lev Spodyneiko. Thermal hall conductance and a relative topological invariant of gapped two-dimensional systems. *Phys. Rev. B*, 101:045137, Jan 2020.

[116] T. Senthil and Michael Levin. Integer quantum hall effect for bosons. *Phys. Rev. Lett.*, 110:046801, Jan 2013.

[117] Alexei Kitaev. Anyons in an exactly solved model and beyond. *Annals of Physics*, 321(1):2–111, 2006.

[118] Sven Bachmann, Alex Bols, Wojciech De Roeck, and Martin Fraas. A many-body index for quantum charge transport. *Commun. Math. Phys.*, 375(2):1249–1272, 2020.

[119] Sven Bachmann, Alex Bols, Wojciech De Roeck, and Martin Fraas. Rational indices for quantum ground state sectors. *J. Math. Phys.*, 62(1):011901, 2021.

[120] A. Kapustin and N. Sopenko. Hall conductance and the statistics of flux insertions in gapped interacting lattice systems. *J. Math. Phys.*, 61(10):101901, 2020.

[121] Robert B Laughlin. Quantized hall conductivity in two dimensions. *Phys. Rev. B*, 23(10):5632, 1981.

[122] Joseph E Avron, Ruedi Seiler, and Barry Simon. Charge deficiency, charge transport and comparison of dimensions. *Commun. Math. Phys.*, 159(2):399–422, 1994.

[123] Michael DeMarco and Xiao-Gang Wen. A commuting projector model with a non-zero quantized hall conductance. *arXiv preprint arXiv:2102.13057*, 2021.

[124] Sergey Bravyi, Matthew B. Hastings, and Spyridon Michalakis. Topological quantum order: Stability under local perturbations. *J. Math. Phys.*, 51(9):093512, 2010.

[125] Spyridon Michalakis and Justyna P Zwolak. Stability of frustration-free hamiltonians. *Commun. Math. Phys.*, 322(2):277–302, 2013.

[126] Matthew B Hastings and Spyridon Michalakis. Quantization of hall conductance for interacting electrons on a torus. *Commun. Math. Phys.*, 334(1):433–471, 2015.

[127] Sven Bachmann, Alex Bols, Wojciech De Roeck, and Martin Fraas. Quantization of conductance in gapped interacting systems. *Annales H. Poincaré*, 19(3):695–708, 2018.

[128] Joseph E Avron and Ruedi Seiler. Quantization of the hall conductance for general, multiparticle schrödinger hamiltonians. *Phys. Rev. Lett.*, 54(4):259, 1985.

[129] Domenico Monaco, Gianluca Panati, Adriano Pisante, and Stefan Teufel. Optimal decay of wannier functions in chern and quantum hall insulators. *Commun. Math. Phys.*, 359(1):61–100, 2018.

[130] Michael Levin. Protected edge modes without symmetry. *Phys. Rev. X*, 3:021009, May 2013.

[131] Andreas W. W. Ludwig, Matthew P. A. Fisher, R. Shankar, and G. Grinstein. Integer quantum hall transition: An alternative approach and exact results. *Phys. Rev. B*, 50:7526–7552, Sep 1994.

[132] Etienne Granet and Carolyn Zhang, to appear.

[133] Yuan Miao, Vladimir Gritsev, and Denis V Kurlov. The floquet baxterisation. *arXiv preprint arXiv:2206.15142*, 2022.

[134] Siu-Hung Ng, Andrew Schopieray, and Yilong Wang. Higher gauss sums of modular categories. *Selecta Mathematica*, 25(4):53, 2019.

[135] Siu-Hung Ng, Eric C Rowell, Yilong Wang, and Qing Zhang. Higher central charges and witt groups. *Advances in Mathematics*, 404:108388, 2022.

[136] Justin Kaidi, Zohar Komargodski, Kantaro Ohmori, Sahand Seifnashri, and Shu-Heng Shao. Higher central charges and topological boundaries in 2+ 1-dimensional tqfts. *SciPost Physics*, 13(3):067, 2022.

[137] Ryohei Kobayashi, Taige Wang, Tomohiro Soejima, Roger SK Mong, and Shinsei Ryu. Extracting higher central charge from a single wave function. *arXiv preprint arXiv:2303.04822*, 2023.

[138] Nikita Sopenko. Chiral topologically ordered states on a lattice from vertex operator algebras. *arXiv preprint arXiv:2301.08697*, 2023.

[139] Deepak Naidu and Eric C Rowell. A finiteness property for braided fusion categories. *Algebras and representation theory*, 14:837–855, 2011.

[140] Carlos Mochon. Anyon computers with smaller groups. *Phys. Rev. A*, 69:032306, Mar 2004.

[141] Shawn X Cui, Seung-Moon Hong, and Zhenghan Wang. Universal quantum computation with weakly integral anyons. *Quantum Information Processing*, 14:2687–2727, 2015.

[142] Nathanan Tantivasadakarn, Ashvin Vishwanath, and Ruben Verresen. A hierarchy of topological order from finite-depth unitaries, measurement and feedforward. *arXiv preprint arXiv:2209.06202*, 2022.

[143] Sergey Bravyi, Isaac Kim, Alexander Kliesch, and Robert Koenig. Adaptive constant-depth circuits for manipulating non-abelian anyons. *arXiv preprint arXiv:2205.01933*, 2022.

[144] C. L. Kane, Ranjan Mukhopadhyay, and T. C. Lubensky. Fractional quantum hall effect in an array of quantum wires. *Phys. Rev. Lett.*, 88:036401, Jan 2002.

[145] Tobias Meng. Coupled-wire constructions: a luttinger liquid approach to topology. *The European Physical Journal Special Topics*, 229(4):527–543, 2020.

[146] Yin-Chen He, Subhro Bhattacharjee, R. Moessner, and Frank Pollmann. Bosonic integer quantum hall effect in an interacting lattice model. *Phys. Rev. Lett.*, 115:116803, Sep 2015.

[147] Bin-Bin Chen, Ziyu Chen, Shou-Shu Gong, D. N. Sheng, Wei Li, and Andreas Weichselbaum. Quantum spin liquid with emergent chiral order in the triangular-lattice hubbard model. *Phys. Rev. B*, 106:094420, Sep 2022.

[148] Li-Mei Chen, Tyler D Ellison, Meng Cheng, Peng Ye, and Ji-Yao Chen. Chiral fibonacci spin liquid in a $\mathbb{Z}_3$ kitaev model. *arXiv preprint arXiv:2302.05060*, 2023.